2023 Fall

"Phase Transformation *in* Materials"

11.27.2023

Eun Soo Park

Office: 33-313
Telephone: 880-7221
Email: espark@snu.ac.kr
Office hours: by an appointment

Contents for today's class

< Phase Transformation in Solids > Long range diffusion

1) **Diffusional Transformation** **(a) Precipitation** : Nucleation & Growth

Q1: Overall Transformation Kinetics–TTT diagram

Q2: Precipitation in Age-Hardening Alloys

Q3: Age Hardening

Q4: How can you design an alloy with high strength at high T?

Q5: Quenched-in vacancies vs Precipitate-free zone

Q6: Spinodal Decomposition

Q7: Precipitation of Ferrite from Austenite (γ→α)

(b) Eutectoid Transformation (5.8 절)

Short range diffusion

(c) Order-disorder Transformation (1.3.7 절)

(d) Massive Transformation (5.9 절)

(e) Polymorphic Transformation

Q7: Precipitation of Ferrite from Austenite ($\gamma \rightarrow \alpha$)

5.6. The Precipitation of Ferrite from Austenite (γ→α)

(Most important nucleation site: Grain boundary and the surface of inclusions)

The Iron-Carbon Phase Diagram

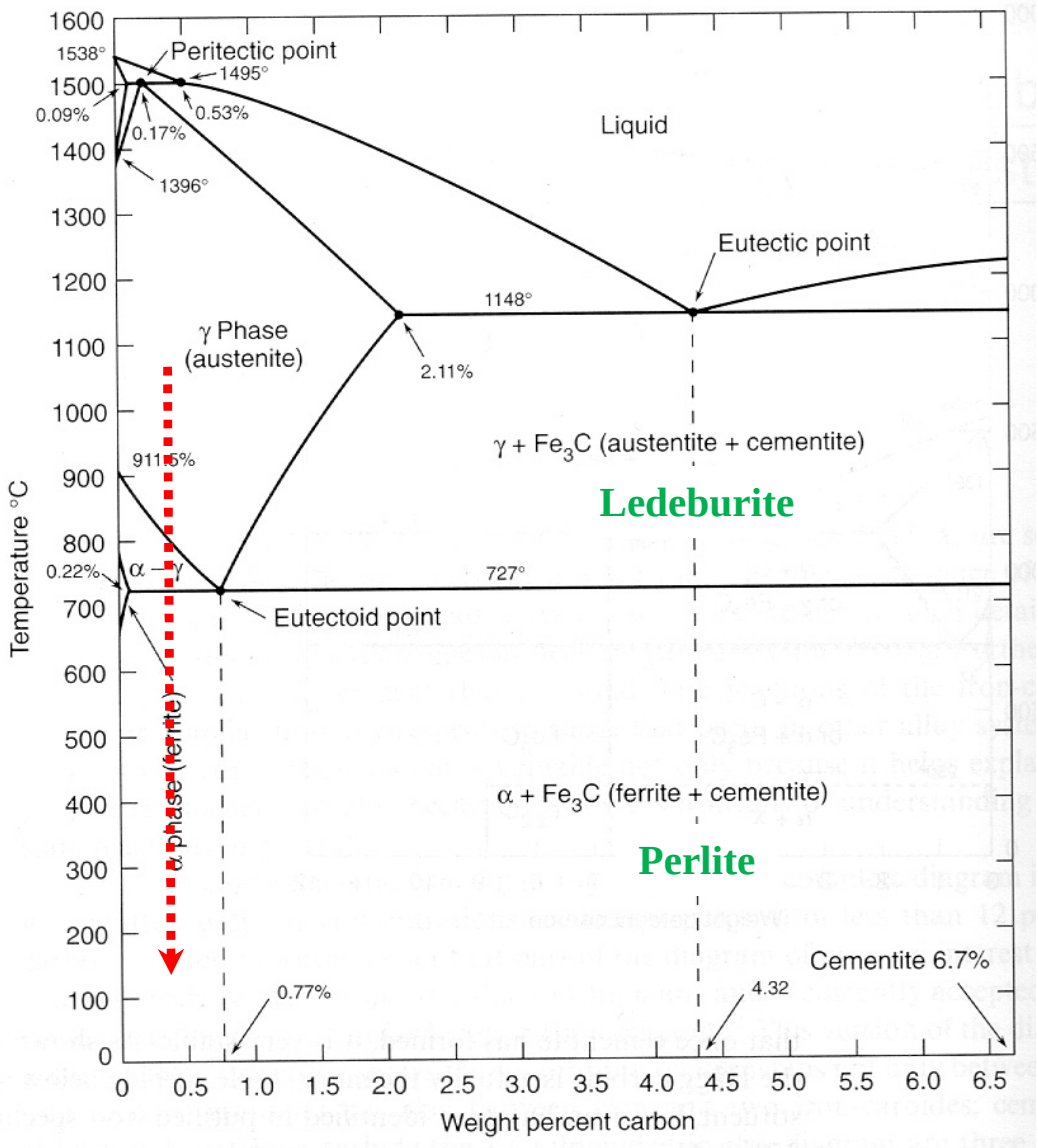

Microstructure (0.4 wt%C) evolved by slow cooling (air, furnace) ?

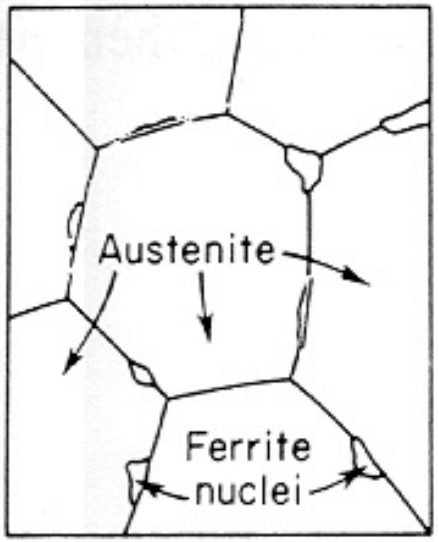

The most important nucleation sites are grain boundaries and the surfaces of inclusions.

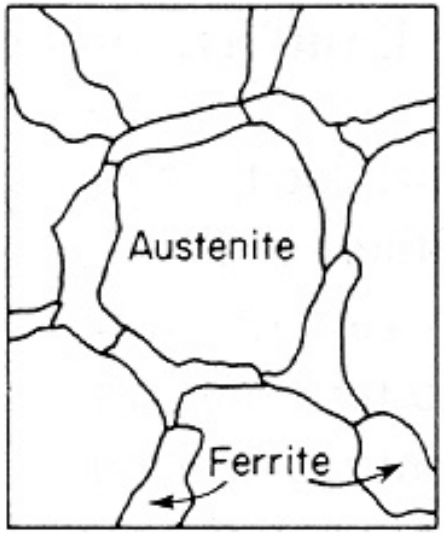

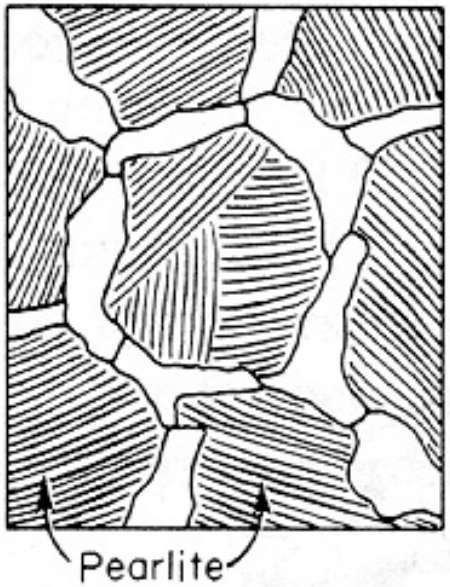

* Orientation memory mechanism between γ and α :

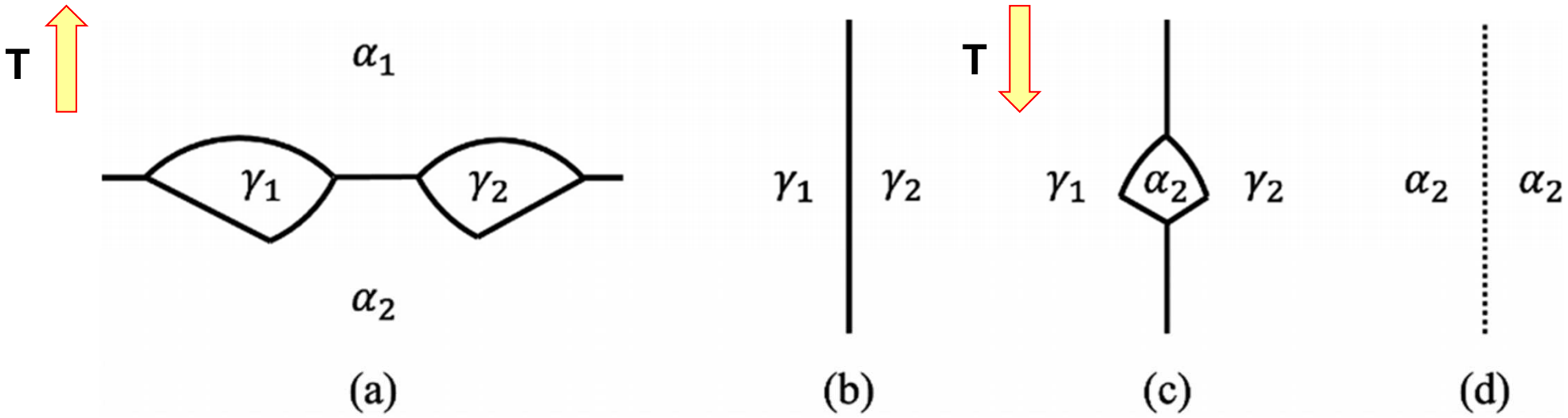

FIGURE 5.46 An orientation memory mechanism. (a) On heating to above A_3, austenite grains nucleate on a grain boundary between two ferrite grains as two variants of, for example, the KS orientation relationship to ferrite grain α_2. (b) The nuclei grow to consume all the ferrite forming an austenite grain boundary. (c) On cooling to below A_3, a ferrite nucleus in the same orientation as α_2 will have an orientation relationship and low-energy interfaces with both austenite grains. (d) After growth of such nuclei, the microstructure contains ferrite grains with the same orientation as existed in the starting microstructure.

5.6. The Precipitation of Ferrite from Austenite

Diffusional Transformation of Austenite into Ferrite

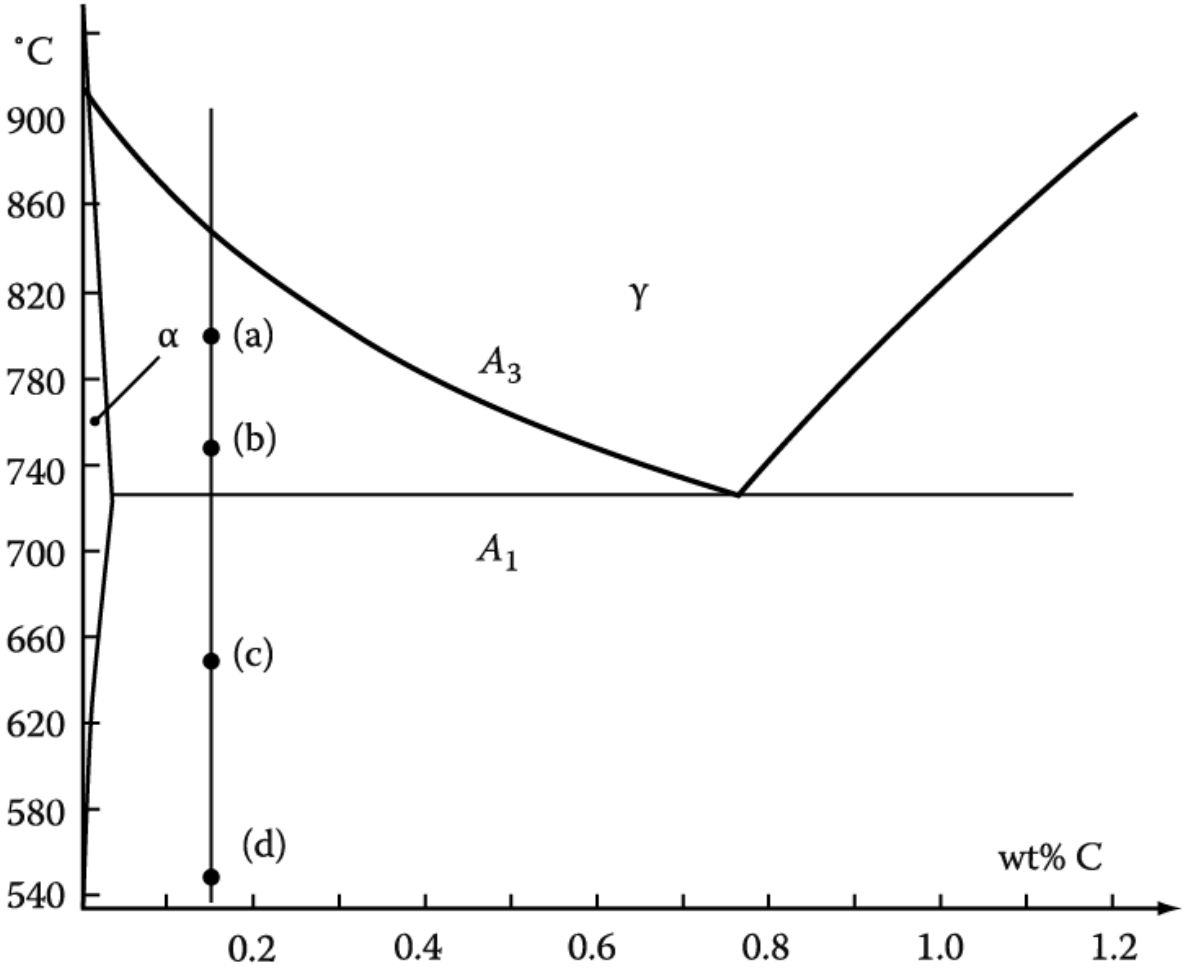

Figure 5.45 Holding temperature for steel in Figure. 5.46

Fe-0.15 wt%C

After being austenitized, held at

(a) 800°C for 150 s

(b) 750°C for 40 s

(c) 650°C for 9 s

(d) 550°C for 2 s and

then quenched to room T.

What would be the microstructures?

Microstructures of an austenitized Fe-0.15%C alloy (x 100 except (d, x300))

White: α ferrite/ Gray: M formed from untransformed γ/ fine constituent: a mixture of ferrite and carbide

Primary ferrite allotriomorphs with a few plates ⇨ Many more plates, mostly growing from GBs/ inside α grain

Smaller ΔT

(a)
800°C
for 150 s

(입계타형) G.B. allotriomorphs
"blockey" manner/
Smoothly curved
& faceted α/γ
Interface are present

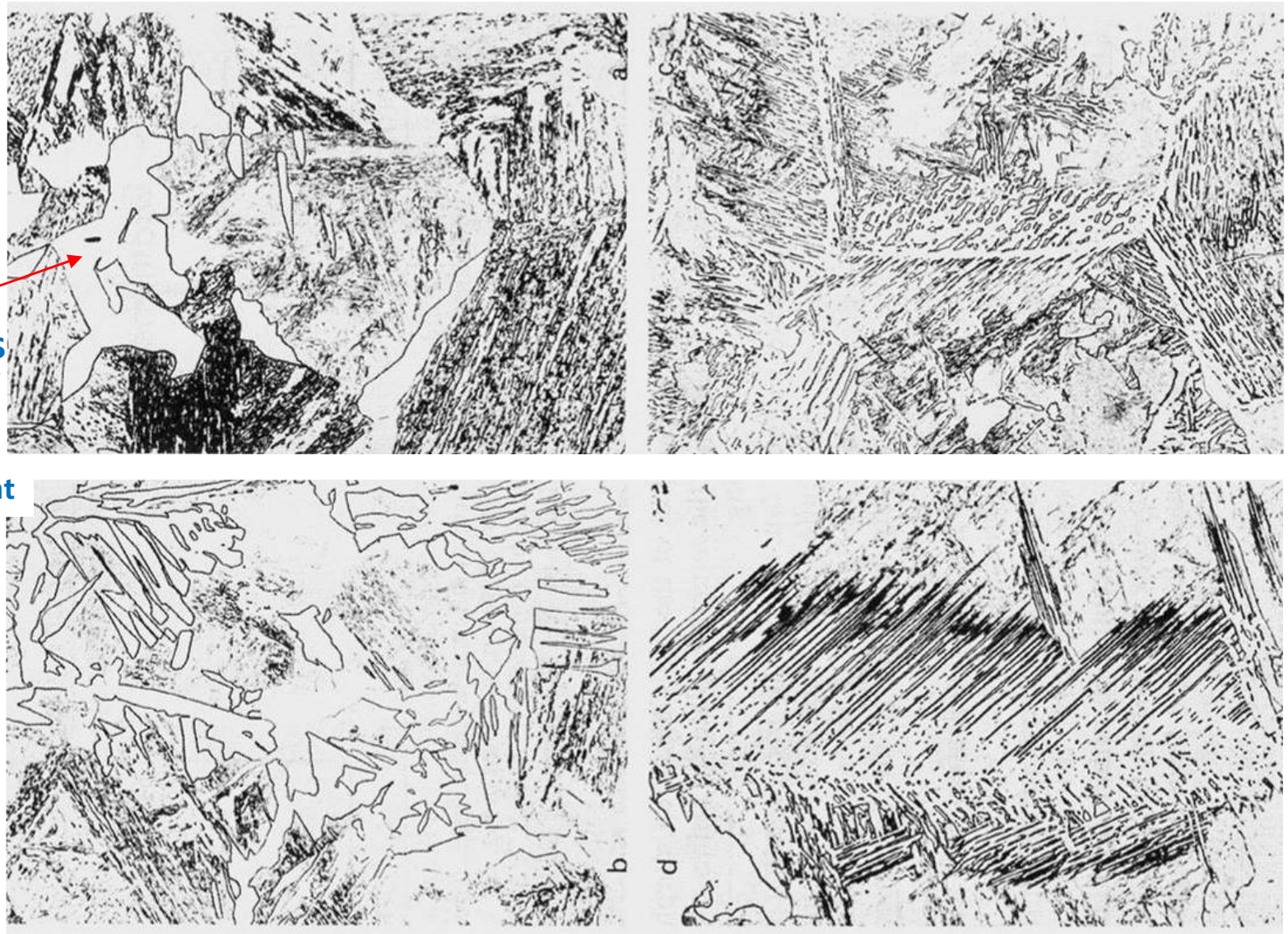

(b)
750°C
for 40 s

(c)
650°C
for 9 s

(d)
550°C
for 2 s

larger ΔT

Widmanstätten ferrite side-plates (b), (c), (d) _ Finer & faceted coherent interface with increasing "undercooling"

* Grain boundary allotriomorph 입계타형

Grain boundary precipitation → **Faster than allowed by volume diffusion**
involves three steps

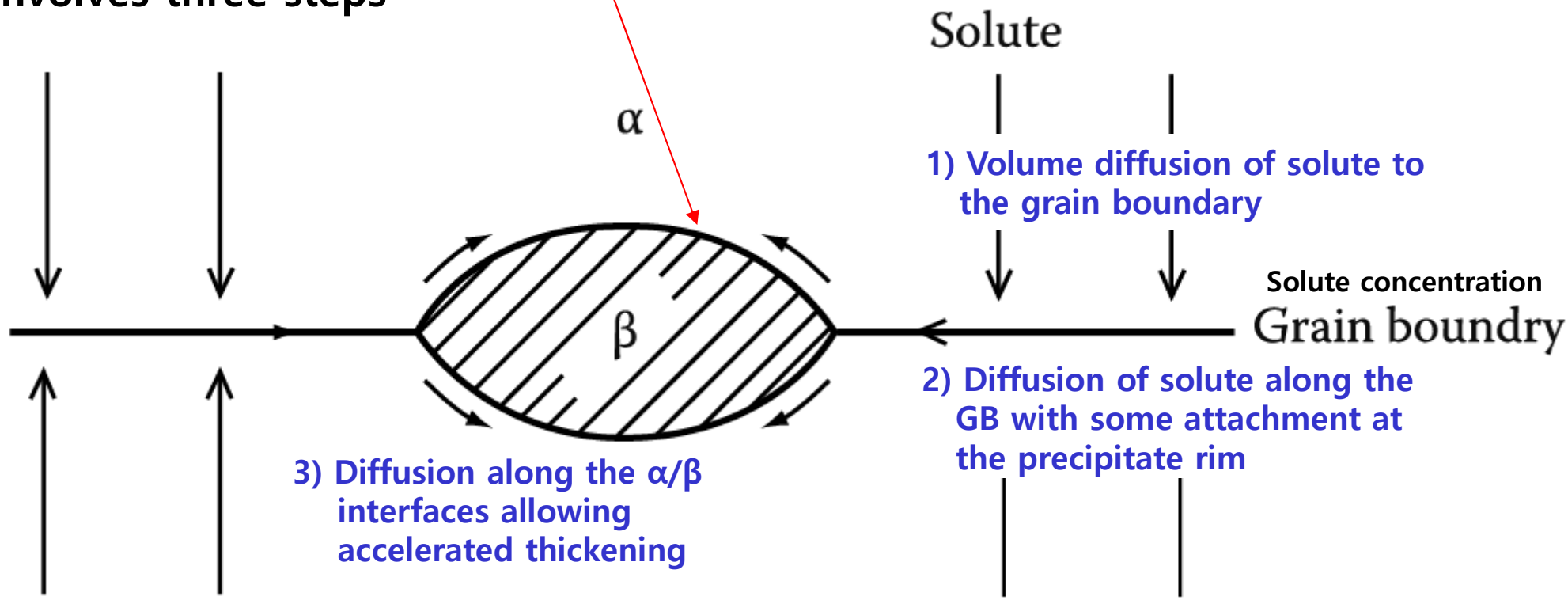

치환형 확산이 일어나는 경우 매우 중요/ 침입형 고용체에서는 체적 확산 속도가 크기 때문에 입계나 전위를 통한 단거리 확산은 상대적으로 중요하지 않음.

Fig. 5.18 Grain-boundary diffusion can lead to rapid lengthening and thickening of grain boundary precipitates, especially by substitutional diffusion.

The reason for the **transition from grain boundary allotriomorphs to Widman -stätten side-plates** with increasing undercooling is not fully understood.

→ possible answer: **Relative Velocity of Incoherent & Semicoherent Interfaces vary with undercooling**

a) At small undercoolings, both semi-coherent and incoherent interfaces ~similar rates

b) At large undercoolings, only incoherent interfaces~full use of increased driving force

(Continuous growth)

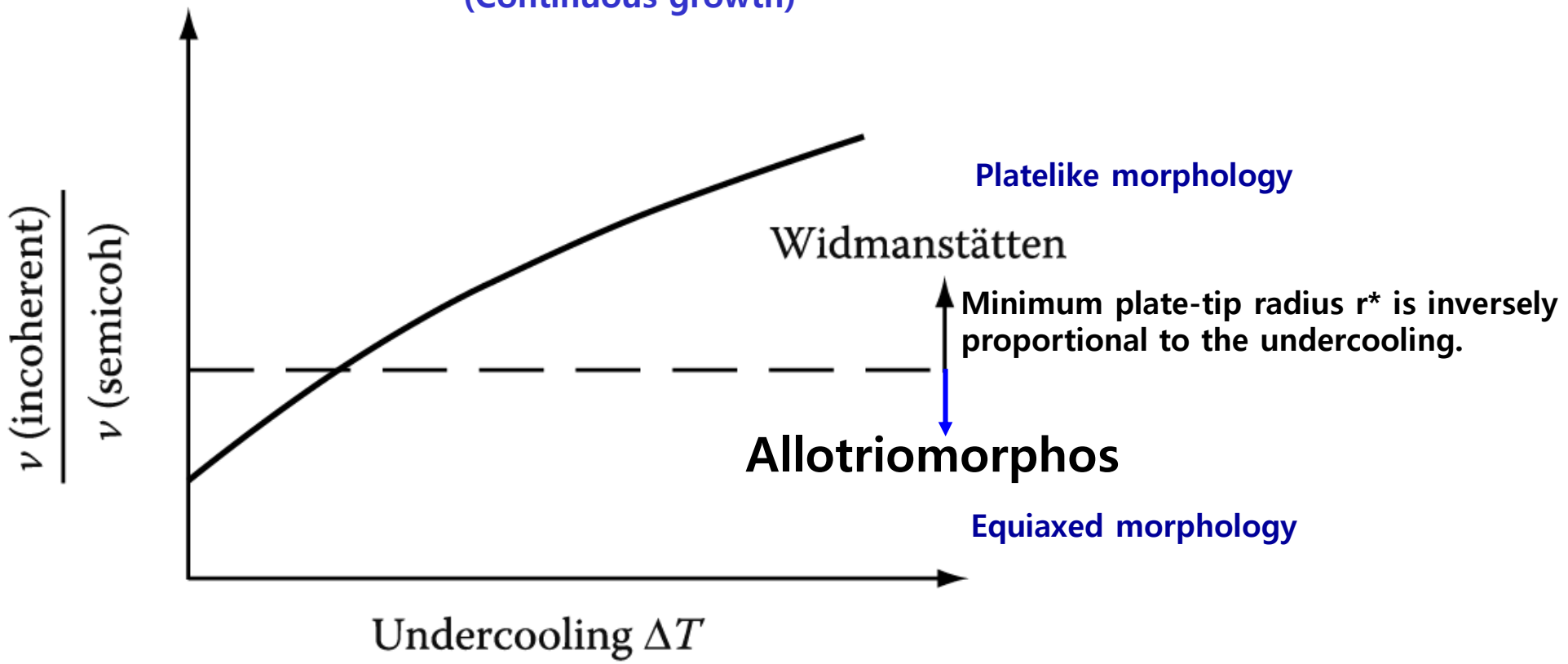

* Intragranular ferrite in large-grained specimen

: ferrite can also precipitate within the austenite grains (Fig. in page 17)
suitable heterogeneous nucleation site~inclusions and dislocations
generally equiaxed at low undercooling ↔ more platelike at higher undercoolings

5.6. The Precipitation of Ferrite from Austenite

Typical TTT curve for $\gamma \rightarrow \alpha$ transformation $\rightarrow f(t,T)$

J-M-A Eq. $f = 1 - \exp(-kt^n)$

$-\frac{\pi}{3} Iv^3$

***k*:** sensitive with T ***f*(*I*, *v*)**

***n*:** 1 ~ 4 **(depend on nucleation mechanism)**

a) Time for a given percentage transformation will decrease as the constant *k* increase

b) *k* increases with increases in ΔT or total # of nucleation sites

→ Thus, decreasing the austenite grain size has the effect of shifting the C curve to shorter transformation times.

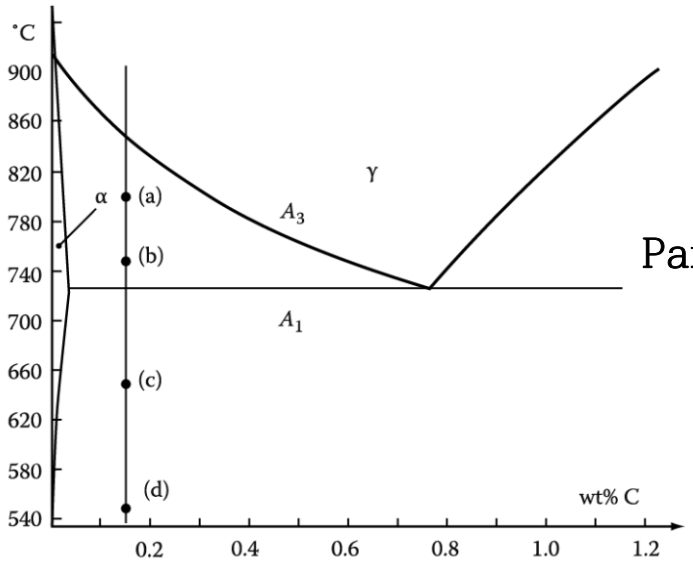

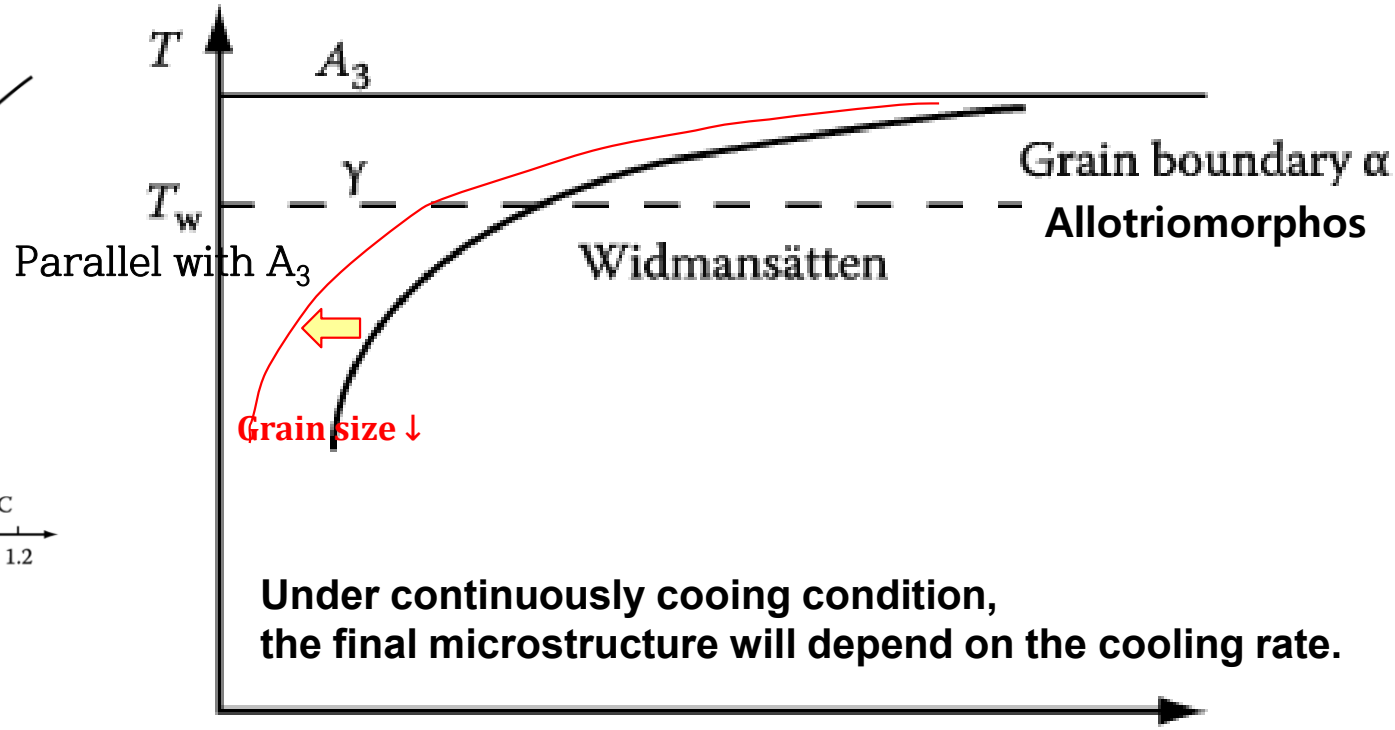

(a)

Figure 5.48 (a) typical TTT curve for $\gamma \rightarrow \alpha$ transformation in a hypoeutectoid steel: a typical C shape.

For alloys of different carbon content, A_3 and T_w vary and show parallel manner each other.

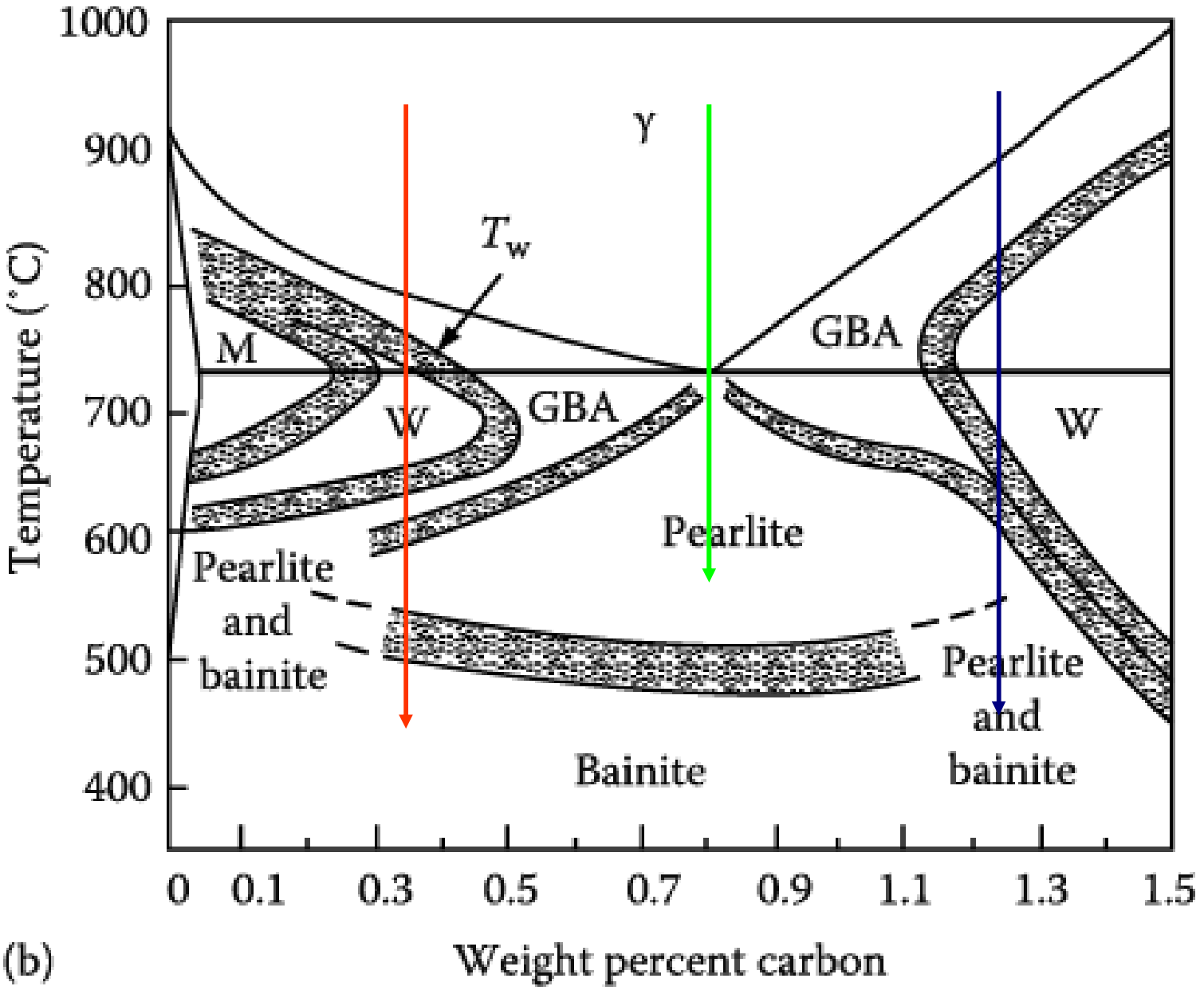

(GBA: GB allotriomorphs, W: Widmanstatten sideplates/intermolecular plates, M: Massive ferrite)

Figure 5.48 (b) Temperature-composition regions in which the various morphologies are dominant at late reaction times in specimens with ASTM grain size Nos. 0-1.

FIG 5.49 Microstructures obtained from different heat treatments in plain carbon steels (×40).
The effect of prior austenite grain size can be seen by comparing (a) and (b), which show a 0.23C–1.2Mn steel (wt.%) air-cooled after austenitizing at 900°C and 1150°C, respectively. The effect of cooling rate for the same grain size can be seen by comparing (c) and (d) from a 0.4C steel: (c) furnace cooled, (d) air cooled.

Effect of prior austenite grain size

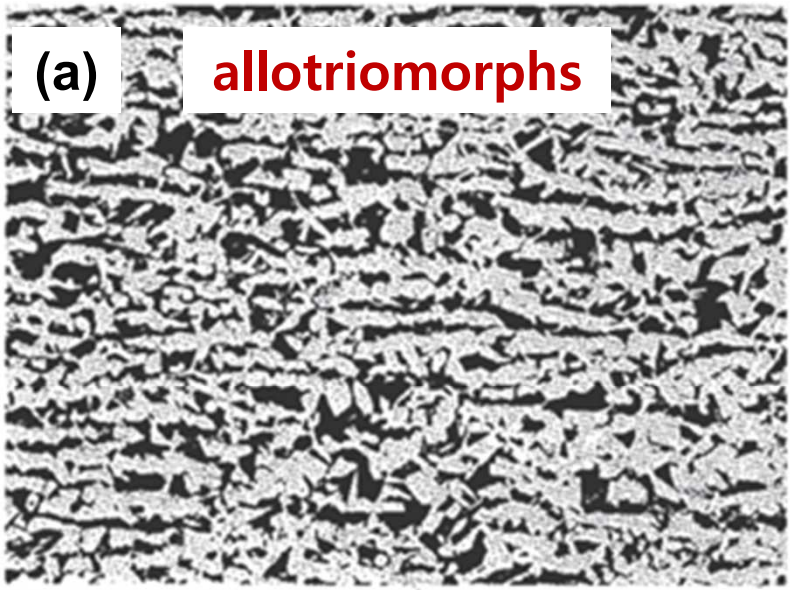

Effect of cooling rate for the same grain size

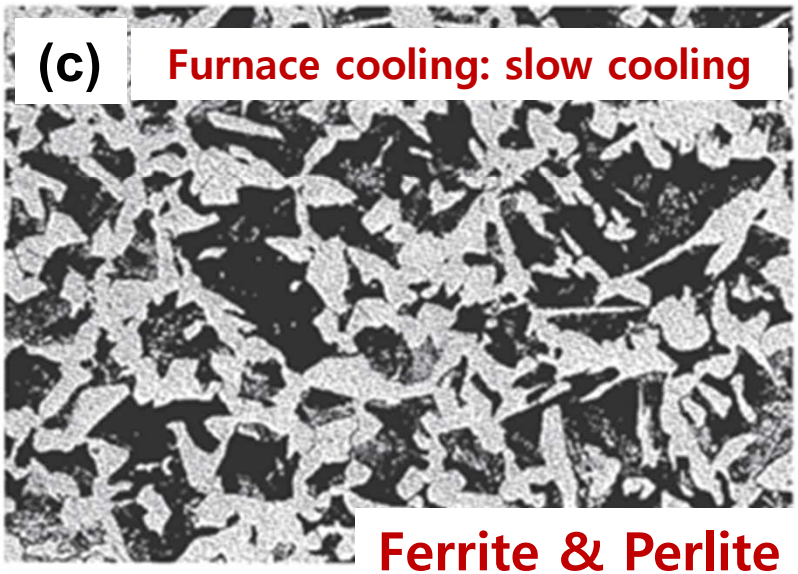

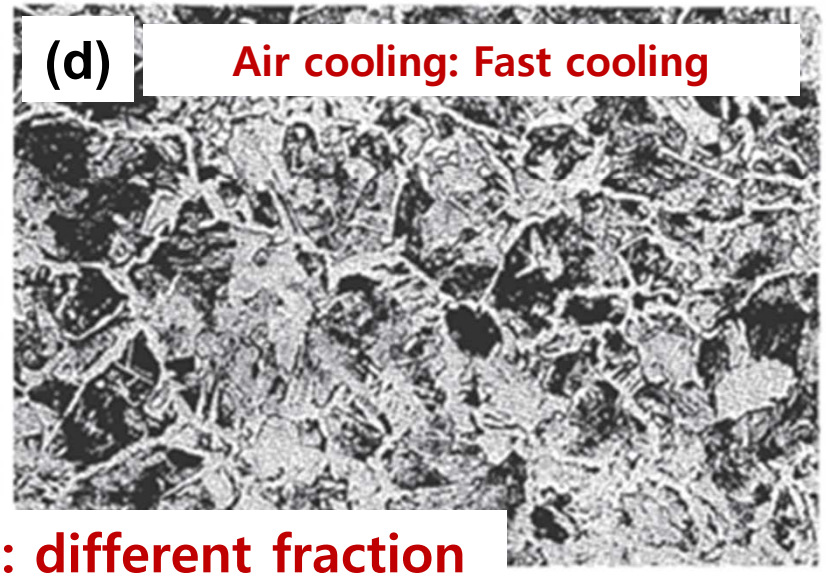

Ferrite & Perlite : different fraction

5.7 Cellular Precipitation

- 입계 석출의 다른 형태
- 형태적으로는 공석변태와 유사

$$\alpha' \rightarrow \alpha + \beta$$

- 불연속 석출 (석출물 조대화로 연속 석출대비 기계적 성질 저하)

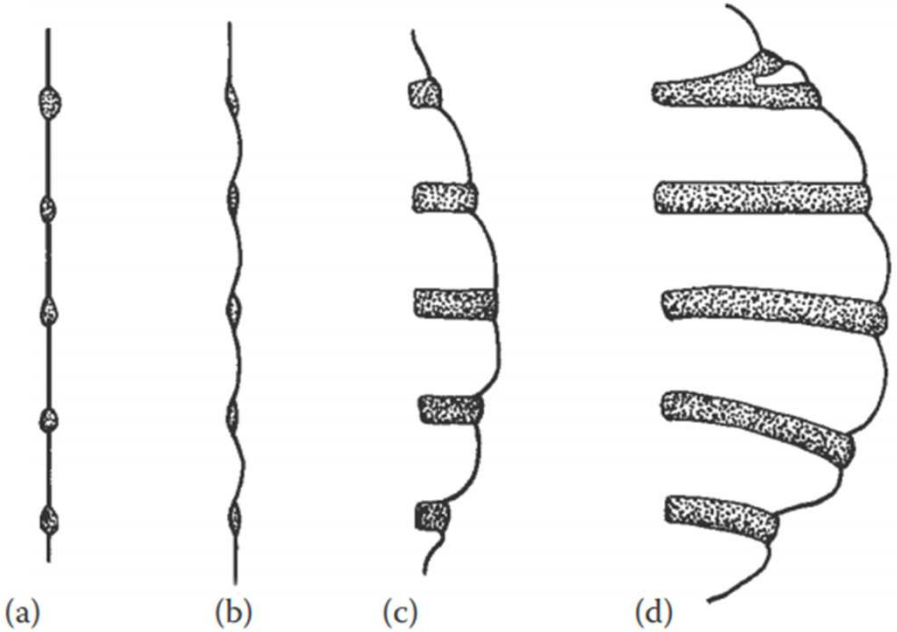

FIGURE 5.51 A schematic diagram showing a possible sequence of steps during the development of cellular precipitation.

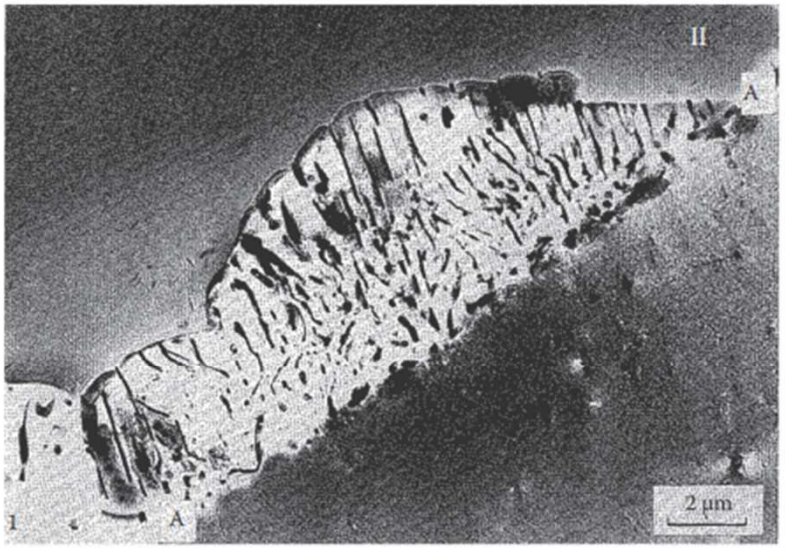

(a)

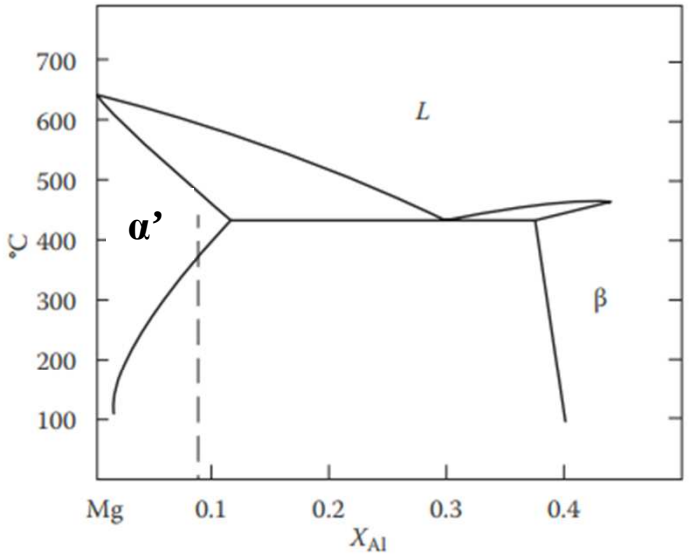

(b)

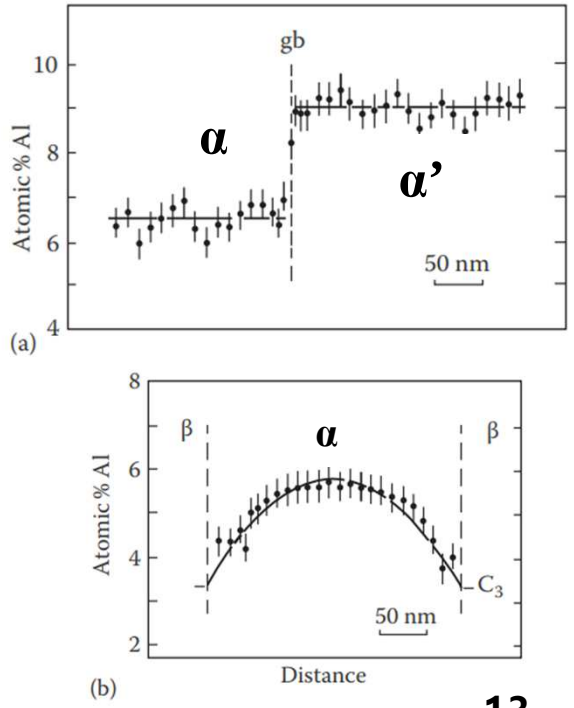

FIGURE 5.52 (a) Cellular precipitation of $Mg_{17}Al_{12}$ in an Mg–9 at.% Al alloy solution treated and aged 1 h at 220°C followed by 2 min at 310°C. Some general $Mg_{17}Al_{12}$ precipitation has also occurred on dislocations within the grains. (b) The relevant part of the Mg–Al phase diagram.

5. Diffusion Transformations in solid

: diffusional nucleation & growth

(a) Precipitation

$$\alpha' \rightarrow \alpha + \beta$$

Metastable supersaturated
Solid solution

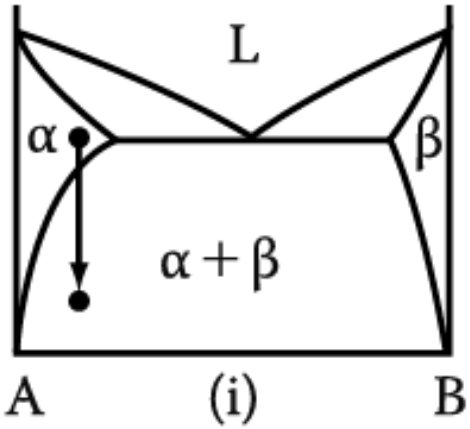

Homogeneous Nucleation

$$\Delta G = -V\Delta G_V + A\gamma + V\Delta G_S$$

Heterogeneous Nucleation

$$\Delta G_{het} = -V(\Delta G_V - \Delta G_S) + A\gamma - \Delta G_d$$

$$N_{\text{hom}} = \omega C_0 \exp\left(-\frac{\Delta G_m}{kT}\right) \exp\left(-\frac{\Delta G^*}{kT}\right)$$

➡ suitable nucleation sites ~ nonequilibrium defects
(creation of nucleus~destruction of a defect($-\Delta G_d$))

(b) Eutectoid Transformation

Composition of product phases differs from that of a parent phase.

→ **long-range diffusion**

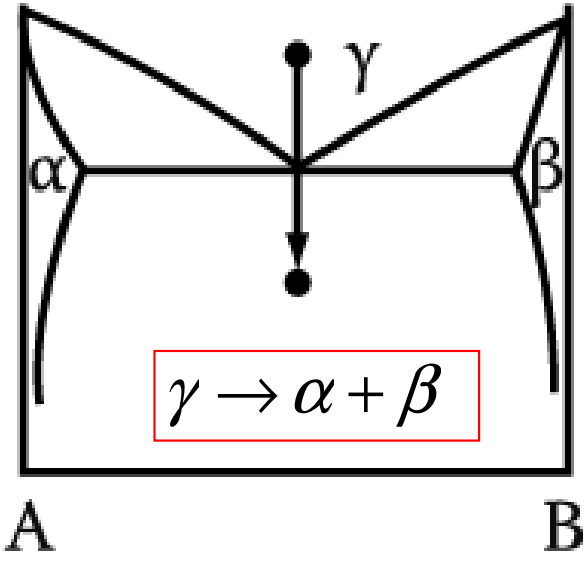

5.8. Eutectoid Transformations

5.8.1 Pearlite in Fe-C Alloys

$$\gamma \rightarrow \alpha + Fe_3C$$

Very similar to a eutectic transformation

Pearlite nodule nucleate on GBs and grow with a roughly constant radial velocity into the surrounding austenite grains.

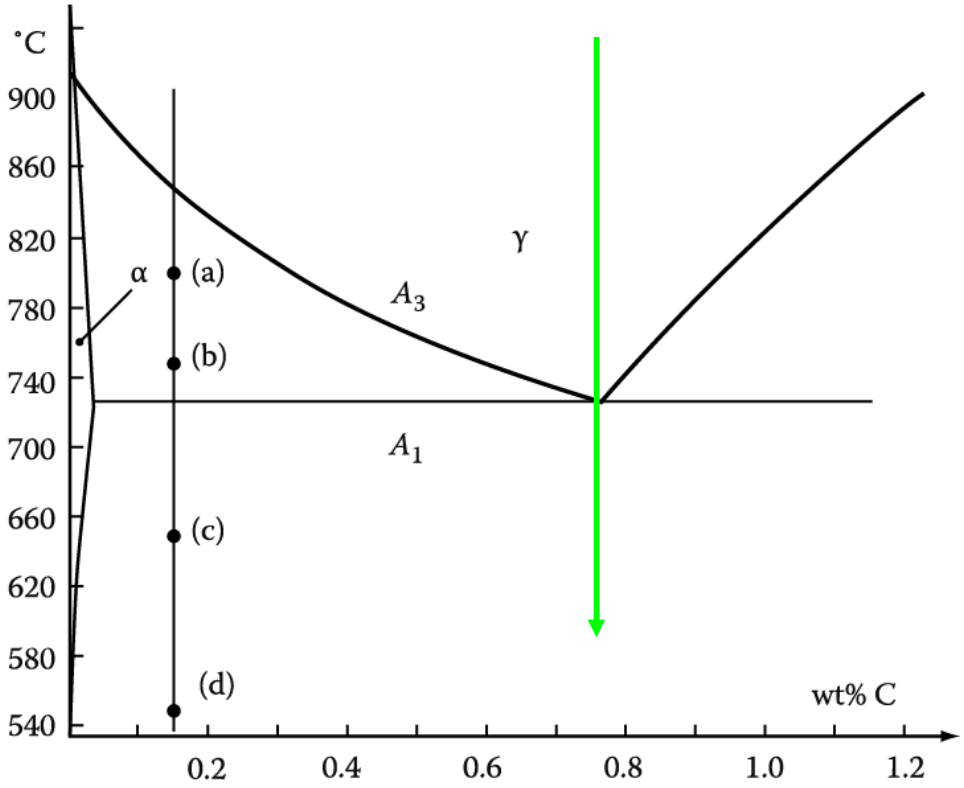

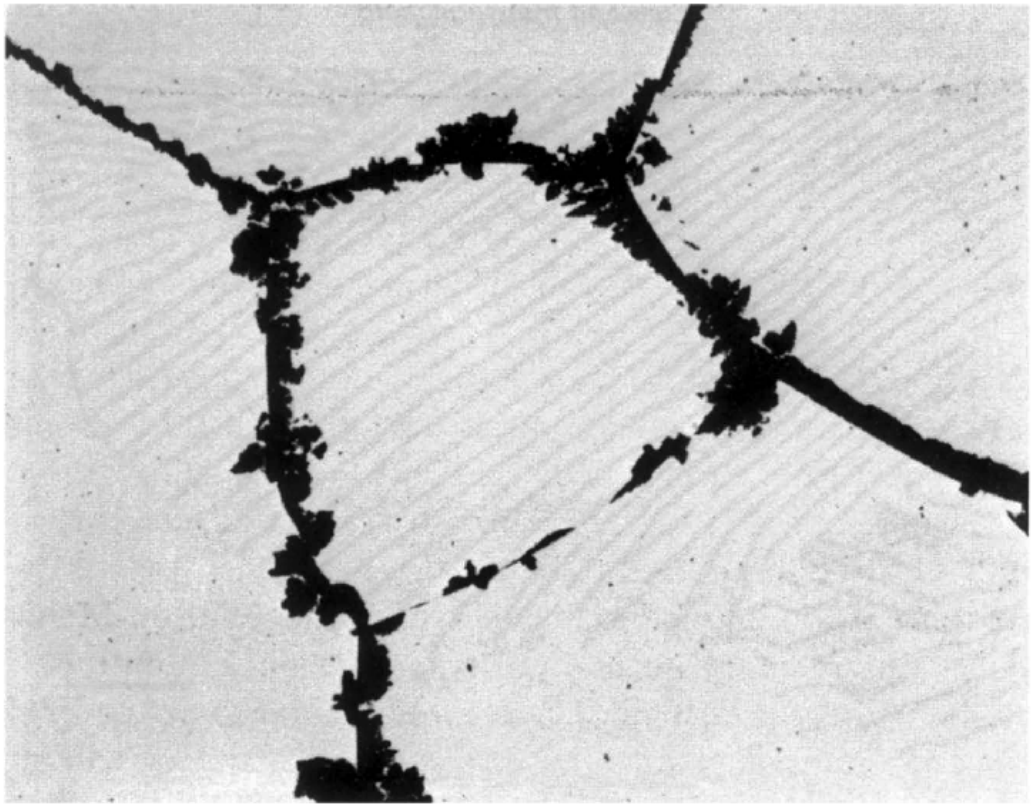

* At large undercooling,

: the nucleation rate is much higher and site saturation occurs, that is all GBs become quickly covered with nodules which grow together forming layers of perlite, Figure 5.61.

* At small undercooling below A_1,

: the number of pearlite nodules that nucleate is relatively small, and the nodules can grow as hemispheres or spheres without interfering with each other.

Pearlite in Fe-C Alloys: nucleation and growth

Nucleation: depend on GB structures and composition

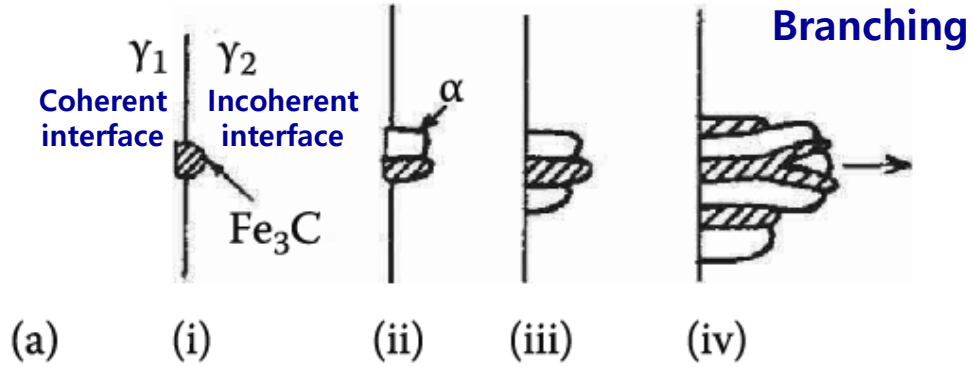

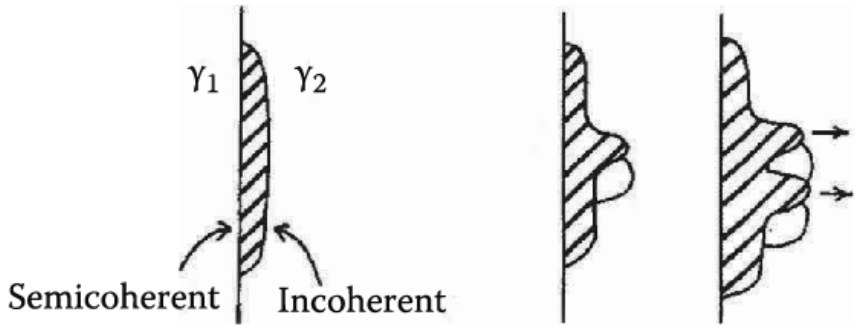

Peralite will nucleate and grow on the incoherent side

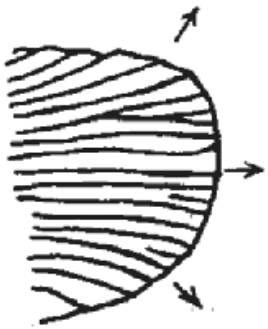

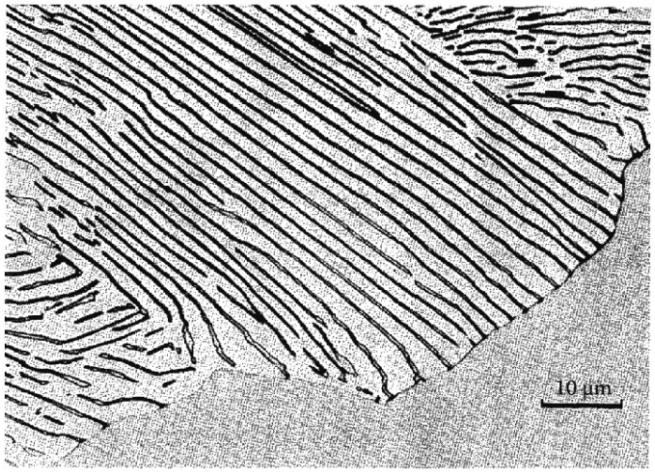

(c) A perlite colony at a later stage of growth

(a) On a "clean" GB.

(i) **Cementite nucleates on GB with coherent interface and orientation relationship with γ_1 and incoherent interface with γ_2.**

(ii) **α nucleates adjacent to cementite also with a coherent interface and orientation relationship with γ_1. (This also produces an orientation relationship between the cementite and the ferrite).**

(iii) **The nucleation process repeats side ways, while incoherent interfaces grow into γ_2.**

(iv) **New plates can also form by a branching mechanism.**

(b) When a proeutectoid phase (cementite or ferrite) already exists on that boundary, pearlite will nucleate and grow on the incoherent side. A different orientation relationship between the cementite and the ferrite results in this case.

(c) Pearlite colony at a latest stage of growth.

Pearlite grows into the austenite grain with which it does not have an orientation relationship.

Growth of Pearlite: analogous to the growth of a lamellar eutectic

Min. possible: (S*) $\propto 1/\Delta T$ / Growth rate : mainly lattice diffusion $v = kD_c^{\gamma}(\Delta T)^2$

Interlamellar spacing of pearlite colonies mainly boundary diffusion $v = kD_b(\Delta T)^3$

Relative Positions of the Transformation curves for Pearlite and Bainite in Plain Carbon Eutectoid Steels.

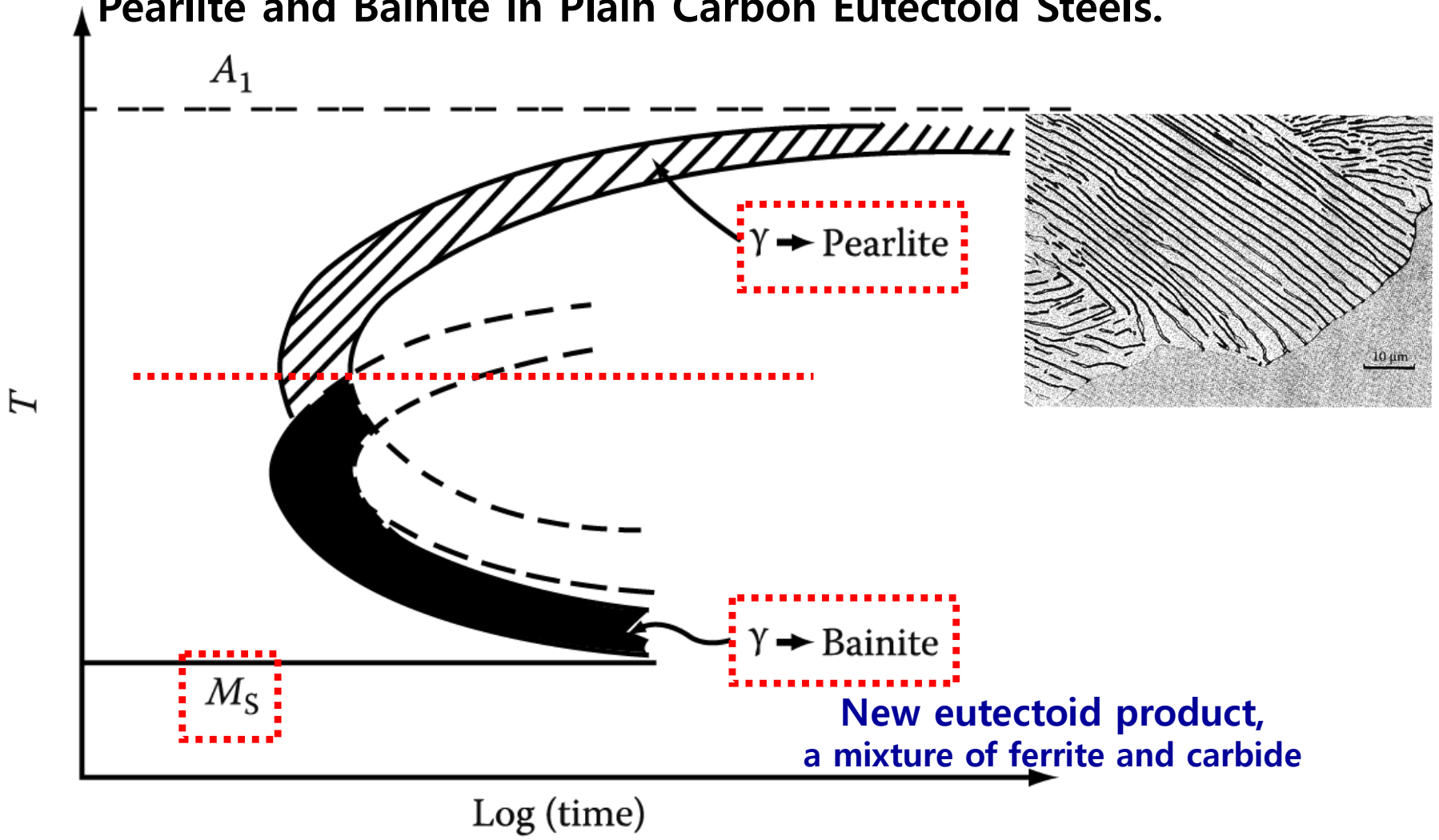

Figure 5.64 Schematic diagram showing relative positions of the transformation curves for pearlite and bainite in plain carbon eutectoid steel.

5.8.1.3 Pearlite in off-eutectoid Fe-C Alloys

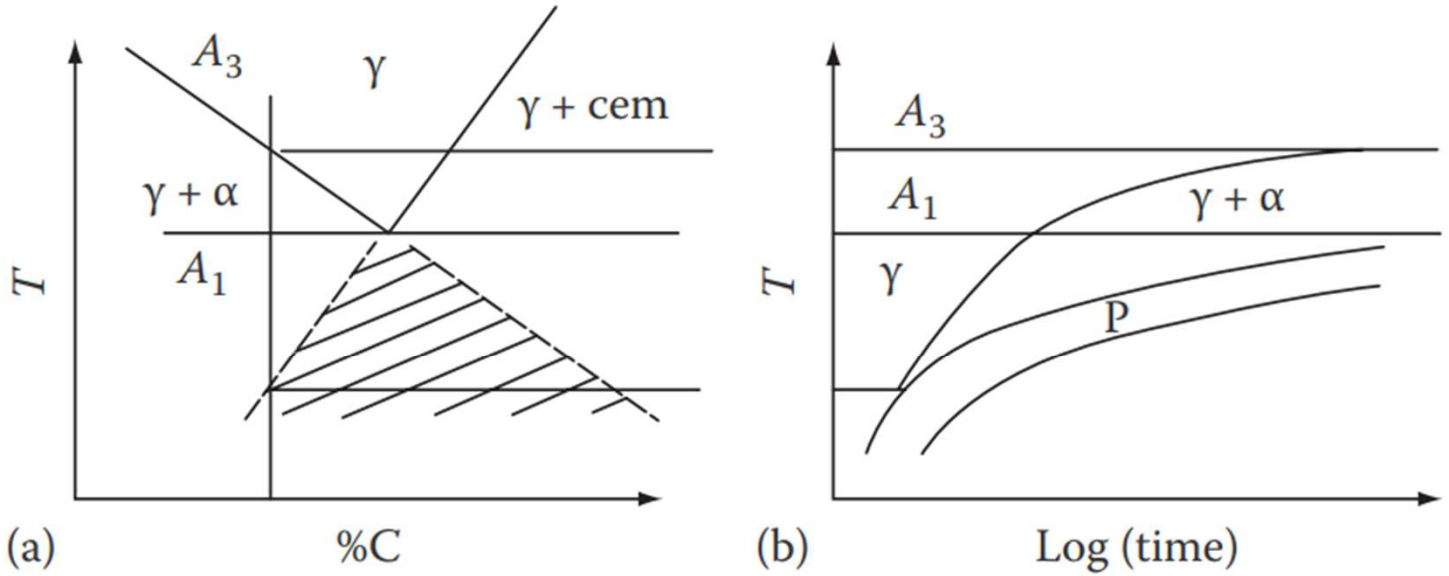

FIGURE 5.61 Effect of transformation temperature on the volume fraction of proeutectoid ferrite.

5.8.2 Bainite Transformation

The microstructure of bainite depends mainly on the temperature at which it forms.

Upper Banite in medium-carbon steel

At high temp. 350 ~ 550°C, ferrite laths, K-S relationship, similar to Widmanstäten plates

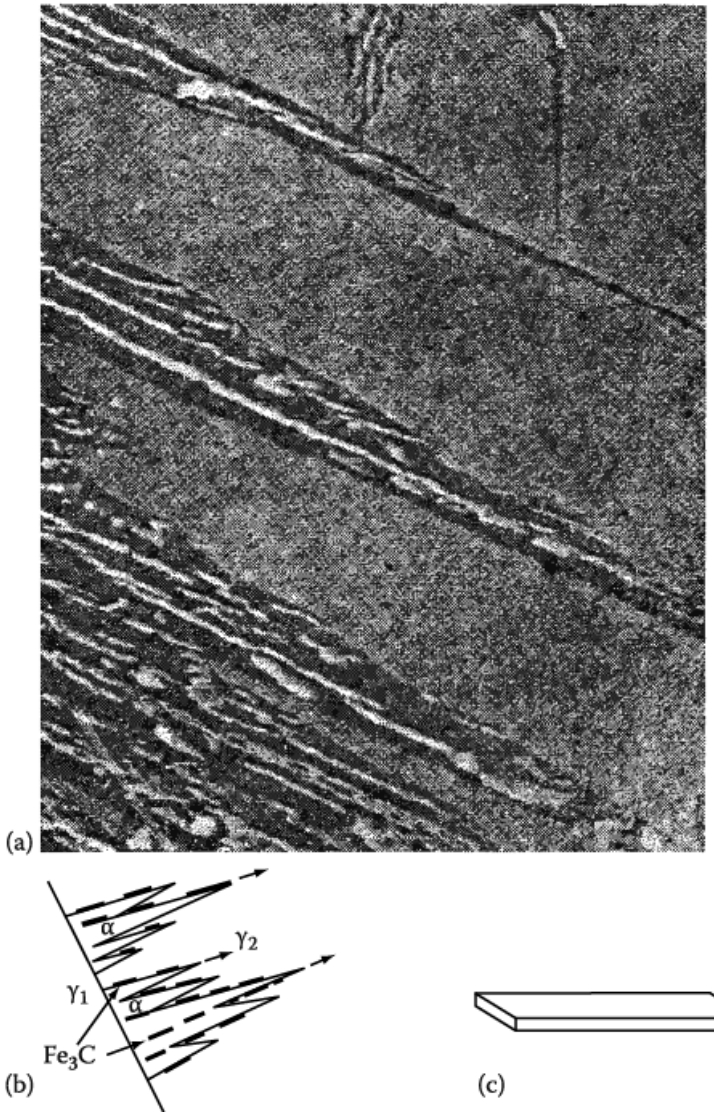

(b) Schematic of growth mechanism. Widmanstatten ferrite laths growth into γ_2. Cementite plates nucleate in carbon-enriched austenite.

Lower Bainite in 0.69wt% C low-alloy steel

At sufficiently low temp. laths → plates
Carbide dispersion becomes much finer, rather like in tempered M.

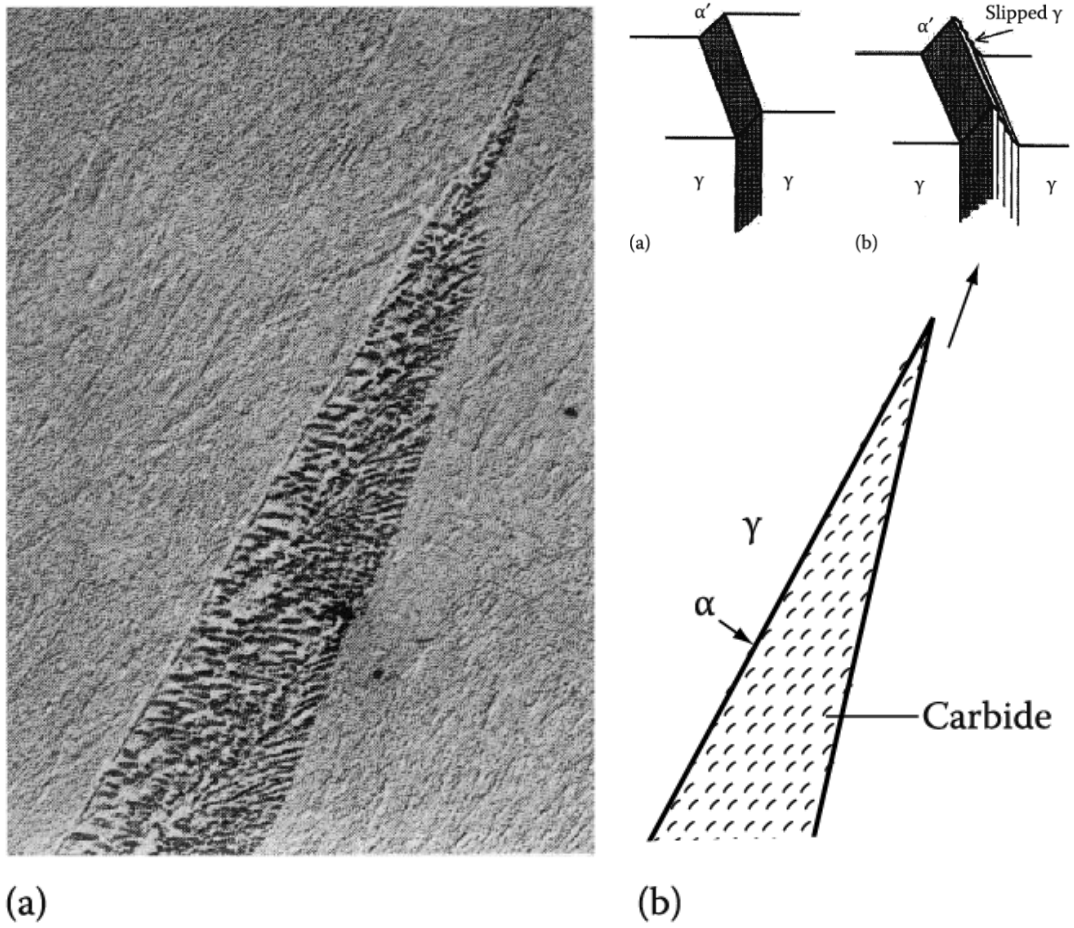

Surface tilts by bainite trans. like M trans.
Due to Shear mechanism/ordered military manner

(b) A possible growth mechanism. α/γ interface advances as fast as carbides precipitate at interface thereby removing the excess carbon in front of the α.

At the highest temp. where pearlite and bainite grow competitively.

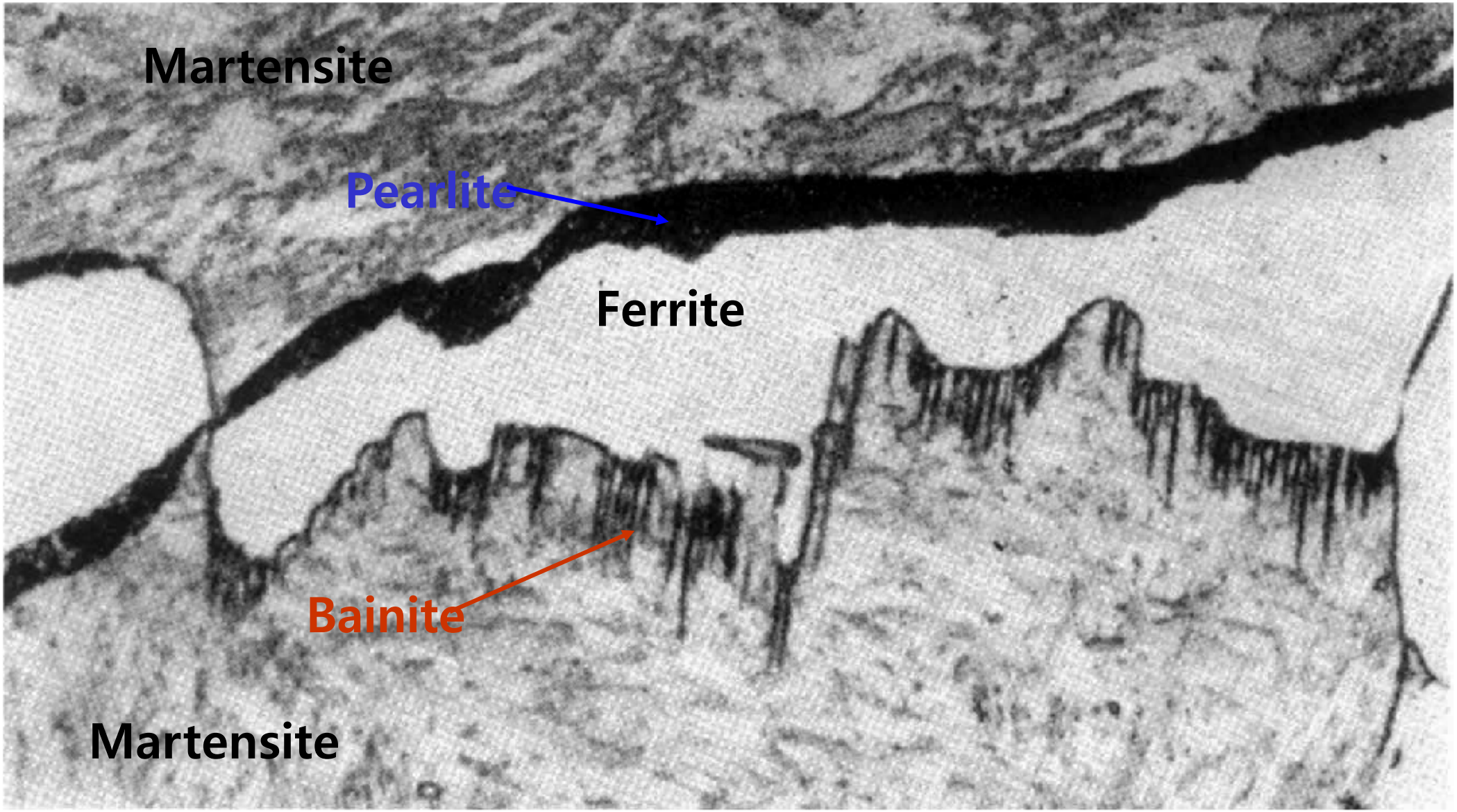

Fig. 5.67 Hypoeutectoid steel (0.6% C) partially transformed for 30 min at 710 ℃. Inefficiently quenched. Bainitic growth into lower grain of austenite and pearlitic growth into upper grain during quench (x1800).

Pearlite : no specific orientation relationship

Bainite : orientation relationship

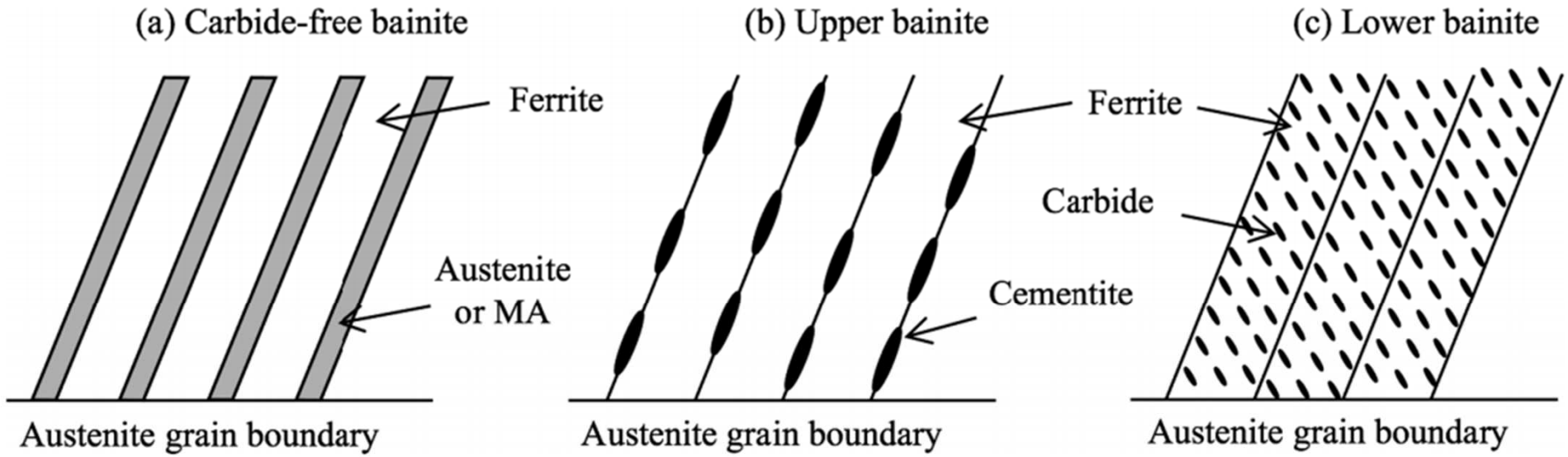

FIGURE 5.63 Idealized morphologies of single bainite packets or sheaves as seen in cross-sections through the ferrite plates or laths. (a) Carbide-free bainite. (b) and (c) Upper and lower bainite morphologies according to Hehemann.[30] MA = mixture of martensite and austenite.

5.8.2.1 Ferrite Growth in Upper Bainite

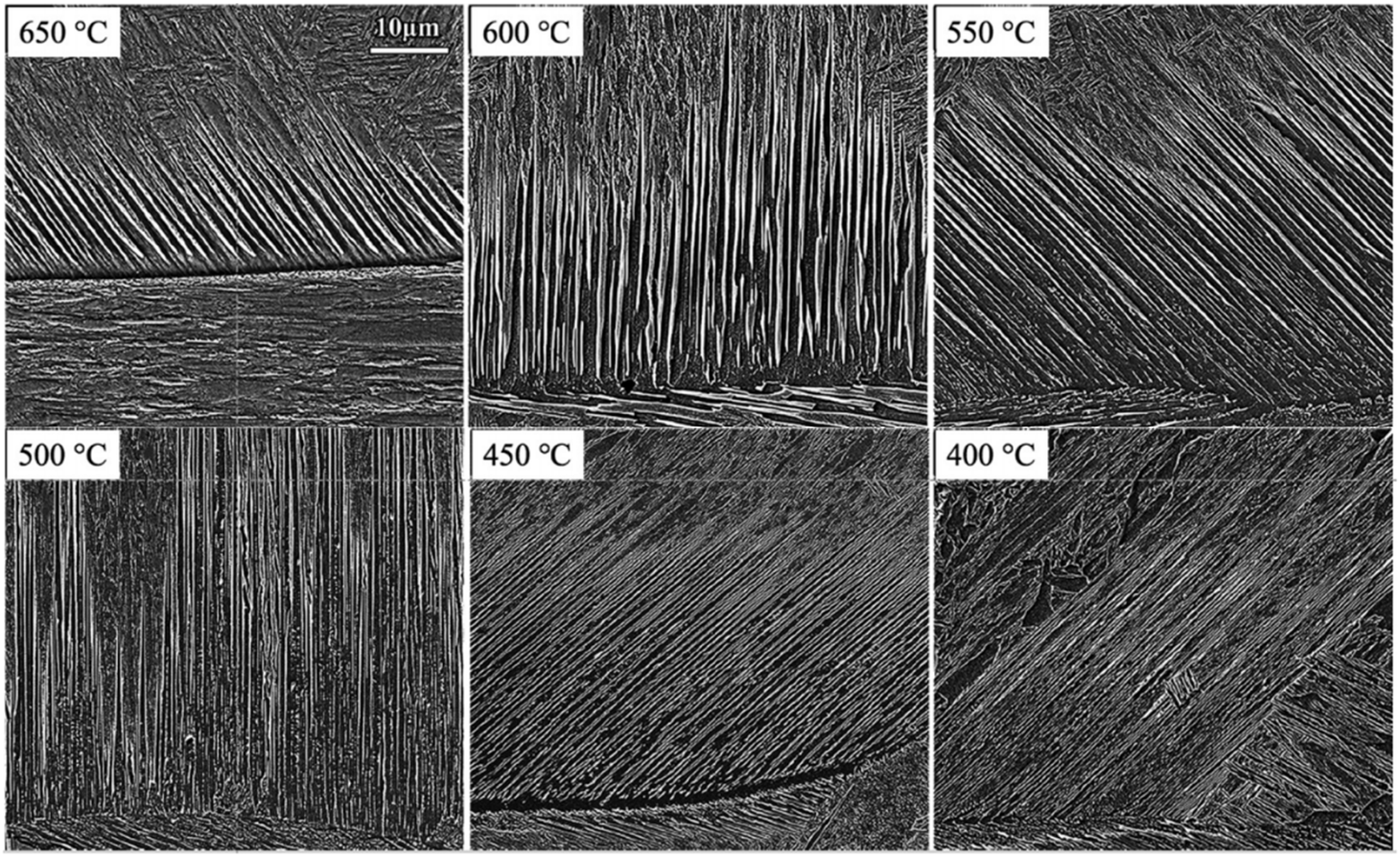

FIGURE 5.64 Side-plates of ferrite that constitute Widmanstätten ferrite and upper bainite at an early stage of growth in an Fe–0.28C–0.52Si alloy (wt.%). Isothermal transformation tem- peratures given. Untransformed austenite appears as martensite formed during final quenching. Specimen sectioning is such that the plates can be seen to extend uninterruptedly from the nucle- ating grain boundaries to the growing tips. Scanning electron microscope images of etched speci- mens. (Reprinted from J. Yin, M. Hillert and A. Borgenstam, Morphology of proeutectoid ferrite, Metallurgical and Materials Transactions, 48A:1425–1443 (2017). Open access under the terms of the Creative Commons CC BY license.)

5.8.2.2 Carbide Morphology in Upper Bainite

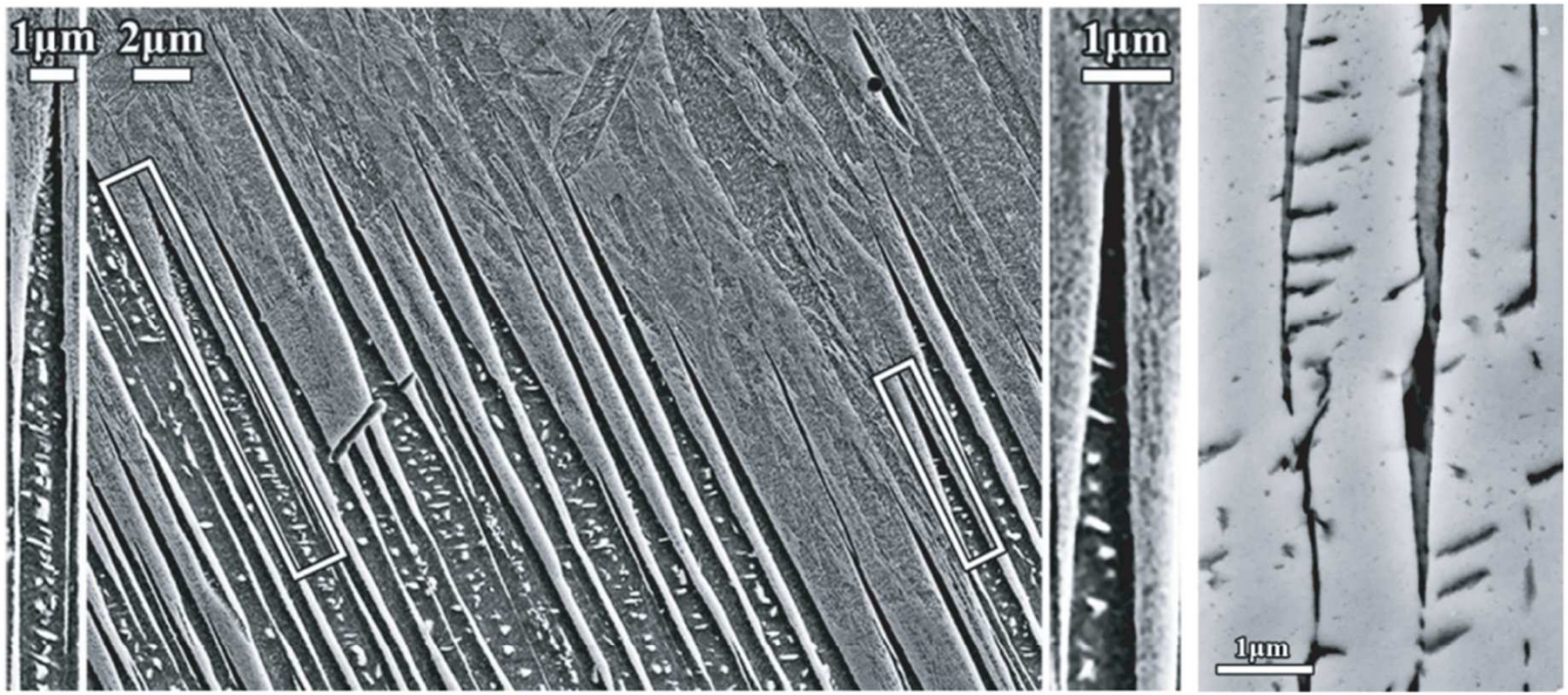

(a) (b)

FIGURE 5.67 (a) Growth front of upper bainite in an Fe–0.27C–0.45Mn (wt.%) alloy after austenitizing at 1,200°C, cooling rapidly to 500°C, holding 2 s and quenching so that austenite remaining at 500°C transforms to martensite. High magnification insert on the right shows a cementite-free lath of ferrite covered by an $\alpha + Fe_3C$ eutectoid layer. Detail on the left shows two cementite-free plates of ferrite separated by a eutectoid layer. Scanning electron microscope image in which cementite and untransformed, carbon-rich austenite appears light and ferrite laths dark. (b) Detail of cementite and interlath austenite in Fe–0.26C–0.51Si–0.48Mn after 6 s at 500°C before final quench. Scanning electron microscope image in which cementite and untransformed, carbon-rich austenite appears dark and ferrite laths appear light. (Reprinted from J. Yin, M. Hillert and A. Borgenstam, *Metallurgical and Materials Transactions*, **48A**:1444–1458 (2017). Open access under the terms of the Creative Commons CC BY license.)

5.8.2.3 Lower Bainite

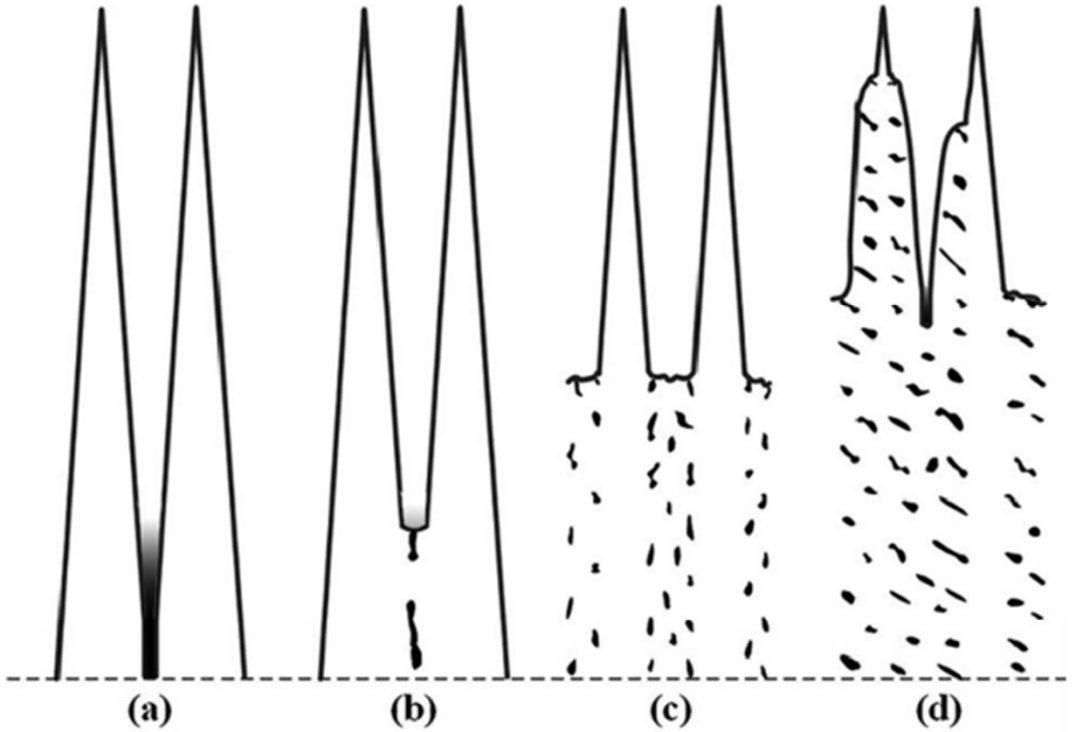

FIGURE 5.68 Schematic illustration of eutectoid transformation of interlath austenite. The vertical scale is greatly compressed. Austenite shading indicates degree of carbon enrichment. (a) No cementite is available and thickening of ferrite laths can continue leading to films of austenite rich in carbon. (b) Late formation of cementite producing cementite aligned along the lath boundaries. (c) The eutectoid reaction is able to transform austenite of a lower carbon content, and there is space for more cooperative growth. (d) Early cementite formation leading to thicker eutectoid layers on the laths. (Reprinted from J. Yin, M. Hillert and A. Borgenstam, *Metallurgical and Materials Transactions*, **48A**:1444–1458 (2017). Open access under the terms of the Creative Commons CC BY license.)

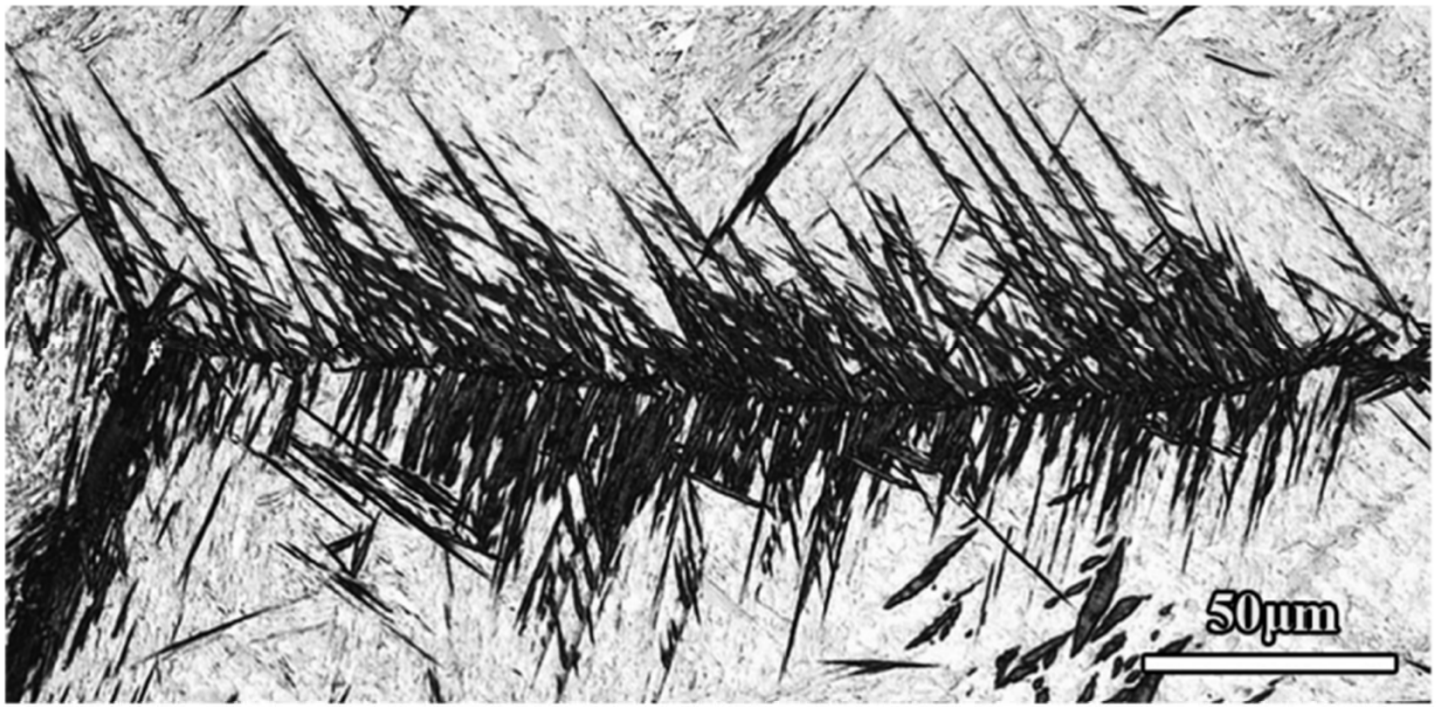

FIGURE 5.69 Low-magnification light optical micrograph of lower bainite sheaves nucleated on a grain boundary and within the grains in an Fe–0.7C (wt.%) alloy after austenitizing at 1,100°C, cooling rapidly to 300°C, holding 60 s and quenching so that austenite remaining at 300°C transforms to martensite (light contrast). (J. Yin, M. Hillert and A. Borgenstam, *Metallurgical and Materials Transactions*, **48A**:4006–4024 (2017). Open access under the terms of the Creative Commons CC BY license.)

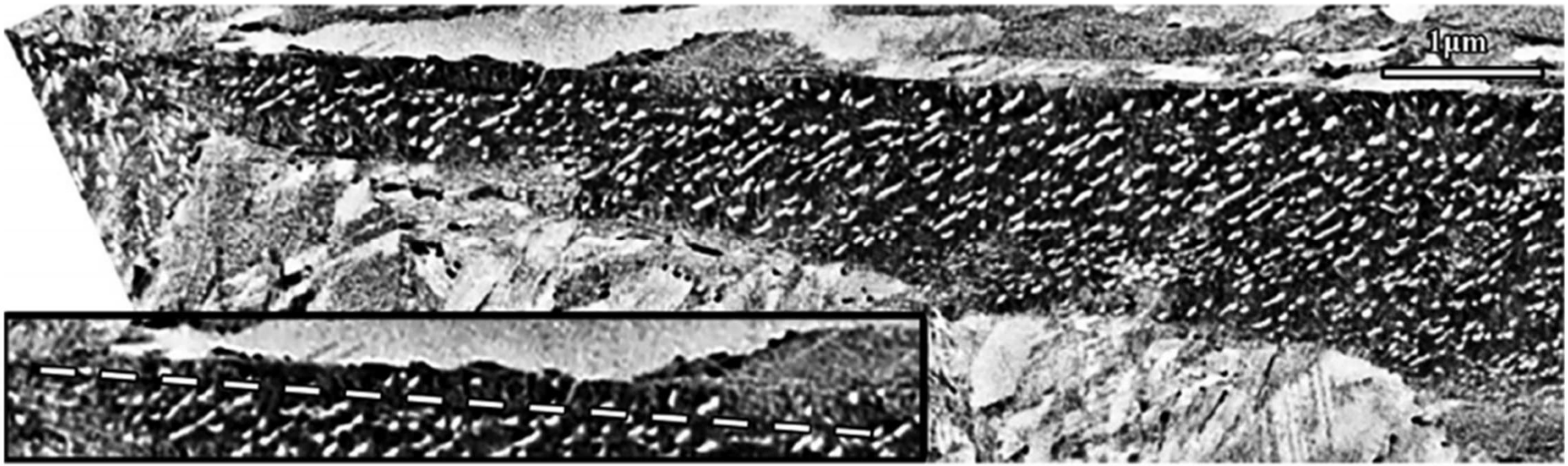

FIGURE 5.70 Same alloy as in the previous figure but held 50 s at 350°C. Scanning electron microscope image of a packet of bainitic ferrite plates containing inclined carbide platelets. Note the small size of the carbides. Bainitic ferrite dark, carbides light, martensite formed during final quench grey. Separate ferrite plates are hard to resolve. One is identified in the inset. (From J. Yin, M. Hillert and A. Borgenstam, *Metallurgical and Materials Transactions*, **48A**:4006–4024 (2017). Open access under the terms of the Creative Commons CC BY license.)

5.8.2.4 Transformation Shear and Stored Energy

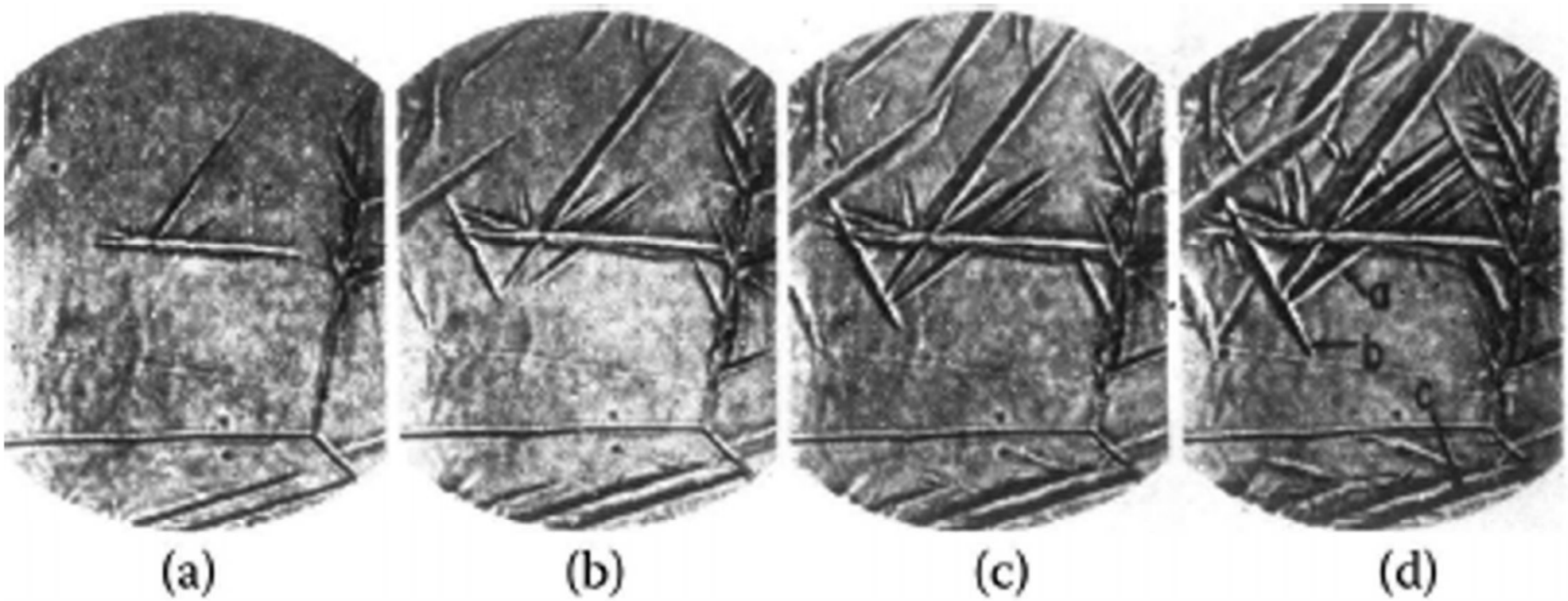

FIGURE 5.71 Photos taken with a hot-state microscope showing the nucleation and growth of bainite plates at 350°C. The contrast is due to surface relief. (a) 14.75 min, (b) 16.2 min, (c) 17.25 min, and (d) 19.2 min. (After Speich, G.R., in *Decomposition of Austenite by Diffusional Processes*, Interscience, New York, 1962.)

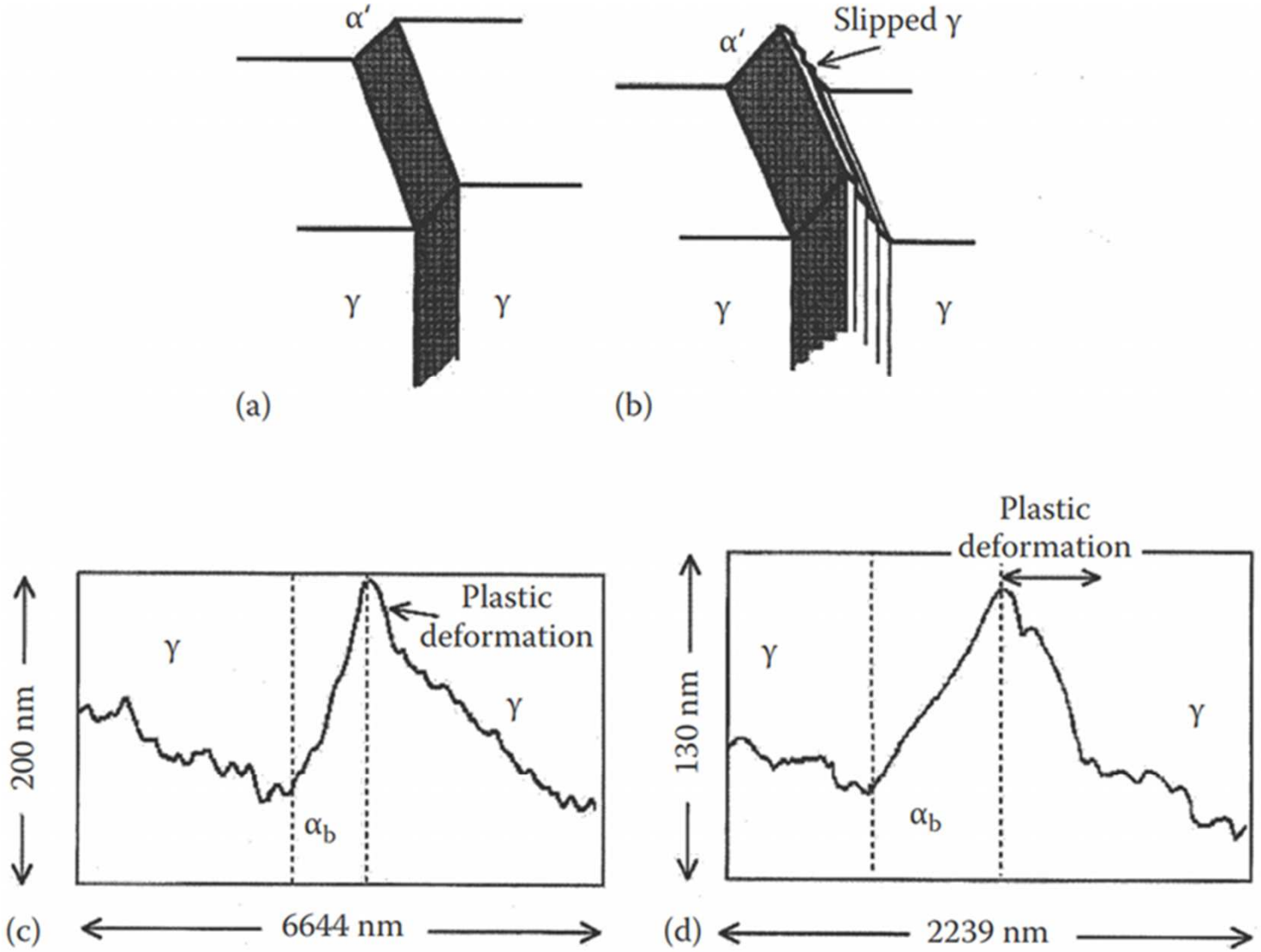

FIGURE 5.72 (a) Surface relief caused by an invariant plane strain without constraint. (b) Plastic relaxation in the adjacent matrix. (After Bhadeshia, H.K.D.H., in *Bainite in Steels*, 2nd edn., IOM Communications Ltd., London, 2001.) (c) and (d) are AFM scans across surface relief caused by a bainite subunit. (Originally appeared in Swallow, E. and Bhadeshia, H.K.D.H., *Mater. Sci. Tech. Lond.*, 12, 121, 1996.)

5.8.3 The effect of alloying elements on hardenability

: adding alloying elements to steels → delay to time required for the decomposition into ferrite and pearlite → M trans under slower cooling rate → increase hardenability

* Main factor limiting hardenability is the rate of formation of pearlite at the nose of the C curve in the TTT diagram.

- Austenite stabilizer (Mn, Cu, Ni) – depress A3 temperature
- Ferrite stabilizer (Cr, Mo, Si) – increase A3 temperature

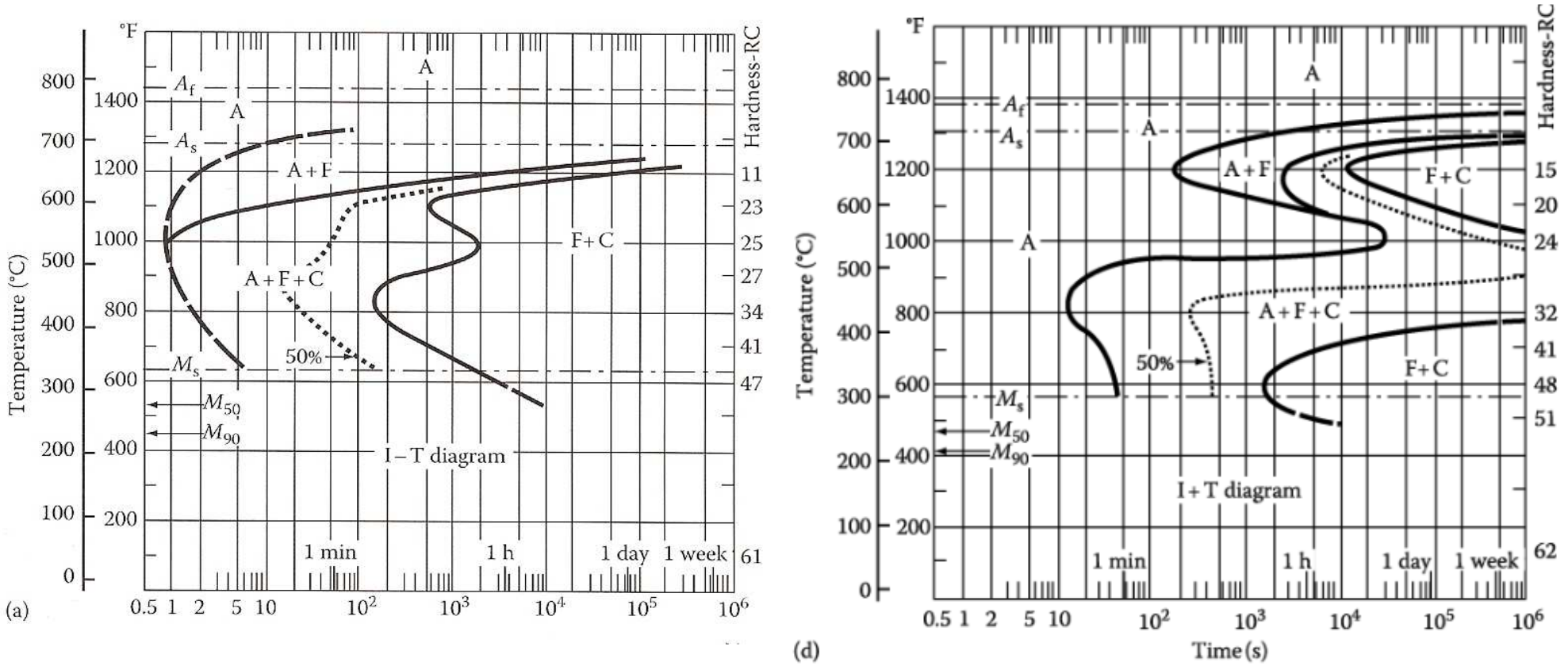

Figure 5.73 TTT diagrams for two commercial low-alloy steels all of which (a) contain roughly 0.4% C and 1% Mn and (b) contains 0.8% Cr, 0.3% Mo, and 1.8% Ni

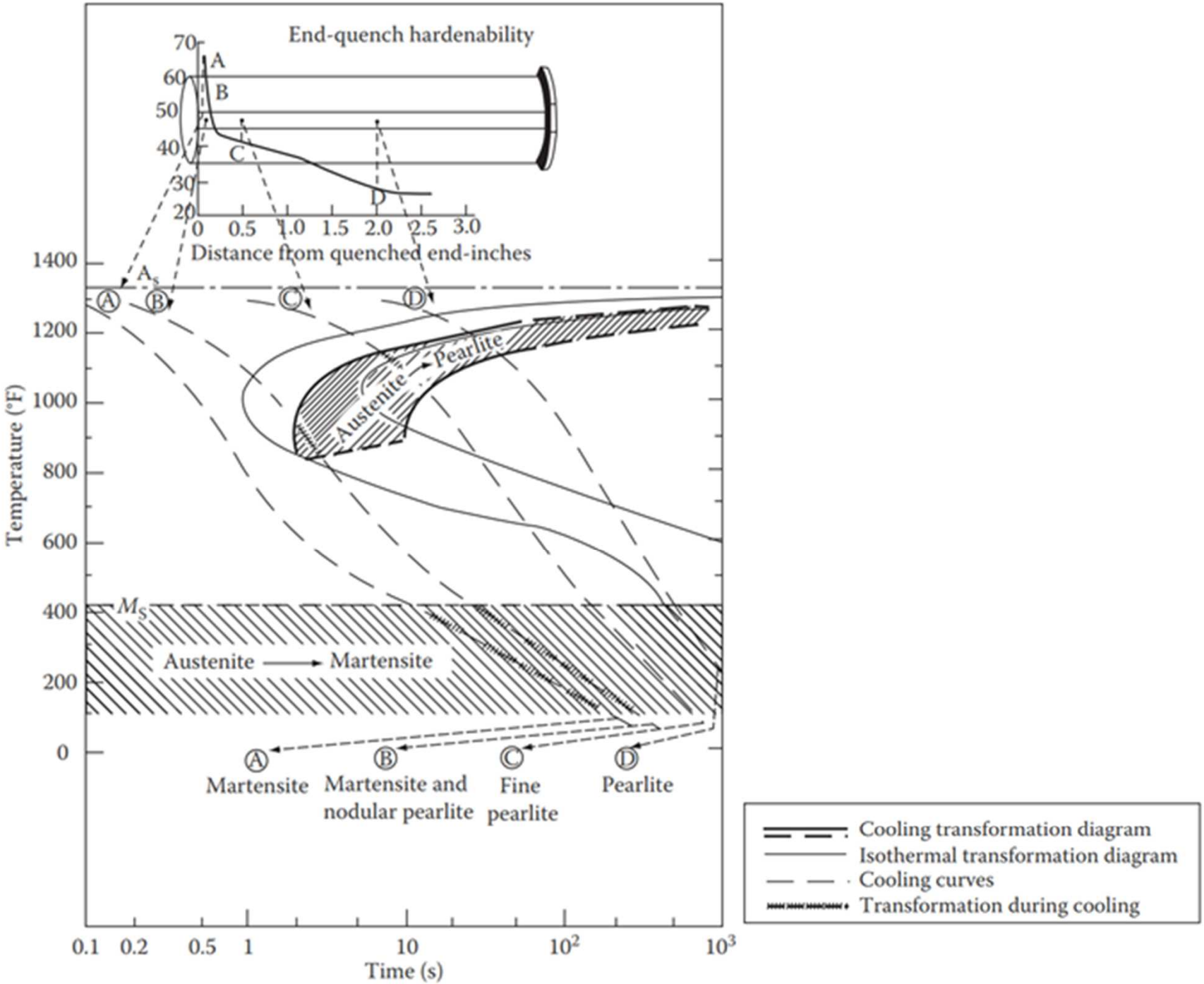

FIGURE 5.77 Correlation of continuous cooling and isothermal transformations with end-quench hardenability test data for eutectoid carbon steel. (*Atlas of Isothermal Transformation and Cooling Transformation Diagrams*, American Society for Metals, 1977, p. 376.)

5.8.5 Fibrous and Interphase precipitation in alloy steels

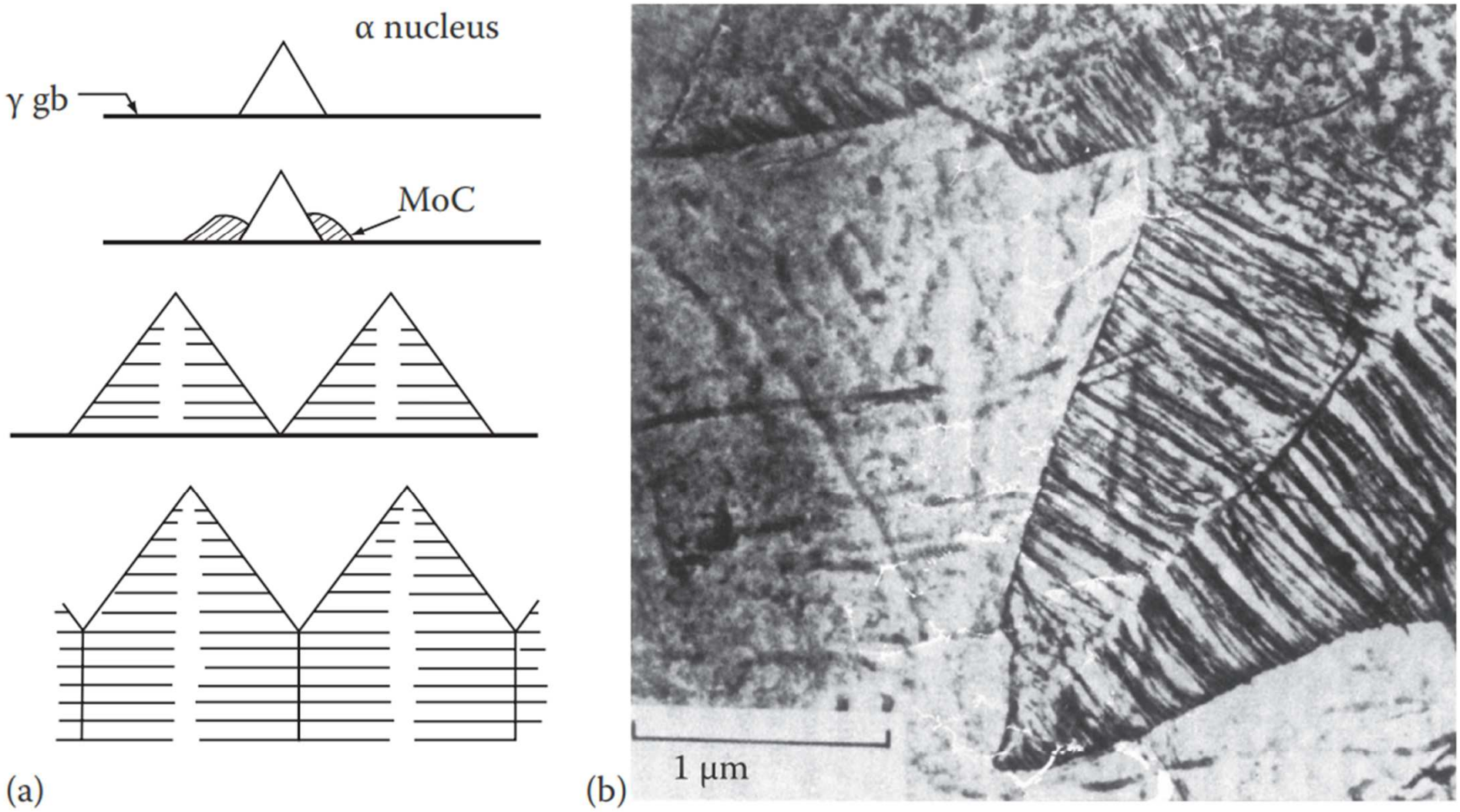

FIGURE 5.79 Fe–4Mo–0.2C (wt.%) transformed 2 h at 650°C. (a) Schematic of possible nucleation and growth mechanism. (b) Thin-foil electron micrograph (× 32, 000). (After R.W.K. Honeycombe, "Transformation from Austenite in Alloy Steels", *Metallurgical Transactions*, 7A:91 (1976), © American Society for Metals and The Metallurgical Society of AIME, 1976, after D.V. Edmonds.)

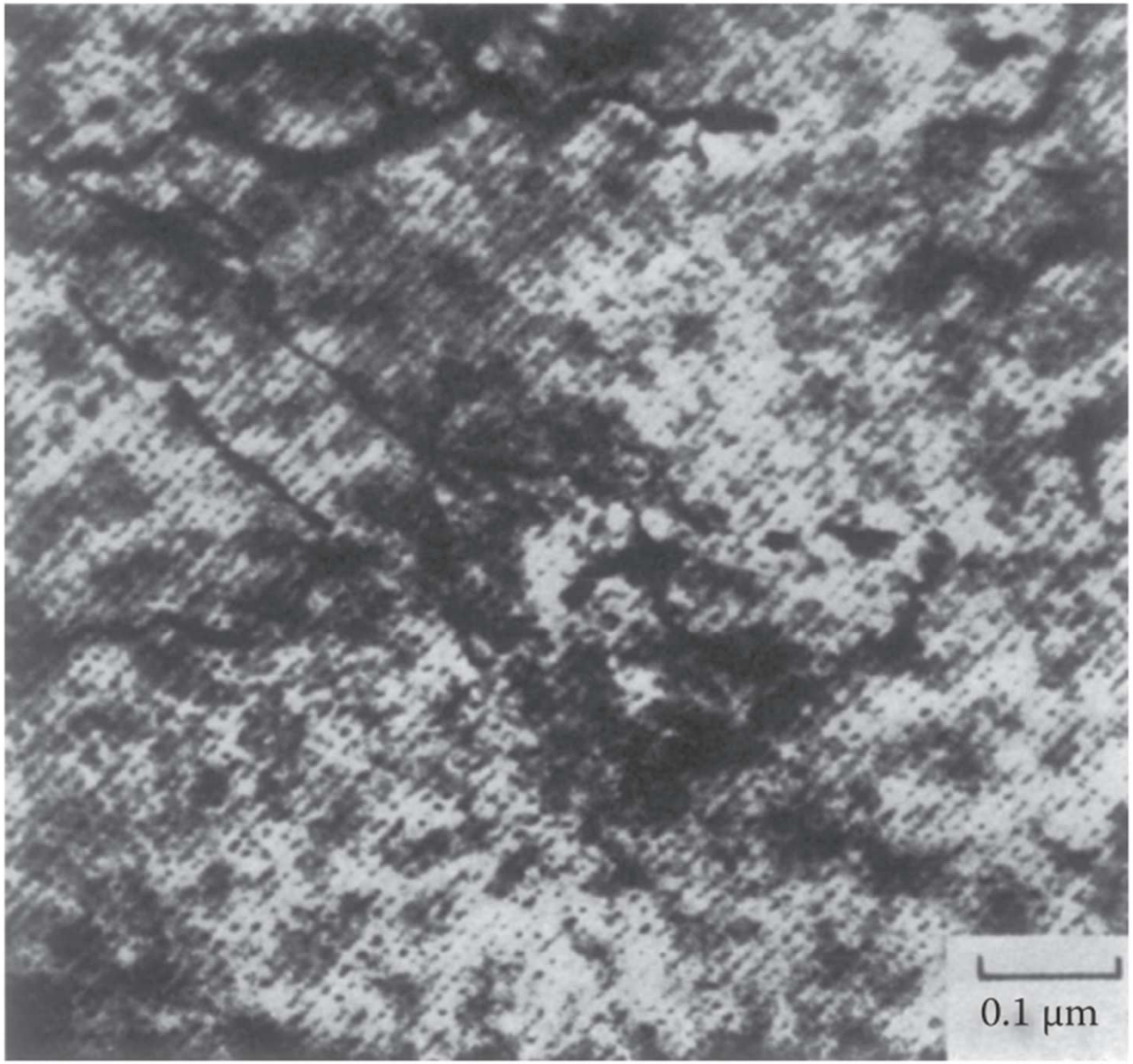

FIGURE 5.80 Fe–0.75V–0.15C (wt.%) after 5 min at 725°C. Thin-foil electron micrograph showing sheets of vanadium carbide precipitates, i.e., interphase precipitation. (After R.W.K. Honeycombe, 'Transformation from Austenite in Alloy Steels', *Metallurgical Transactions*, **7A:**91 (1976), © American Society for Metals and The Metallurgical Society of AIME, 1976, after A.D. Batte.)

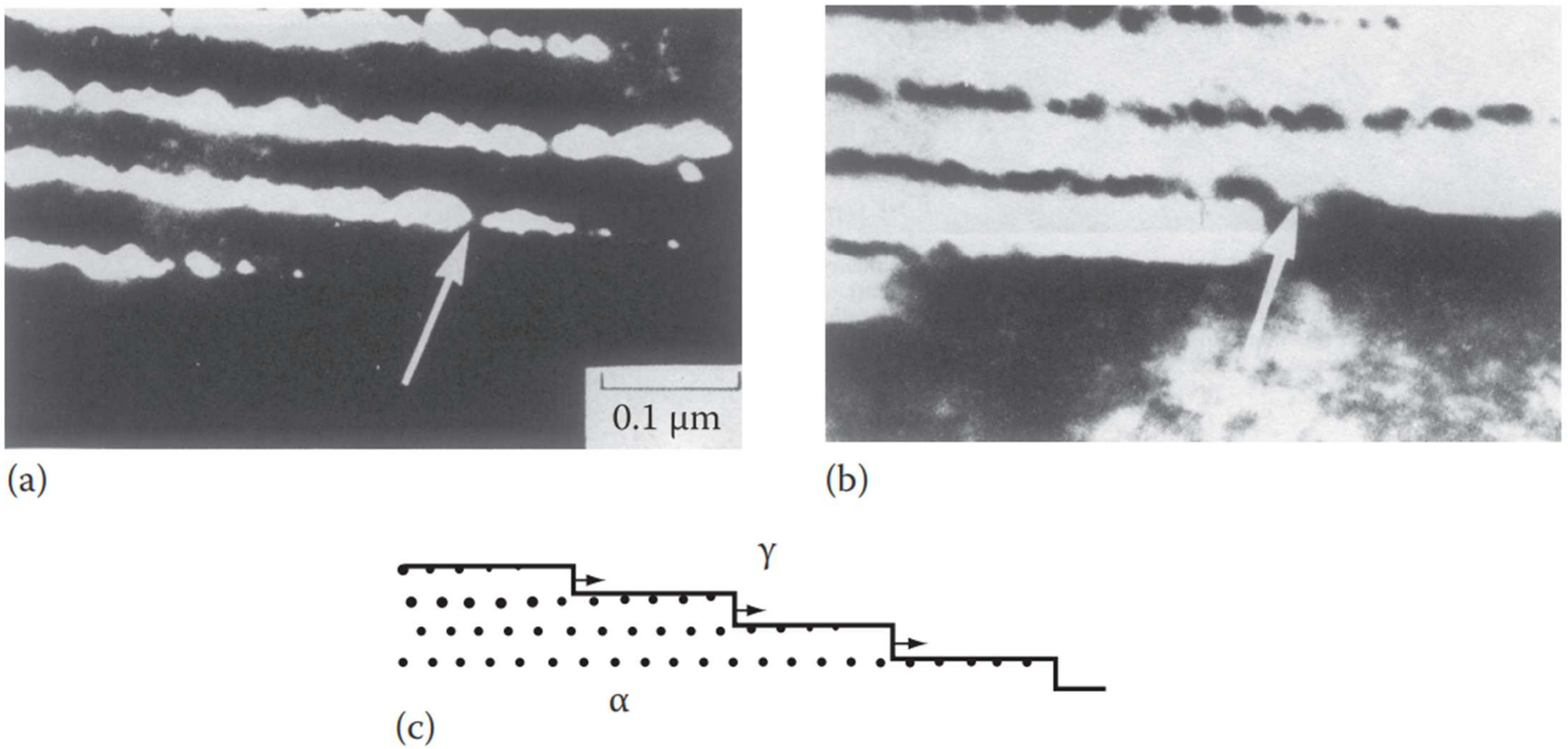

FIGURE 5.81 Fe–12Cr–0.2C (wt.%) transformed 30 min at 650°C. Interphase precipitation of $Cr_{23}C_6$ at the α/γ interface. (a) Dark-field micrograph showing bright precipitates. (b) Bright-field micrograph of same area showing ledges in the α/β interface. Precipitates appear dark. (c) Schematic of nucleation and growth mechanism for interphase precipitation. (After R.W.K. Honeycombe, 'Transformation from Austenite in Alloy Steels', *Metallurgical Transactions* **7A:**91 (1976), © American Society for Metals and The Metallurgical Society of AIME, 1976, after K. Campbell.)

5. Diffusion Transformations in solid

(c) Order-Disorder Transformation

$$\alpha \rightarrow \alpha'$$

Disorder (high temp.) Order (low temp.)

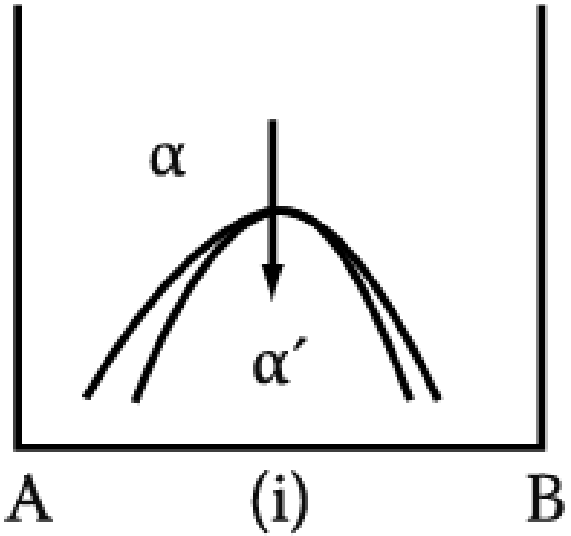

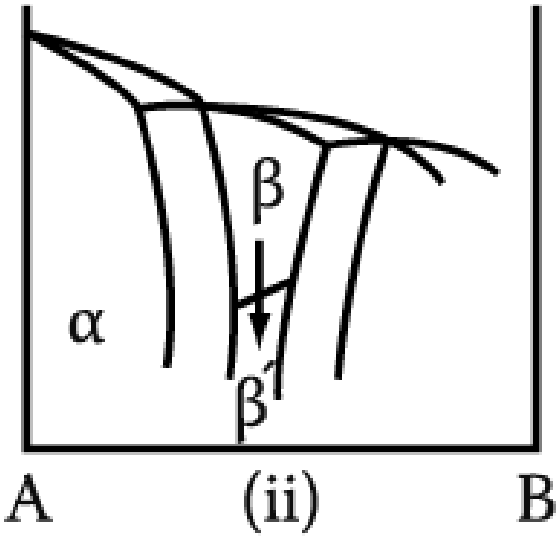

(d) Massive Transformation

: The original phase decomposes into one or more new phases which have the same composition as the parent phase, but different crystal structures.

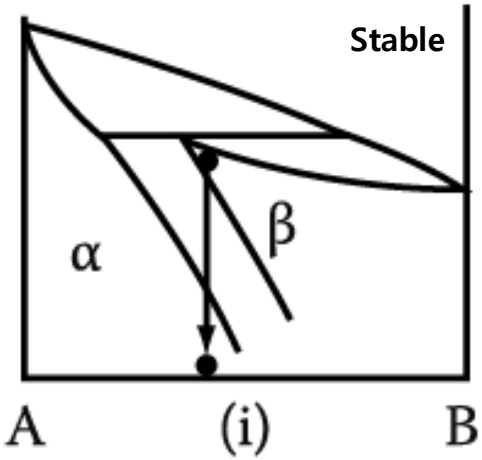

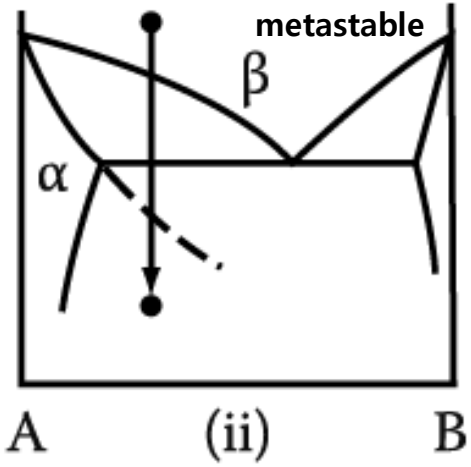

$$\beta \rightarrow \alpha$$

(e) Polymorphic Transformation

In single component systems, different crystal structures are stable over different temper-ature ranges.

5.9 Massive Transformation

: The original phase decomposes into one or more new phases which have the same composition as the parent phase, but different crystal structures.

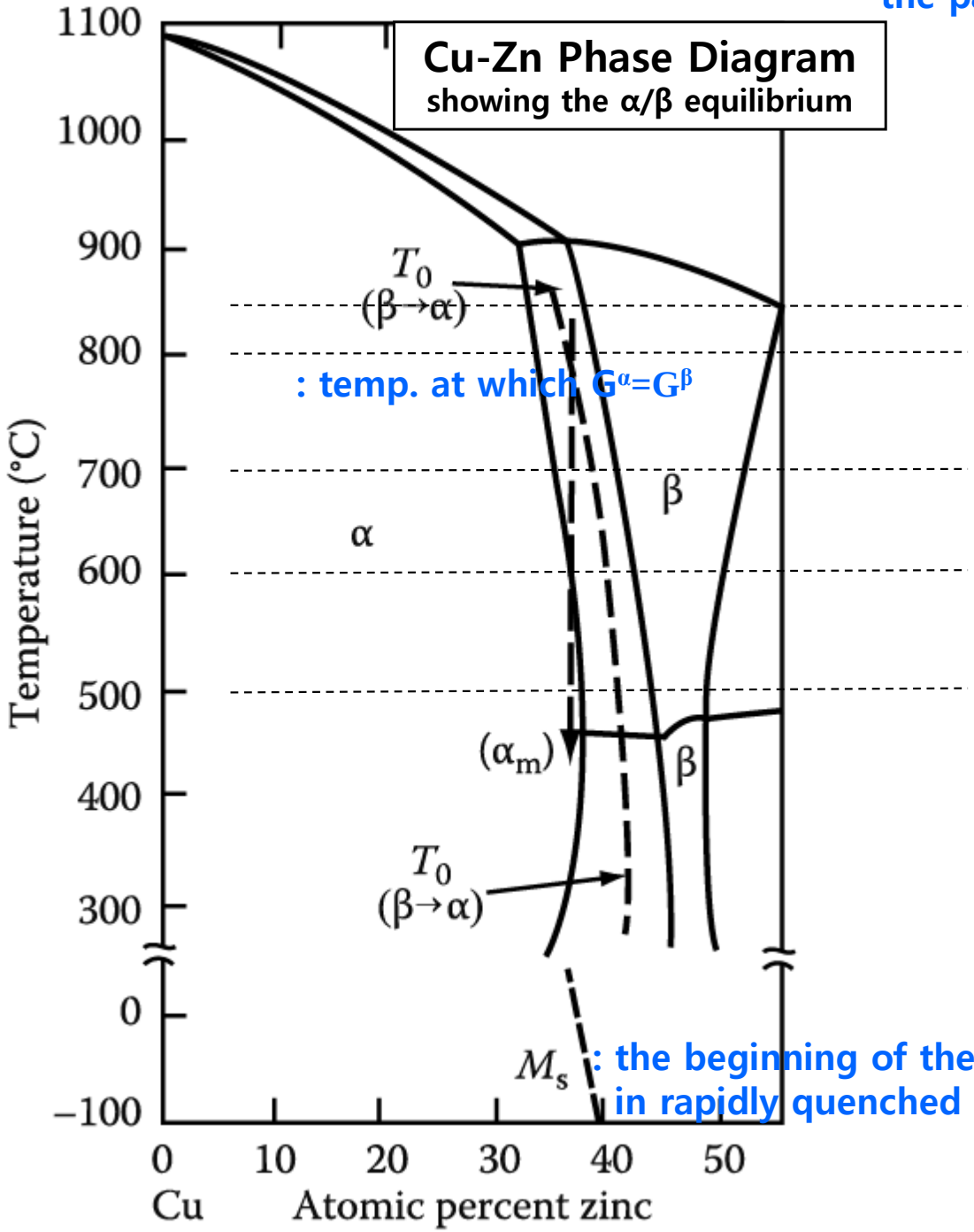

: temp. at which $G^{\alpha}=G^{\beta}$

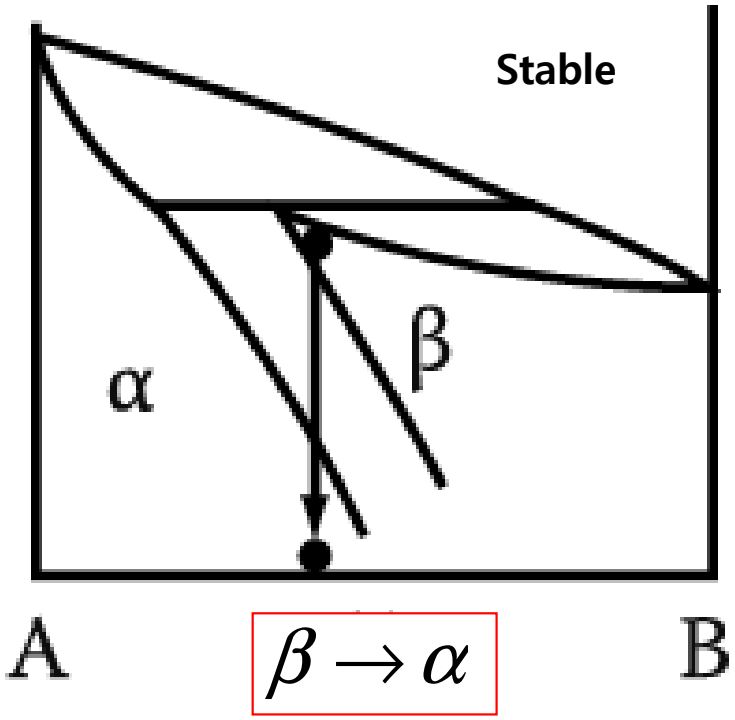

Free energy-composition curves for α and β at 850°C, 800°C, 700°C and 600°C?

M_s : the beginning of the M transformation in rapidly quenched specimens.

5.9 Massive Transformation

Free energy-composition curves for α and β

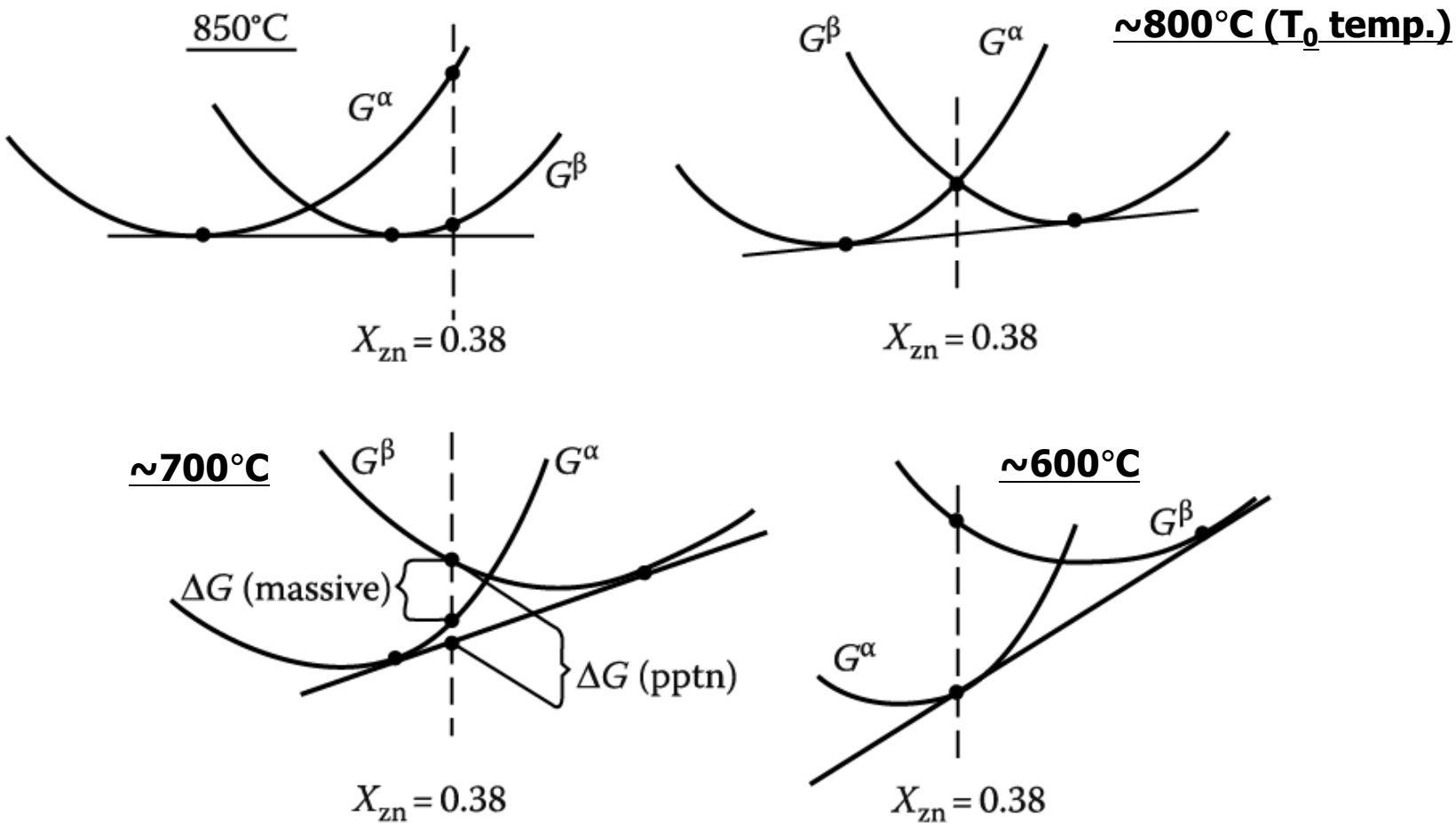

Fig. 5.86 A schematic representation of the free energy-composition curves for α and β in the Cu-Zn system at various temperatures.

At the thermodynamic point of view, it may possible for a massive trans. to occur within the two-phase region of the phase dia. anywhere below the T_0 temp.. But, in practice, there is evidence that massive trans. usually occur only within the "single-phase region" of the phase diagram

5.9 Massive Transformation

Massive α formed at the GBs of β and grow rapidly into the surrounding β

: a diffusionless civilian transformation (change of crystal structure without a change of composition)

Migration of the α/β interfaces~ very similar to the migration of GBs during recrystallization of single-phase material but, driving force ~ orders of magnitude greater than for recrystallization→ rapid growth: a characteristic irregular appearance.

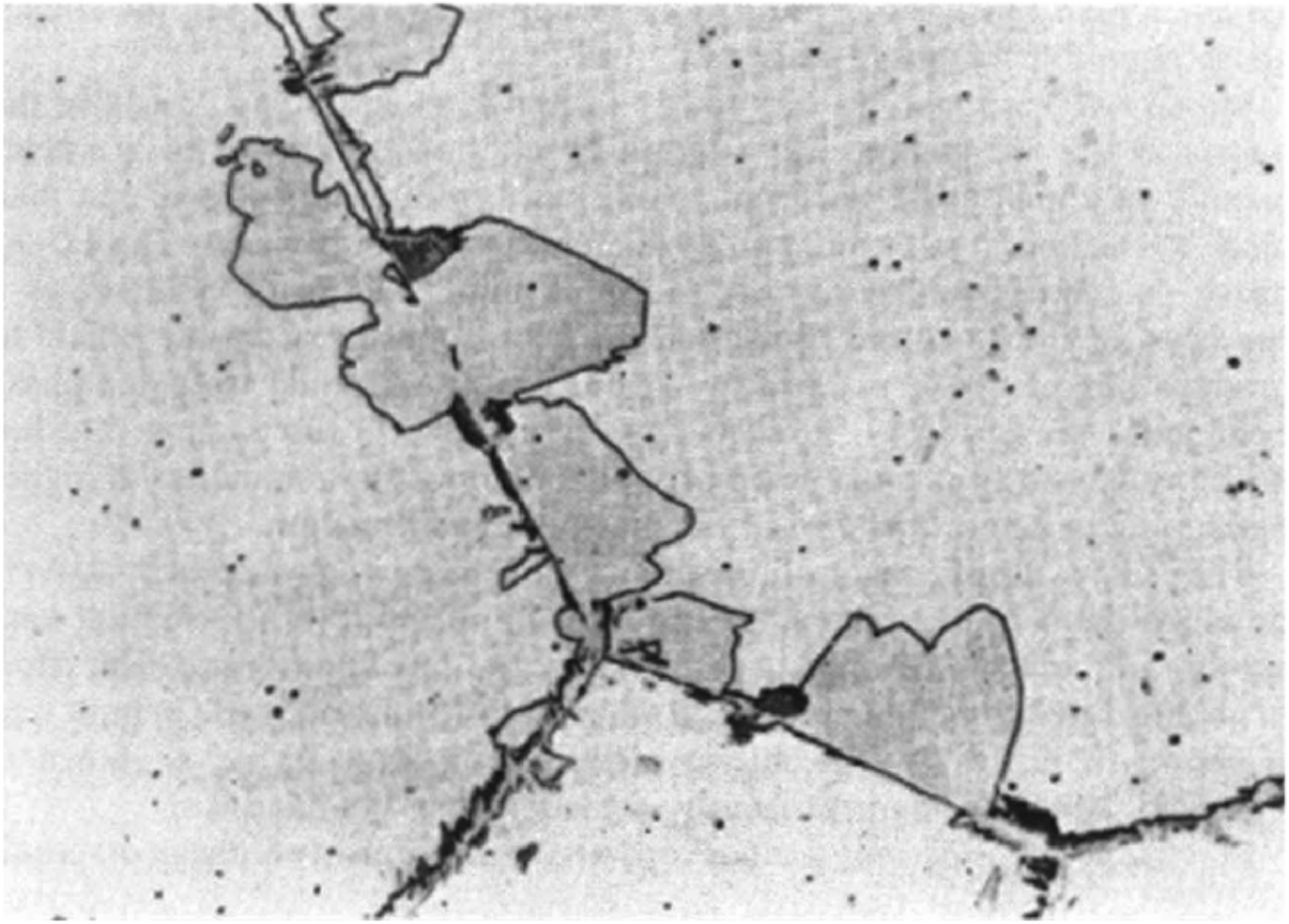

Figure 5.85 Massive a formed at the GBs of β in Cu-38.7wt% Zn quenched from 850℃ in brine at 0℃. Some high temperature precipitation has also occurred on the boundaries.

* Massive, Martensite Transformation

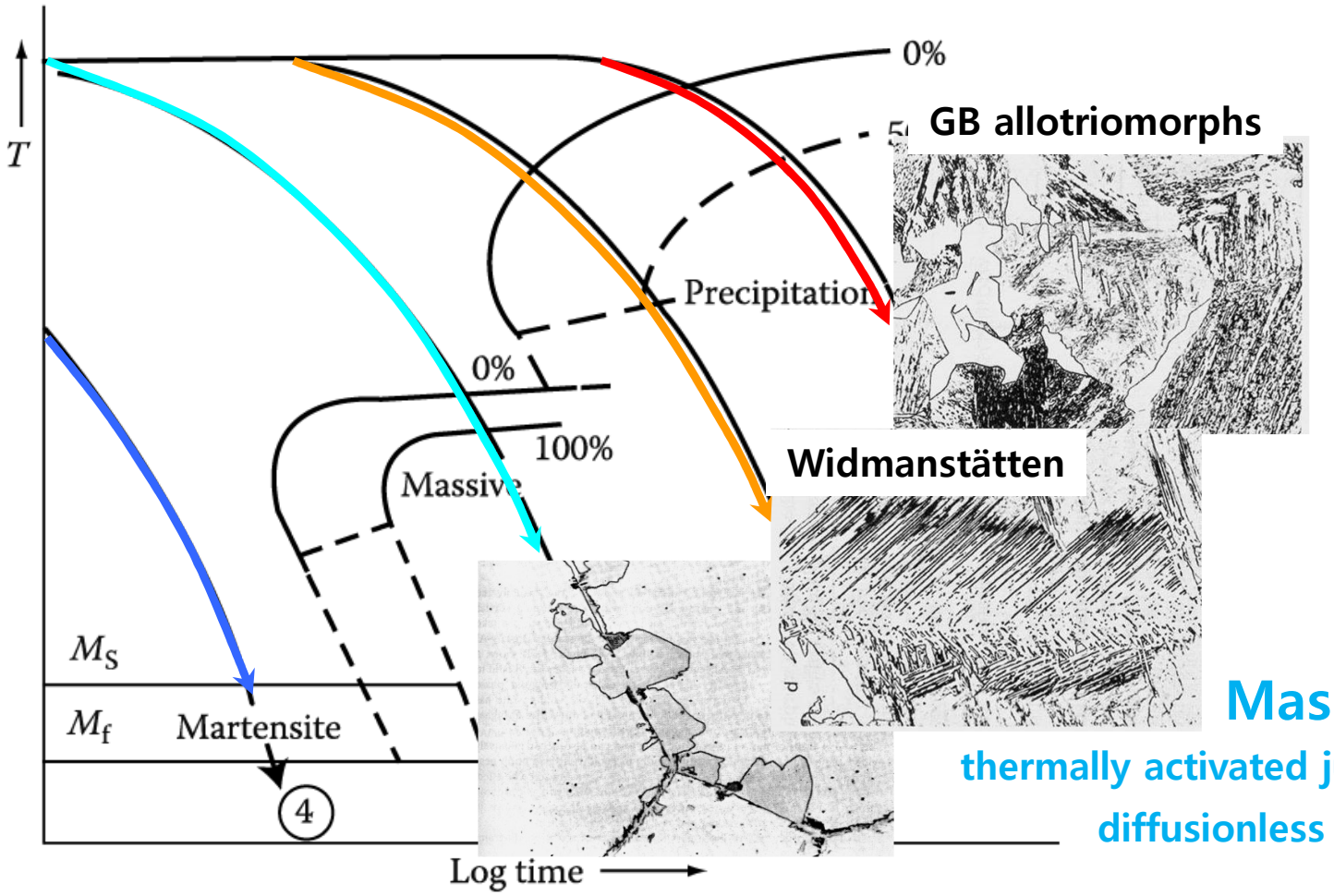

Martensite

Massive Transformation

thermally activated jumping across the α/β interface

diffusionless civilian transformation

Fig. 5.75 A possible CCT diagram for systems showing a massive transformation. Slow cooling (1) produces equiaxed α. Widmanstatten morphologies result from faster cooling (2). Moderately rapid quenching (3) produces the massive transformation, while the highest quench rate (4) leads to a martensitic transformation.

β is sheared into α by the cooperative movement of atoms across a glissile interface

diffusionless military transformation

Martensite Transformation

5.9 Massive Transformation : γ→α transformation in iron and its alloy

Effect of Cooling Rate on the Transformation Temperature at which transformation starts in pure iron

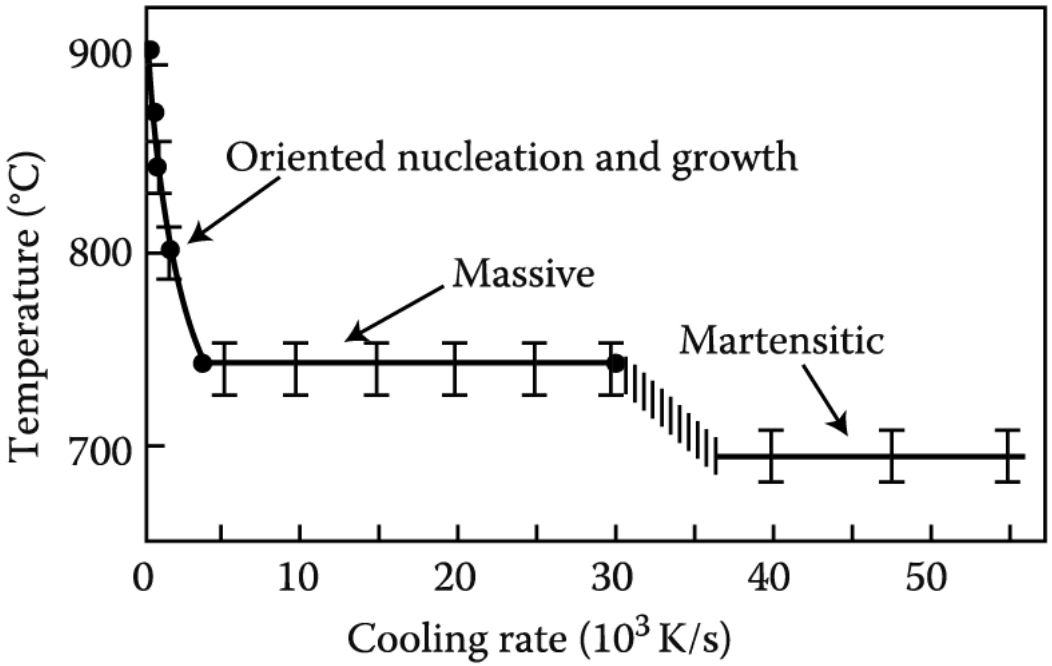

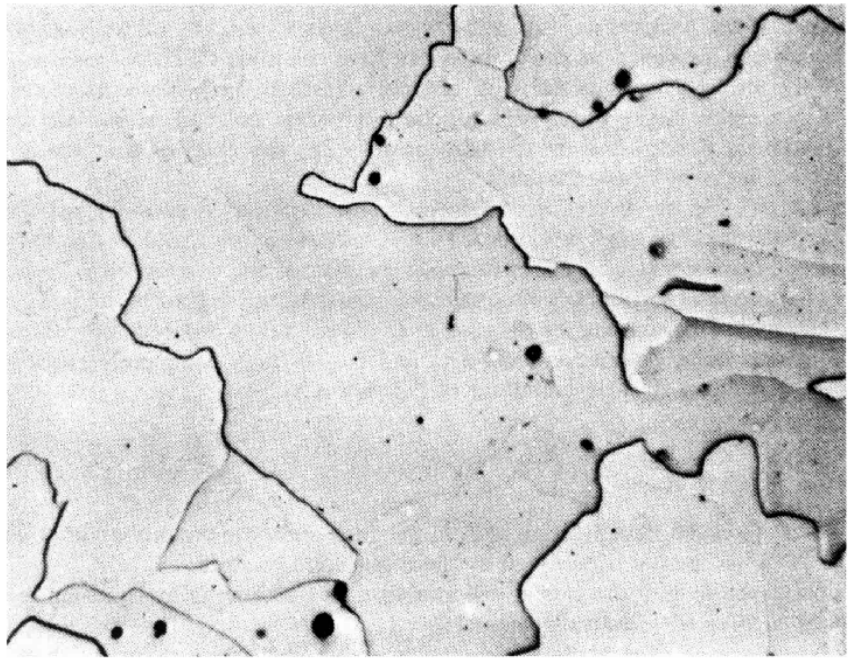

Massive a in an Fe-0.002wt%C
Quenched into iced brine from 1000 °C
: characteristically irregular α/α GBs.

5.9 Massive Transformation

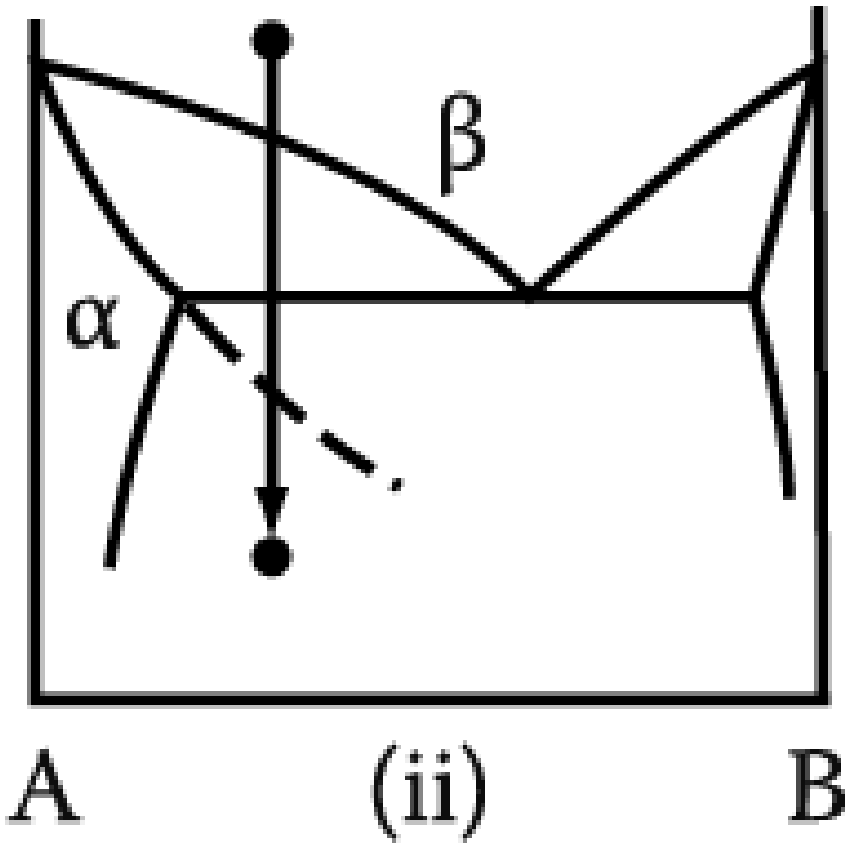

Metastable phases can also form massively.

It is not even necessary for the transformation product to be a single phase: two phases, at least one of which must be metastable, can form simultaneously provided they have the same composition as the parent phase.

5.10 Ordering Transformations

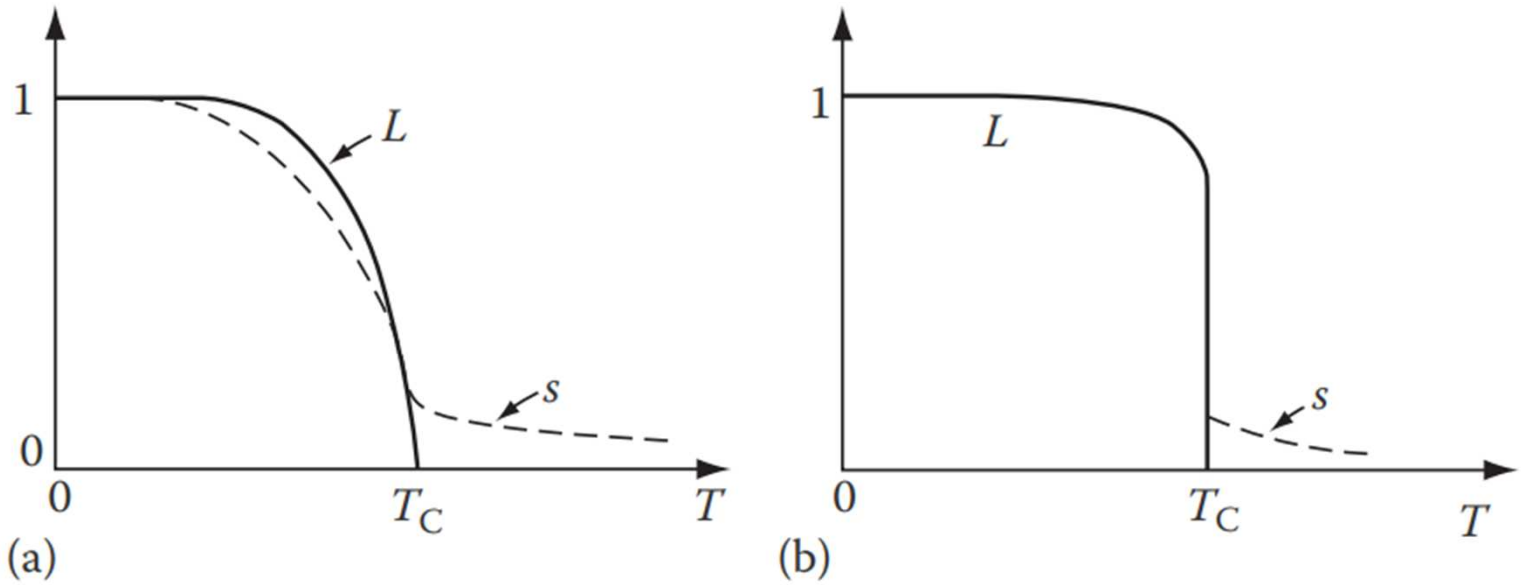

FIGURE 5.87 The variation of long-range order (L) and short-range order (*s*) for (a) CuZn-type and (b) Cu_3Au-type transformations (schematic).

FIG. 5.88 The thermodynamic characteristics of (a) first-order and (b) second-order phase transformations.

$$\left(\frac{\partial^2 G}{\partial T^2}\right)_P = -\left(\frac{\partial S}{\partial T}\right)_P = -\frac{1}{T}\left(\frac{\partial H}{\partial T}\right)_P = -\frac{C_P}{T}$$

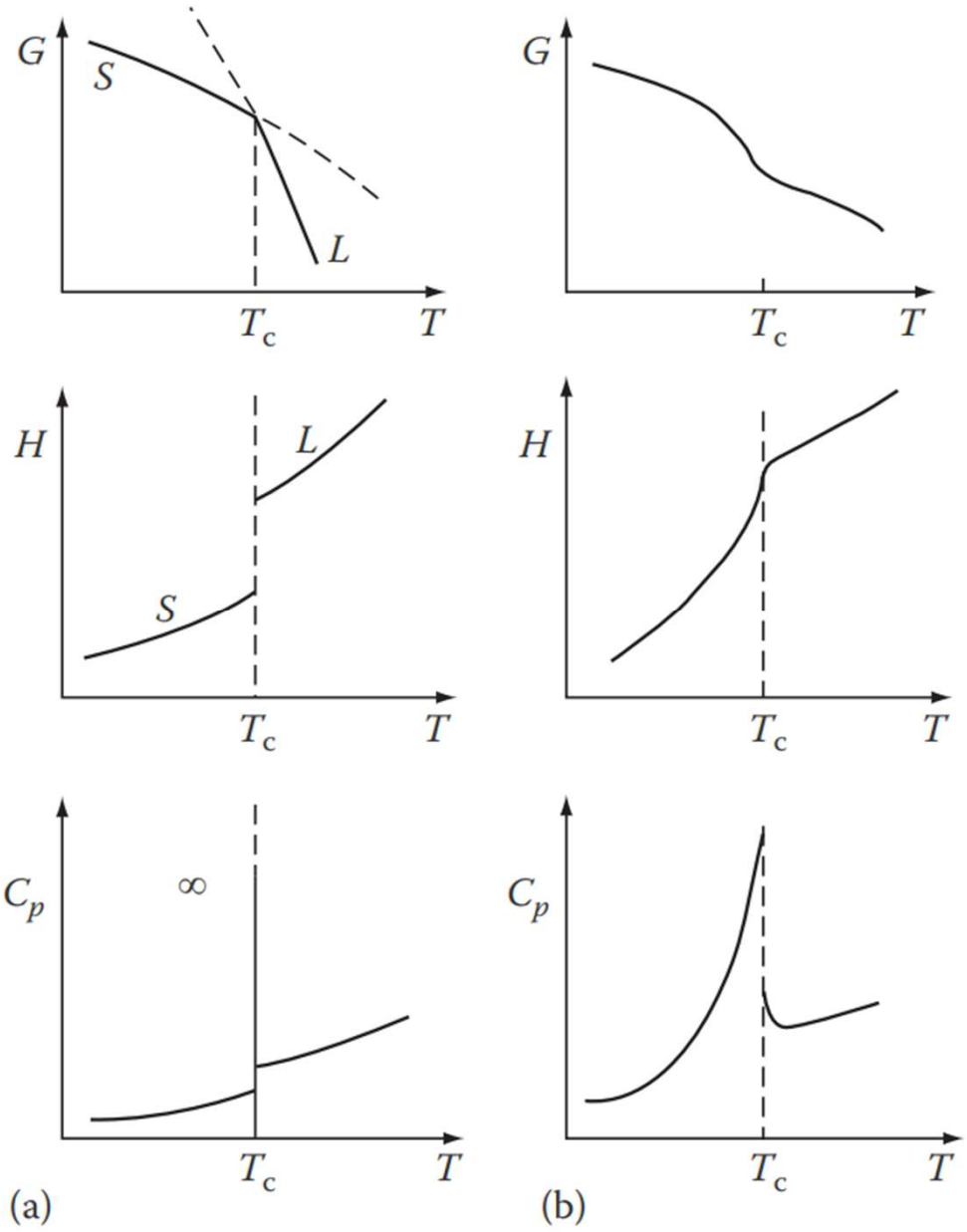

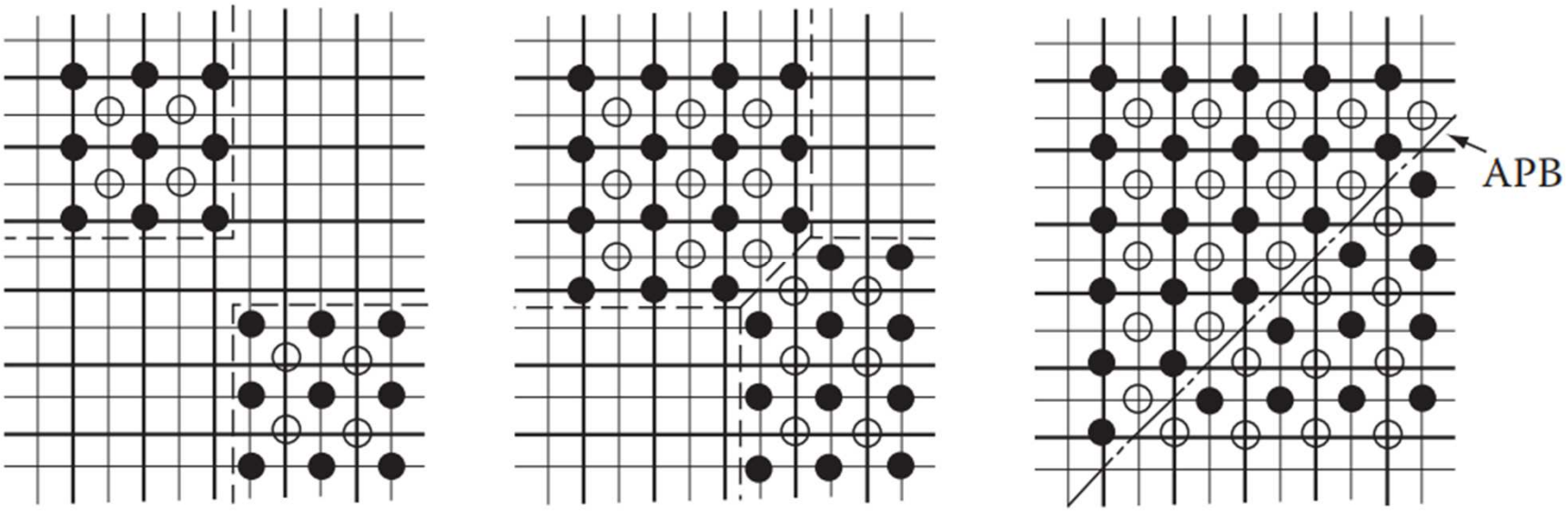

FIGURE 5.89 The formation of an antiphase boundary (APB) when out-of-phase ordered domains impinge. The diagram could represent a {100} plane in Cu_3Au in which case the black and white atoms could represent Cu and Au. (After P. Haasen, *Physical Metallurgy*, Cambridge University Press, Cambridge, 1978.)

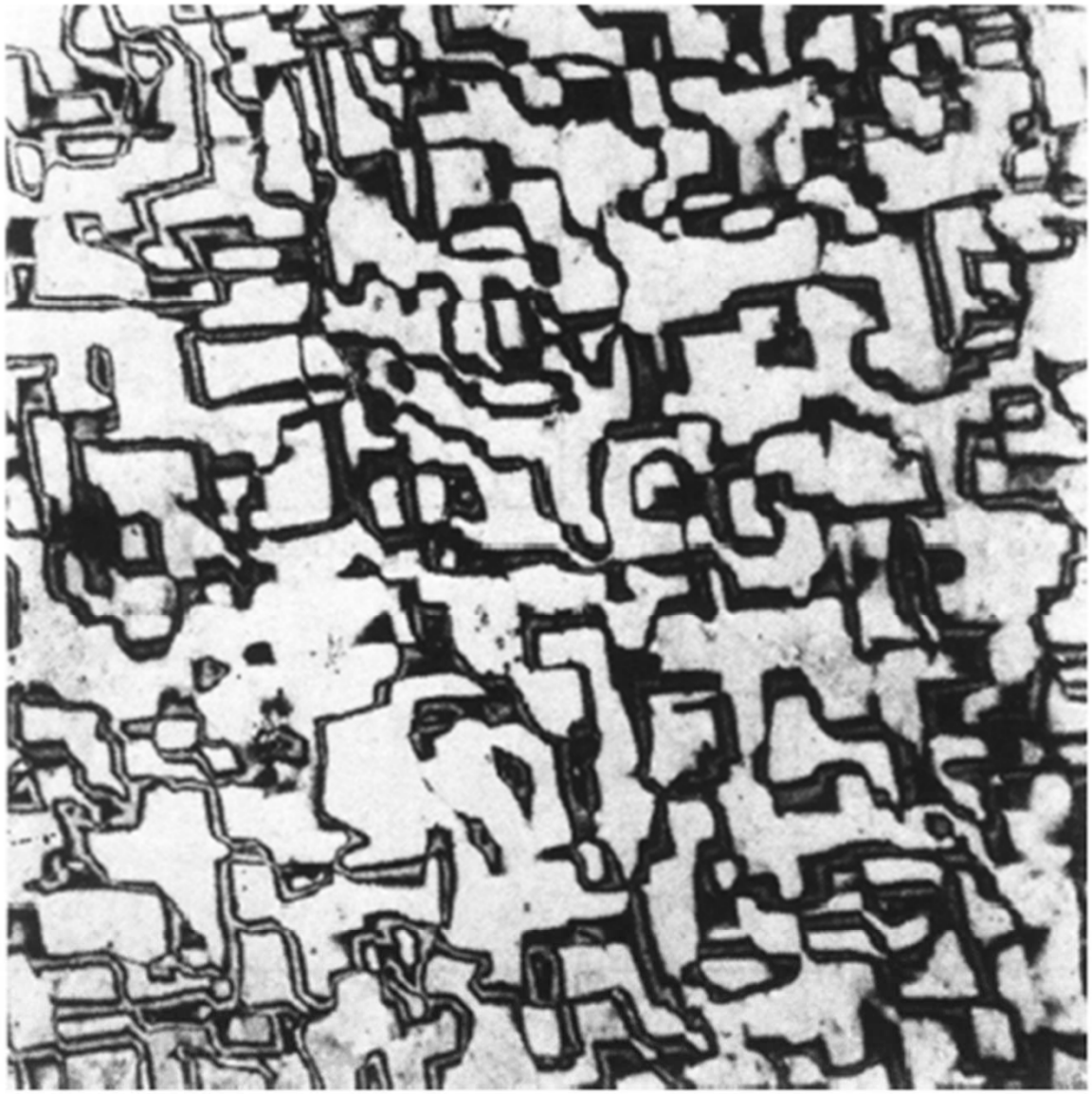

FIGURE 5.90 APBs in ordered Cu_3Au. Thin-foil electron micrograph ×39,000. Note that due to the method of imaging, about one third of the APBs are invisible. (After M.J. Marcinkowski in *Metals Handbook*, 8th edn., Vol. 8, American Society for Metals. 1973, p. 205.)

5.11 CASE Studies skip

5. Diffusion Transformations in solid

: diffusional nucleation & growth

(a) Precipitation

$$\alpha' \rightarrow \alpha + \beta$$

Metastable supersaturated
Solid solution

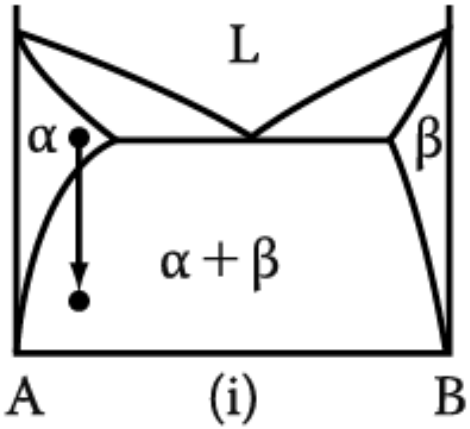

Homogeneous Nucleation

$$\Delta G = -V\Delta G_V + A\gamma + V\Delta G_S$$

Heterogeneous Nucleation

$$\Delta G_{het} = -V(\Delta G_V - \Delta G_S) + A\gamma - \Delta G_d$$

$$N_{\text{hom}} = \omega C_0 \exp\left(-\frac{\Delta G_m}{kT}\right) \exp\left(-\frac{\Delta G^*}{kT}\right)$$

➡ suitable nucleation sites ~ nonequilibrium defects
(creation of nucleus~destruction of a defect($-\Delta G_d$))

(b) Eutectoid Transformation

Composition of product phases differs from that of a parent phase.
→ long-range diffusion

Which transformation proceeds by short-range diffusion?

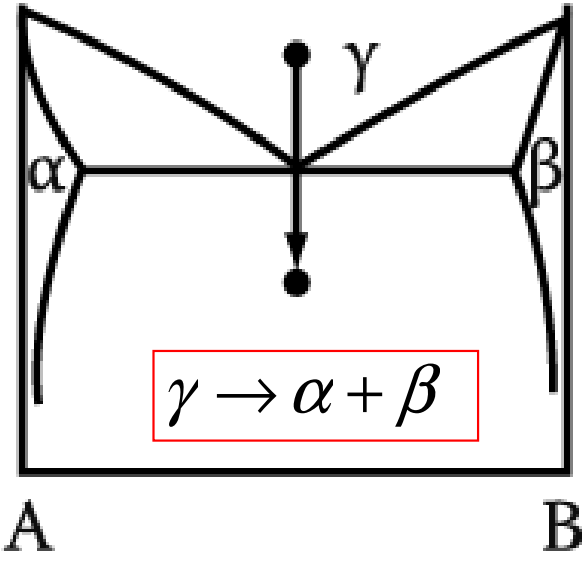

5. Diffusion Transformations in solid

(c) Order-Disorder Transformation

$$\alpha \rightarrow \alpha'$$

Disorder (high temp.) Order (low temp.)

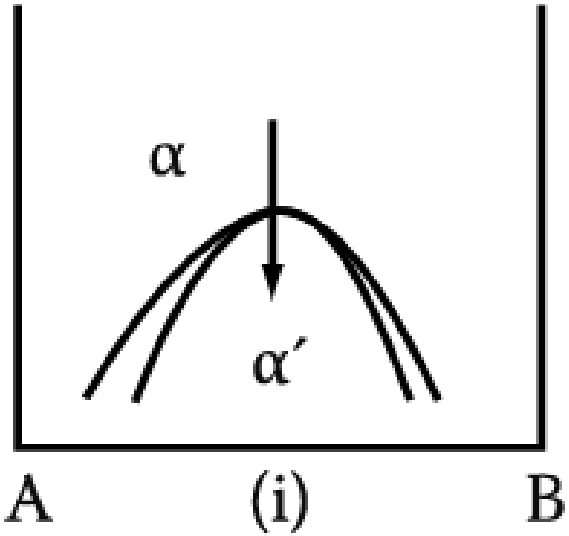

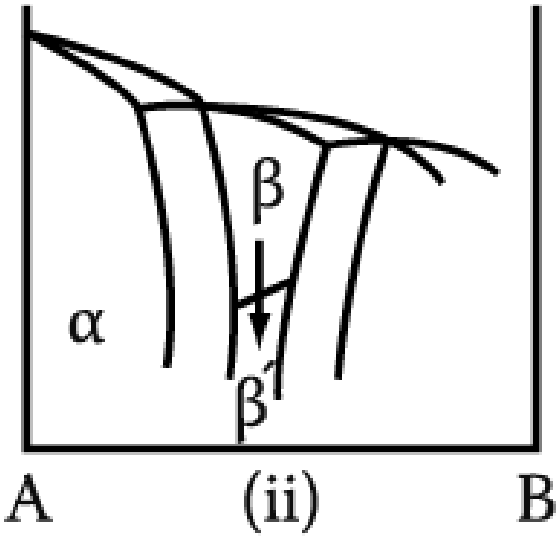

(d) Massive Transformation

: The original phase decomposes into one or more new phases which have the same composition as the parent phase, but different crystal structures.

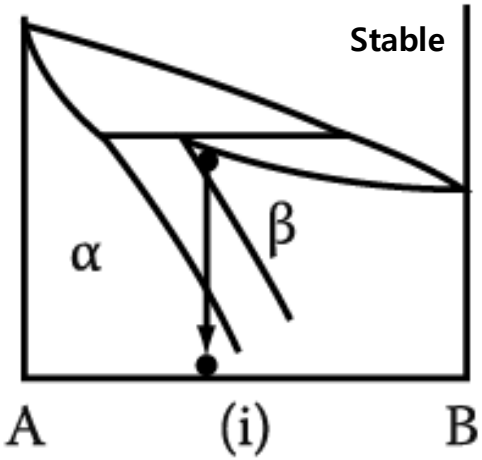

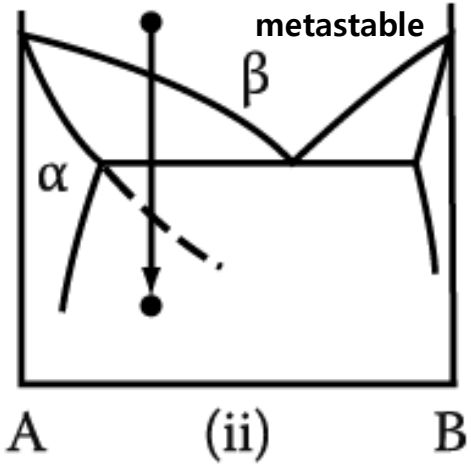

$$\beta \rightarrow \alpha$$

(e) Polymorphic Transformation

In single component systems, different crystal structures are stable over different temperature ranges.

* Homework 6 : Exercises 5 (pages 370-371)

  until 6th December

* Homework 7 : Summary of sections 5.11 & 5.12

  within 5 pages PPT

  Good Luck!!

2023 Fall

"Phase Transformation *in* Materials"

11.29.2023

Eun Soo Park

Office: 33-313
Telephone: 880-7221
Email: espark@snu.ac.kr
Office hours: by an appointment

5. Diffusion Transformations in solid

: diffusional nucleation & growth

(a) Precipitation

$$\alpha' \rightarrow \alpha + \beta$$

Metastable supersaturated
Solid solution

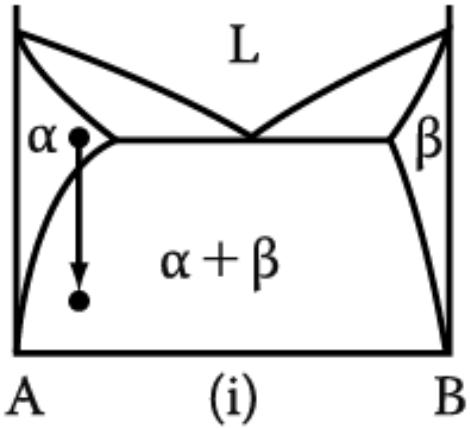

Homogeneous Nucleation

$$\Delta G = -V\Delta G_V + A\gamma + V\Delta G_S$$

Heterogeneous Nucleation

$$\Delta G_{het} = -V(\Delta G_V - \Delta G_S) + A\gamma - \Delta G_d$$

$$N_{\text{hom}} = \omega C_0 \exp\left(-\frac{\Delta G_m}{kT}\right) \exp\left(-\frac{\Delta G^*}{kT}\right)$$

➡ suitable nucleation sites ~ nonequilibrium defects
(creation of nucleus~destruction of a defect($-\Delta G_d$))

(b) Eutectoid Transformation

Composition of product phases differs from that of a parent phase.
→ long-range diffusion

Which transformation proceeds by short-range diffusion?

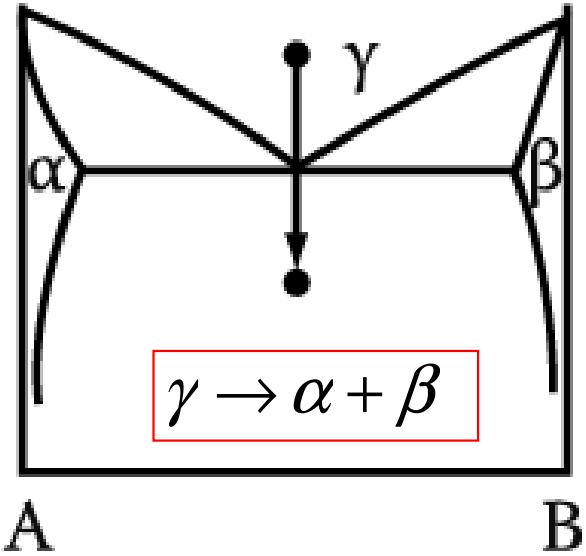

5. Diffusion Transformations in solid

(c) Order-Disorder Transformation

$$\alpha \rightarrow \alpha'$$

Disorder (high temp.) Order (low temp.)

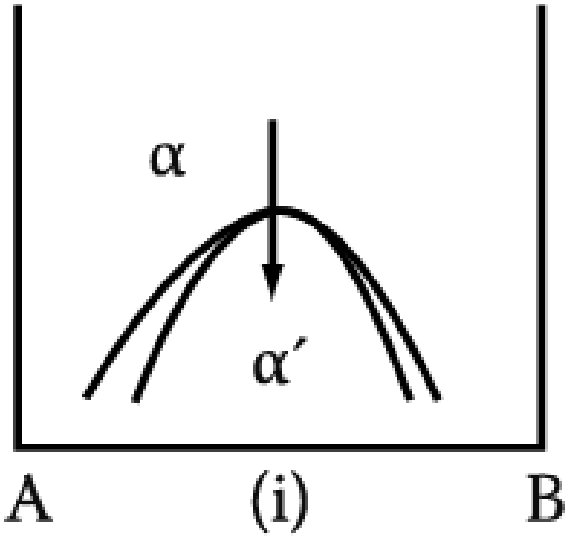

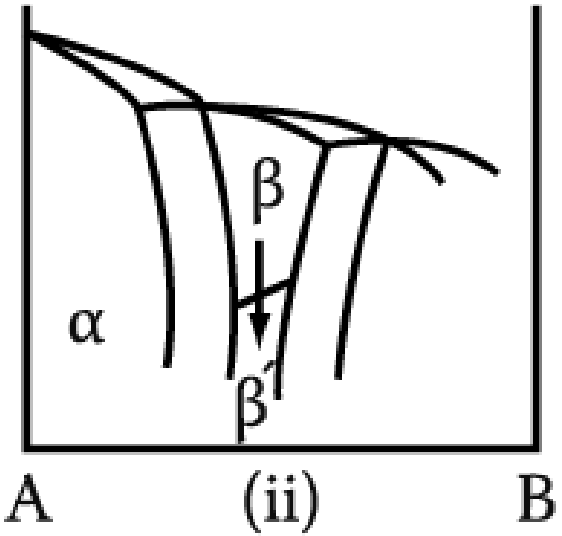

(d) Massive Transformation

: The original phase decomposes into one or more new phases which have the same composition as the parent phase, but different crystal structures.

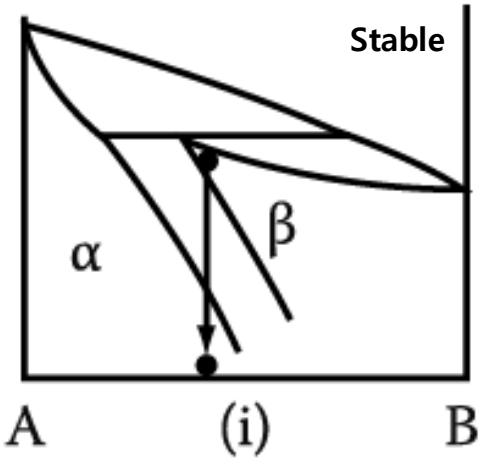

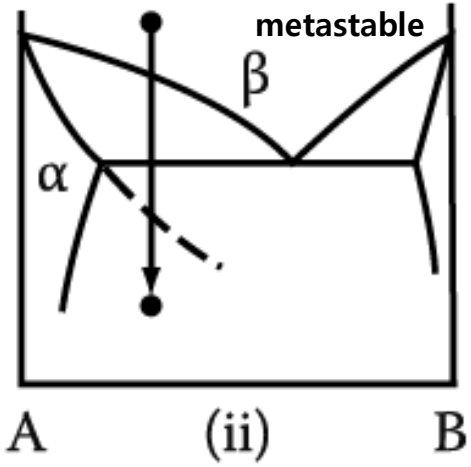

$$\beta \rightarrow \alpha$$

(e) Polymorphic Transformation

In single component systems, different crystal structures are stable over different temper-ature ranges.

5.6. The Precipitation of Ferrite from Austenite (γ→α)

(Most important nucleation site: Grain boundary and the surface of inclusions)

The Iron-Carbon Phase Diagram

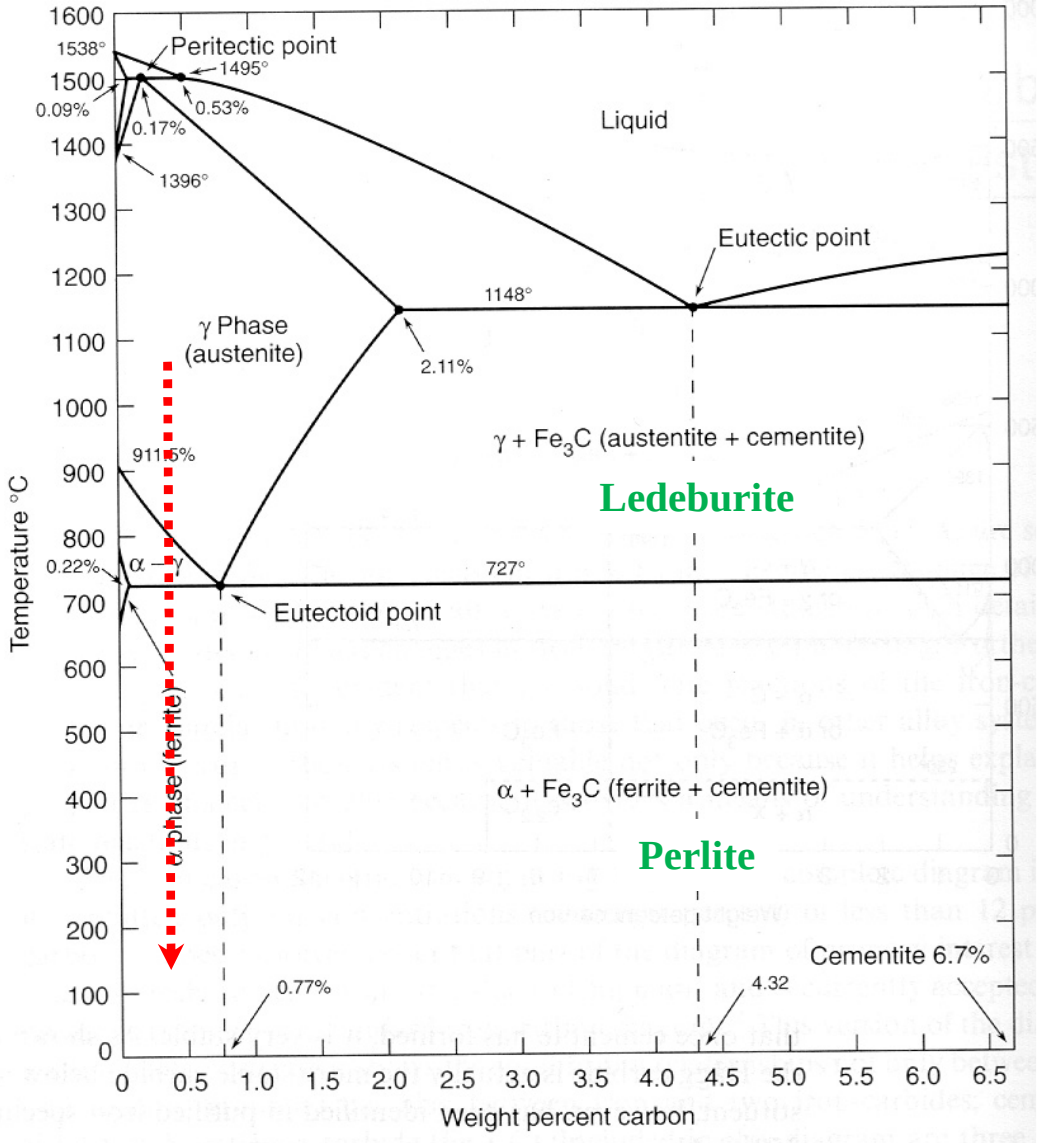

Microstructure (0.4 wt%C) evolved by slow cooling (air, furnace) ?

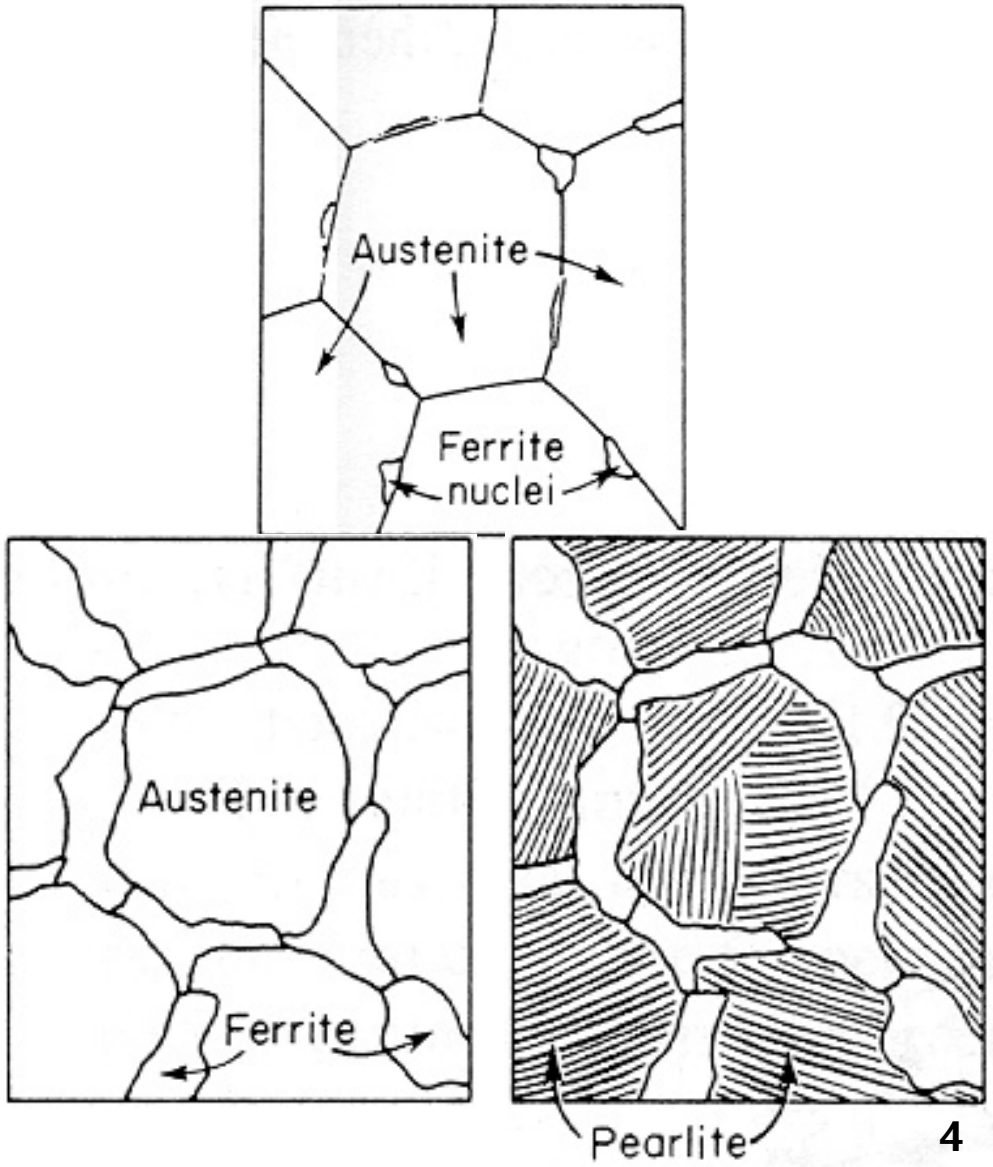

5.6. The Precipitation of Ferrite from Austenite

Diffusional Transformation of Austenite into Ferrite

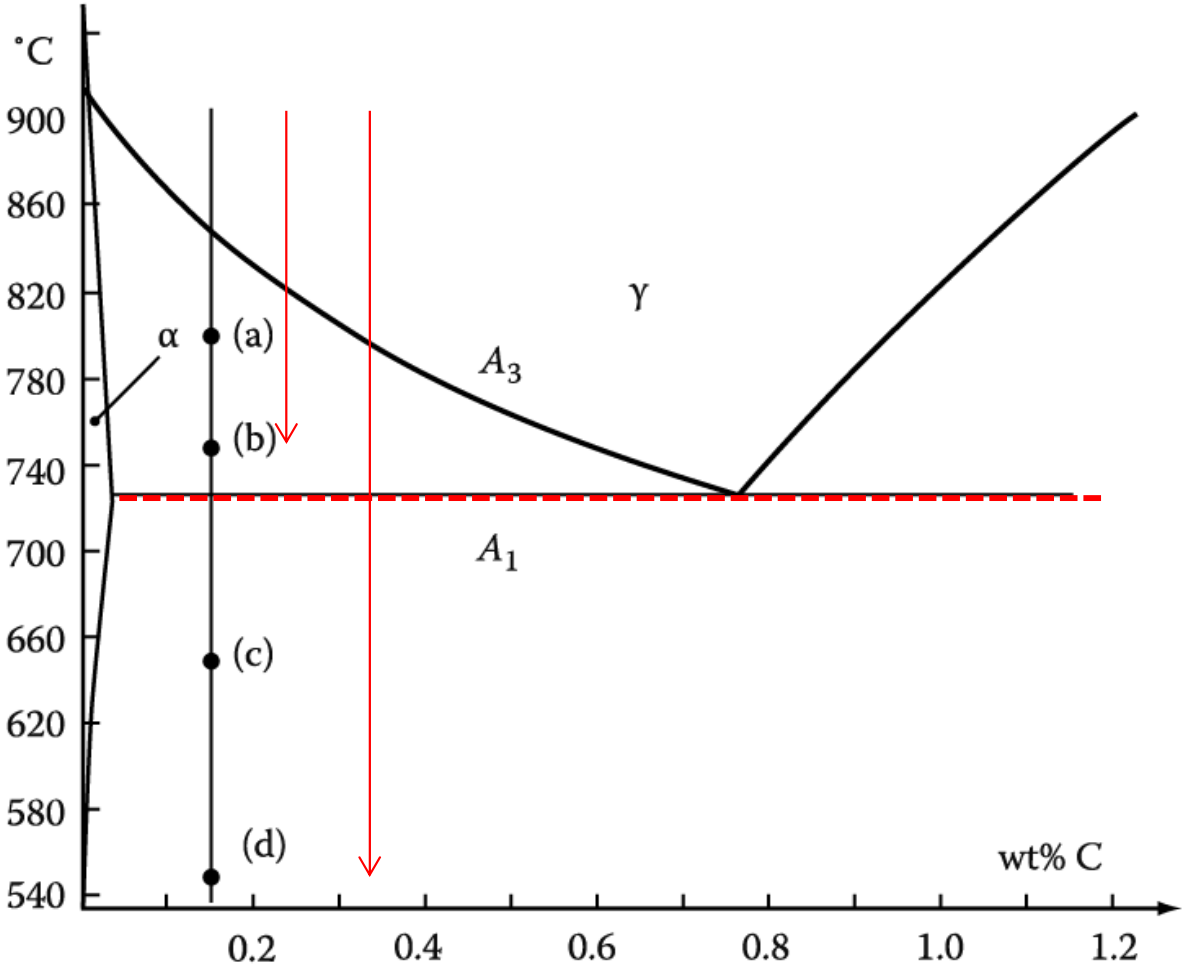

Figure 5.45 Holding temperature for steel in Figure. 5.46

Fe-0.15 wt%C

After being austenitized, held at

(a) 800°C for 150 s

(b) 750°C for 40 s

(c) 650°C for 9 s

(d) 550°C for 2 s and

then quenched to room T.

What would be the microstructures?

For alloys of different carbon content, A_3 and T_w vary and show parallel manner each other.

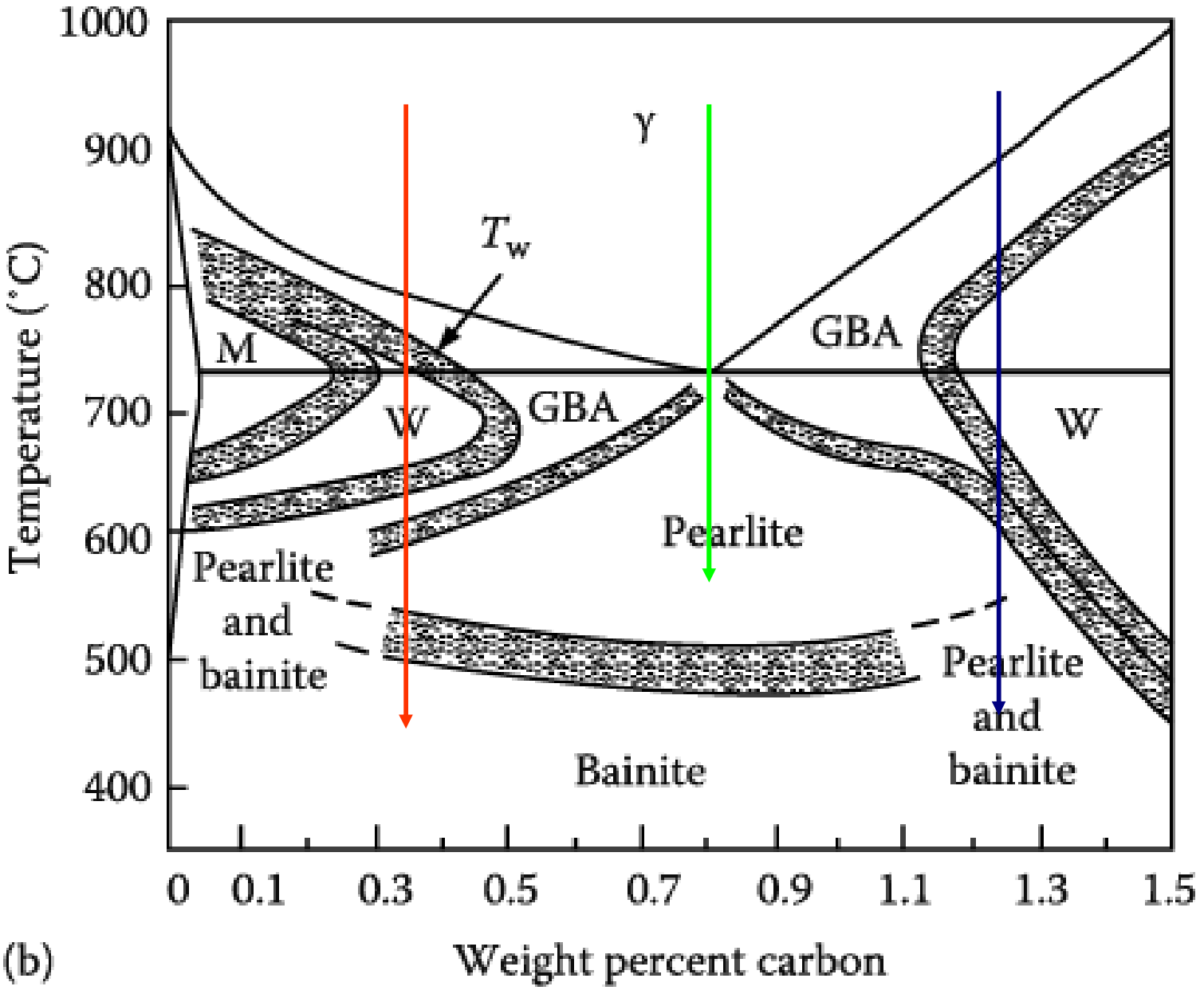

(GBA: GB allotriomorphs, W: Widmanstatten sideplates/intermolecular plates, M: Massive ferrite)

Figure 5.48 (b) Temperature-composition regions in which the various morphologies are dominant at late reaction times in specimens with ASTM grain size Nos. 0-1.

* Massive, Martensite Transformation

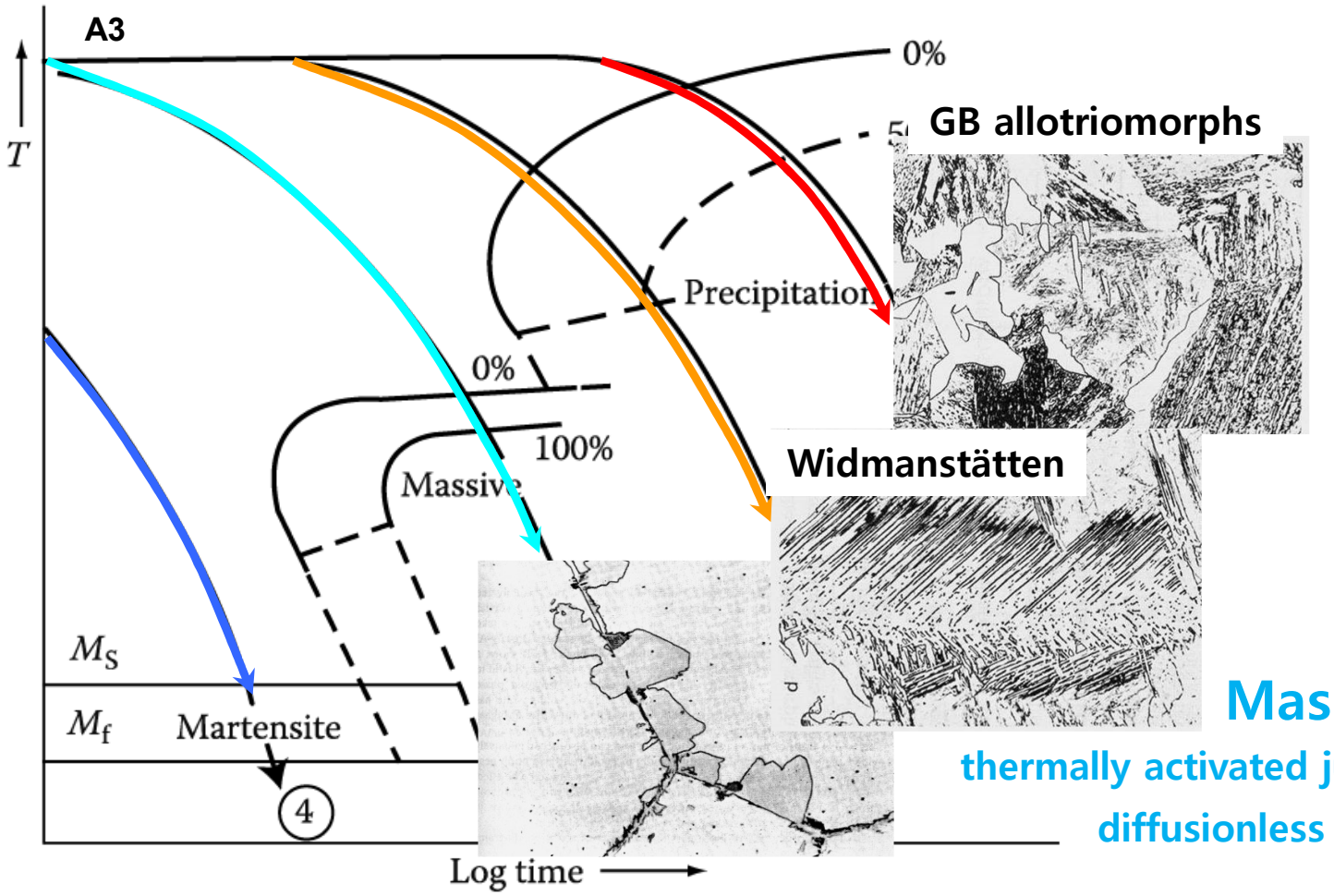

Martensite

Massive Transformation

thermally activated jumping across the α/β interface

diffusionless civilian transformation

↕

β is sheared into α by the cooperative movement of atoms across a glissile interface

diffusionless military transformation

Martensite Transformation

Fig. 5.75 A possible CCT diagram for systems showing a massive transformation. Slow cooling (1) produces equiaxed α. Widmanstatten morphologies result from faster cooling (2). Moderately rapid quenching (3) produces the massive transformation, while the highest quench rate (4) leads to a martensitic transformation.

Growth of Pearlite: analogous to the growth of a lamellar eutectic

Min. possible: (S*) $\propto 1/\Delta T$ / Growth rate : mainly lattice diffusion $v = kD_c^{\gamma}(\Delta T)^2$

Interlamellar spacing of pearlite colonies mainly boundary diffusion $v = kD_b(\Delta T)^3$

Relative Positions of the Transformation curves for Pearlite and Bainite in Plain Carbon Eutectoid Steels.

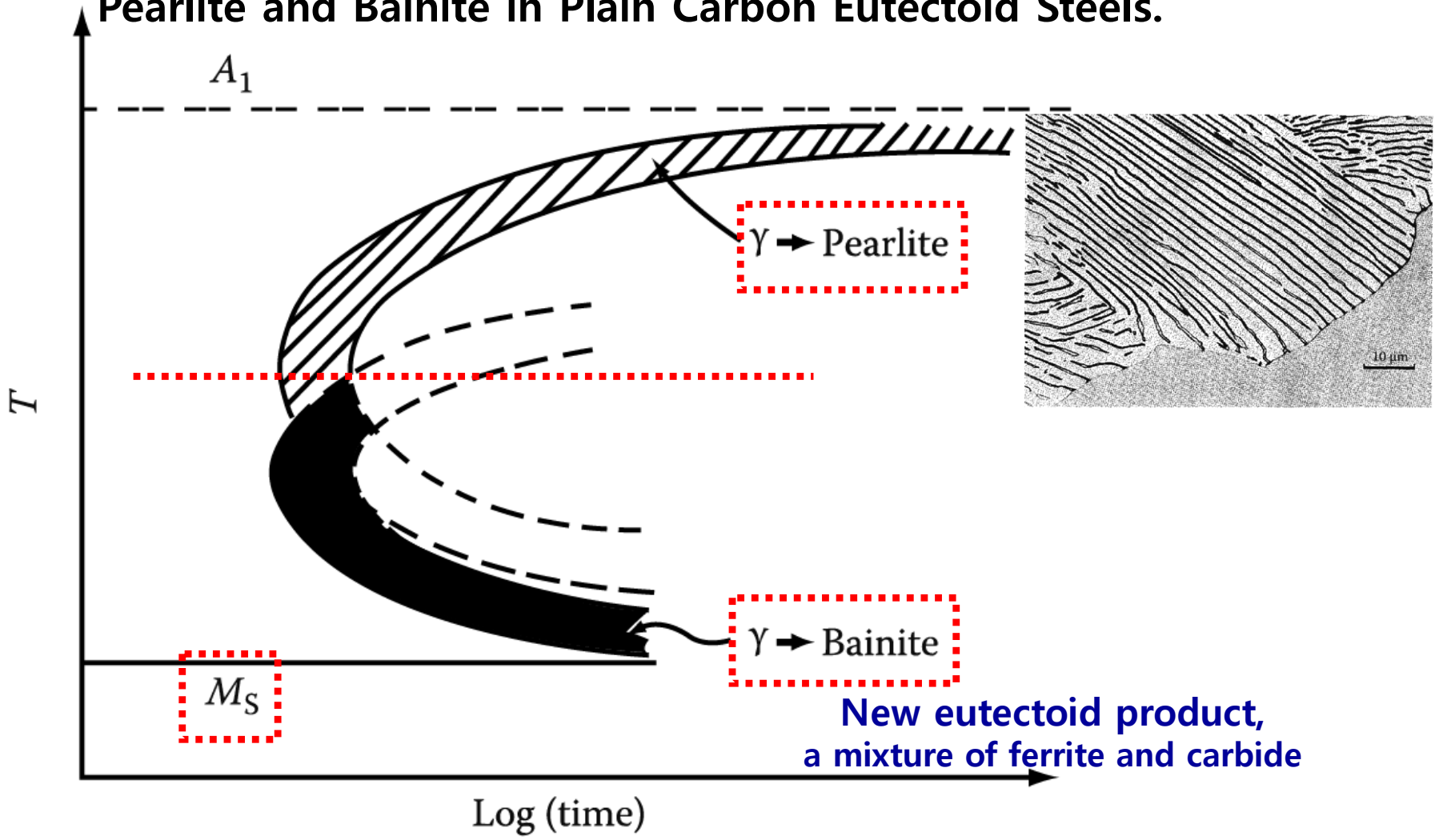

Figure 5.64 Schematic diagram showing relative positions of the transformation curves for pearlite and bainite in plain carbon eutectoid steel.

Contents in Phase Transformation

Background to understand phase transformation

- (Ch1) Thermodynamics and Phase Diagrams
- (Ch2) Diffusion: Kinetics
- (Ch3) Crystal Interface and Microstructure

Representative Phase transformation

- (Ch4) Solidification: Liquid → Solid
- (Ch5) Diffusional Transformations in Solid: Solid → Solid
- (Ch6) Diffusionless Transformations: Solid → Solid

Q1: What is a martensitic transformation?

Chapter 6 Diffusionless Transformation

Individual atomic movements are less than one interatomic spacing.

→ Martensite Transformation

핵생성 및 성장에 의해 일어나는 상변태, 조성변화 없이, 정합계면이나 부분정합계면의 이동으로 전단변형에 의해 결정구조가 변하는, 무확산 변태

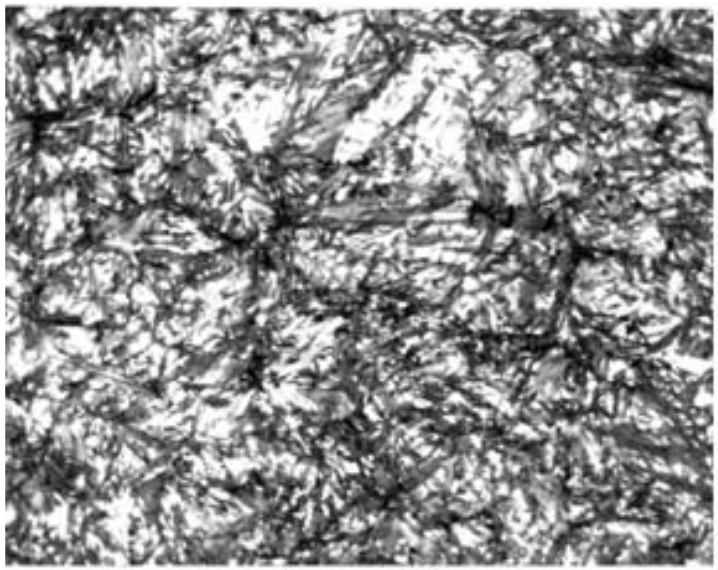

Martensite with some retained austenite

"Needle like" Structure of martensite

(γ→α)

Supersaturated solid solution of carbon in α-Fe

Named for the German metallurgist Adolph Martens, Martensite is the hardened phase of steel that is obtained by cooling Austenite fast enough to trap carbon atoms within the cubic iron matrix distorting it into a body centered tetragonal structure. Now, martensite is used in physical metallurgy to describe any diffusionless trans. product.

One of the most important technological processes is the hardening of steel by quenching.

Military Transformations

- **What is a martensitic transformation?**

  Most phase transformations studied in this course have been diffusional transformations where long range diffusion is required for the (nucleation and) growth of the new phase(s).

- **There is a whole other class of *military transformations* which are *diffusionless transformations* in which the atoms move only short distances (less than one interatomic spacing) in order to join the new phase.**

- **These transformations are *also* subject to the constraints of nucleation and growth. They are (almost invariably) associated with allotropic transformations (동소변태, (a) 조성변화 없음).**

Classification of Transformations

	Civilian	Military
Diffusion Required	**Precipitation, Spinodal Decomposition**	**?**
Diffusionless	**Massive Transformations**	**Martensitic Transformations**

Massive vs. Martensitic Transformations

- There are two basic types of *diffusionless* transformations.
- One is the ***massive transformation***. In this type, a diffusionless transformation takes place ① without a definite orientation relationship. The interphase boundary (between parent and product phases) migrates so as to allow the new phase to grow. It is, however, a ② civilian transformation because the atoms move individually.

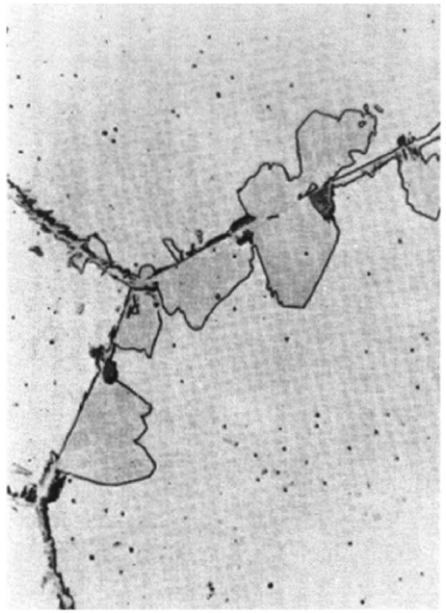

- The other is the ***martensitic transformation***. In this type, the change in phase involves a ① definite orientation relationship because the atoms have to ② move in a coordinated manner. (Military transformation) There is always a ③ change in shape which means that there is a strain associated with the transformation.

Microstructure of Martensite

- The microstructural characteristics of martensite are:
  - **the product (martensite) phase has a (b) well defined crystallographic relationship with the parent (matrix).**

1) martensite(designated α') forms as (c) platelets within grains.

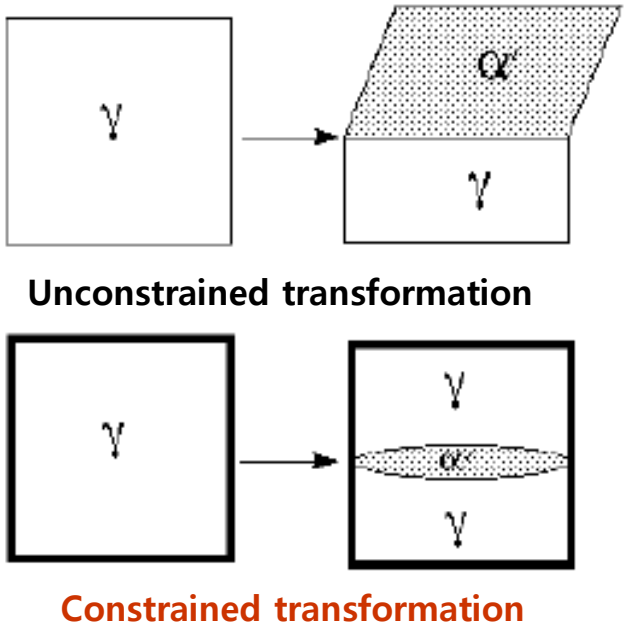

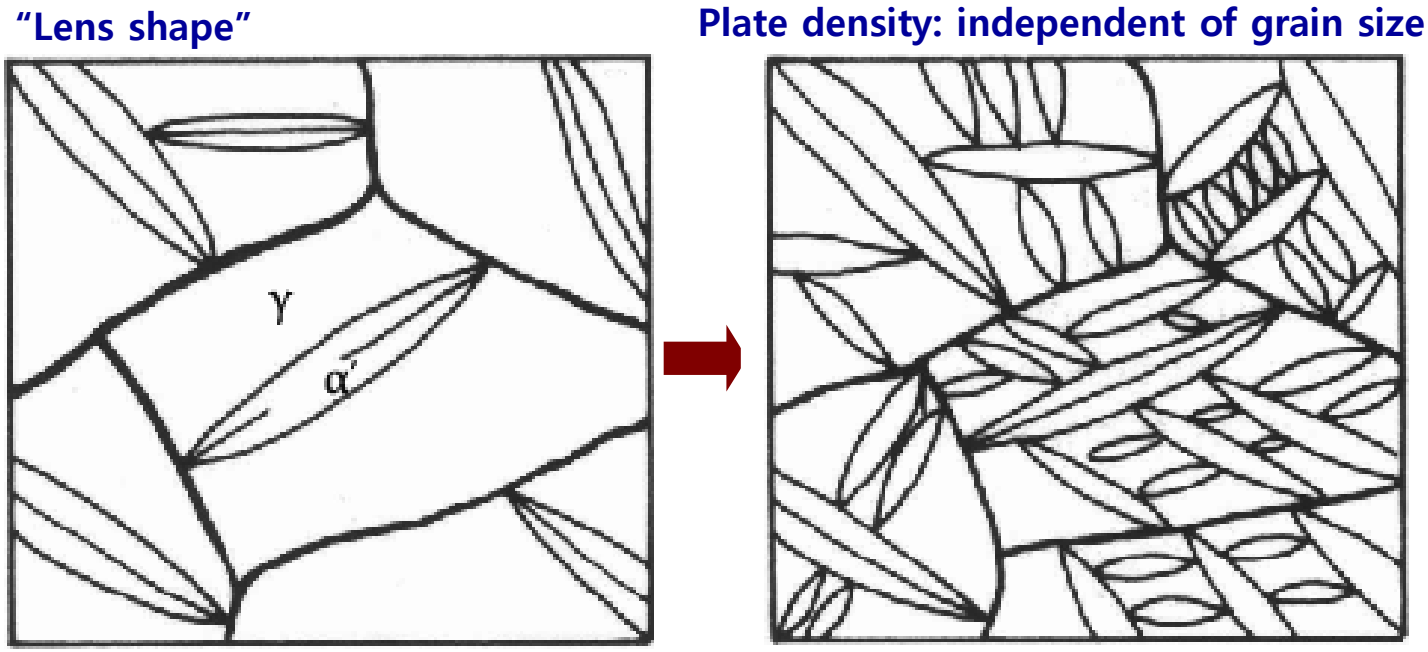

Fig. 6.1 Growth of martensite with increasing cooling below Ms.

→ Martensite formation rarely goes to completion

Microstructure of Martensite

- The microstructural characteristics of martensite are:

2) each platelet is accompanied by a shape change.

- **(d) the shape change appears to be a simple shear parallel to a habit plane (M phase의 중심과 평행한 모상의 특정한 면) and a "uniaxial expansion (dilatation) normal to the habit plane".**

strain associated with the transformation

Polished surface_elastic deformation or tilting
→ but, remain continuous after the transformation

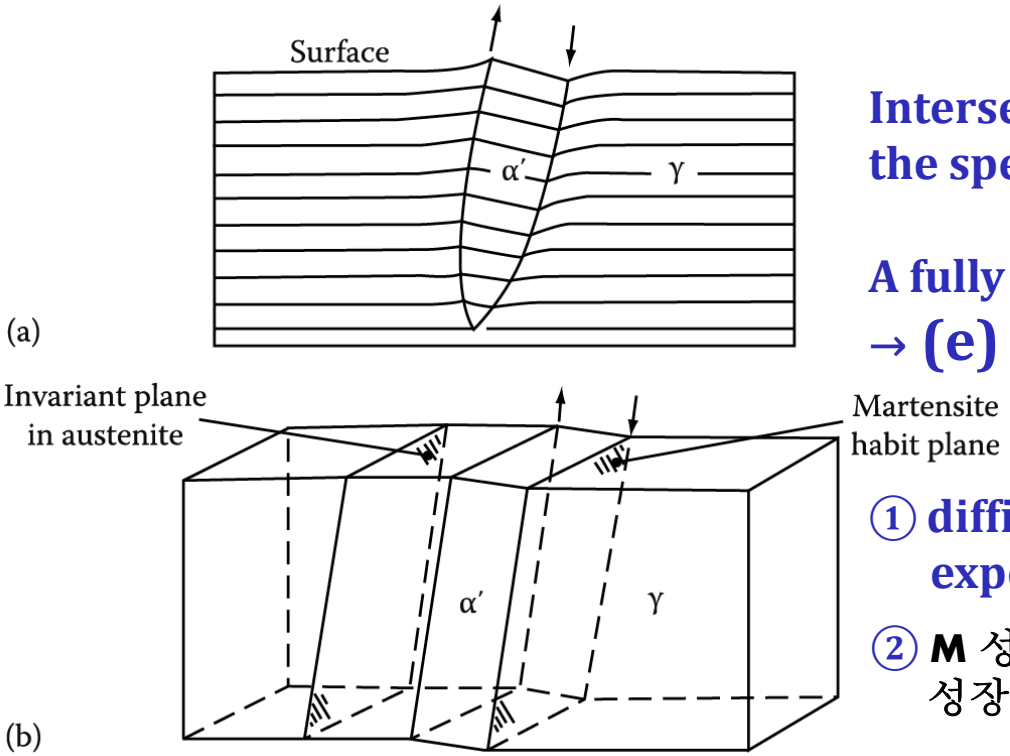

Intersection of the lenses with the surface of the specimen does not result in any discontinuity.

A fully grown plate spanning a whole grain ~10^{-7} sec
→ (e) ν of α'/γ interface ∝ speed of sound in solid

: 변태시 **Click** 소리가 나기도 함

① **difficult process to study M nucleation and growth experimentally**

② **M** 성장속도는 온도에 따른 확연한 변화가 없으며, 성장시 열활성화 거동은 일반적으로 일어나지 않음.

Fig. 6.2 Illustrating how a martensite plate remains macroscopically coherent with the surrounding austenite and even the surface it intersects.

Microstructures

M_f temperature (M finish) corresponds to that temperature below which further cooling does not increase the amount of M.
→ 10-15% retained γ: common feature of higher C content alloys

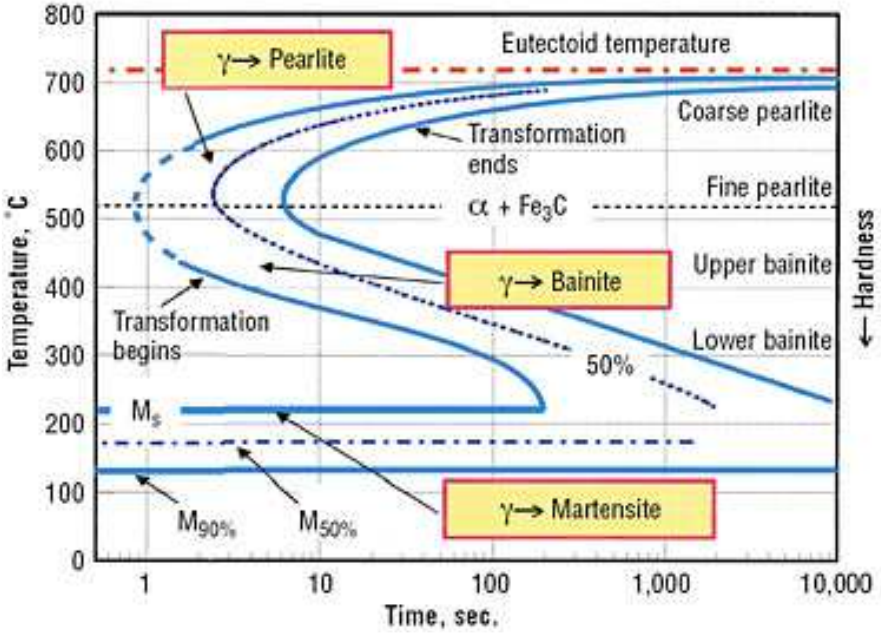

Low C (lath)

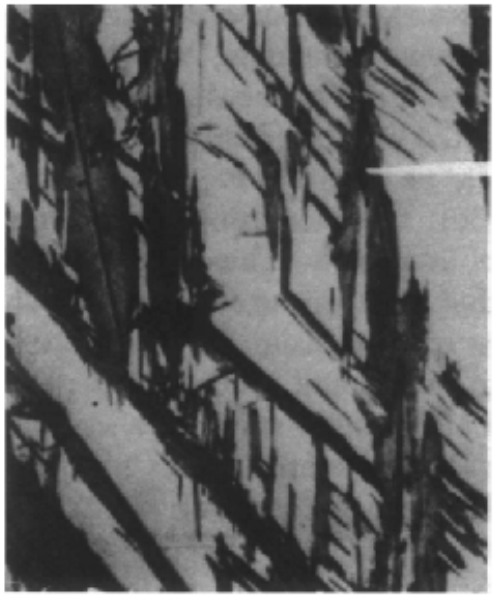

Medium C (plate)

Fe-Ni (plate, some isothermal growth)

Fig. 6.1 (c-e) Different martensite morphologies in iron alloys

Control of Mechanical Properties By Proper Heat Treatment in Iron-Carbon Alloy

Martensite

- Tip of needle shape grain
- Nucleation site of fracture
- Brittle

Proper heat treatment (tempering)

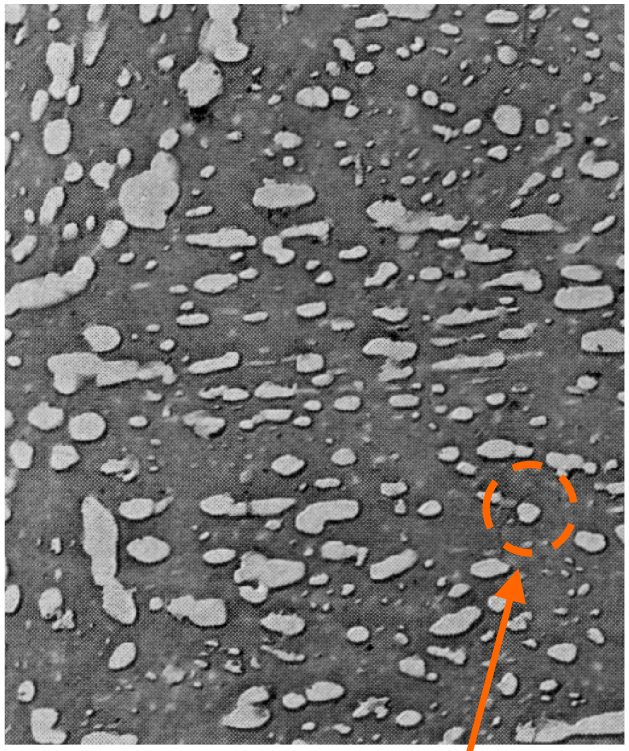

Tempered martensite

- Very small & spherical shape grain
- Good strength, ductility, toughness

Q3:

Driving Forces of Martensitic transformation

- These transformations require ***larger driving forces*** than for diffusional transformations. (= large undercooling, ΔT)

- Why? In order for a transformation to occur without long range diffusion, it must take place ***without a change in composition***.

- This leads to the so-called T_0 **concept**, which is the temperature at which the new phase can appear with **a net decrease in free energy** *at the same composition as the parent (matrix) phase*.

- As the following diagram demonstrates, the temperature, T_0, at which segregation-less transformation becomes possible (i.e. a decrease in free energy would occur), is always less than the liquidus temperature.

Free Energy - Composition: T_0

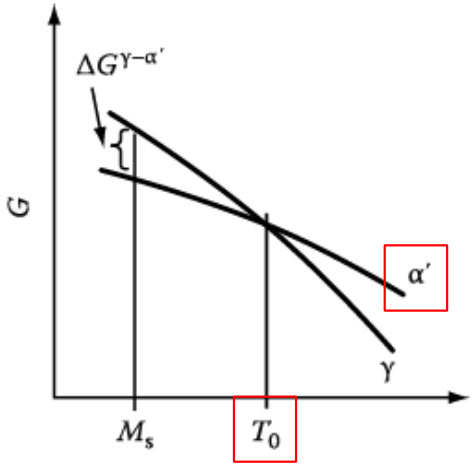

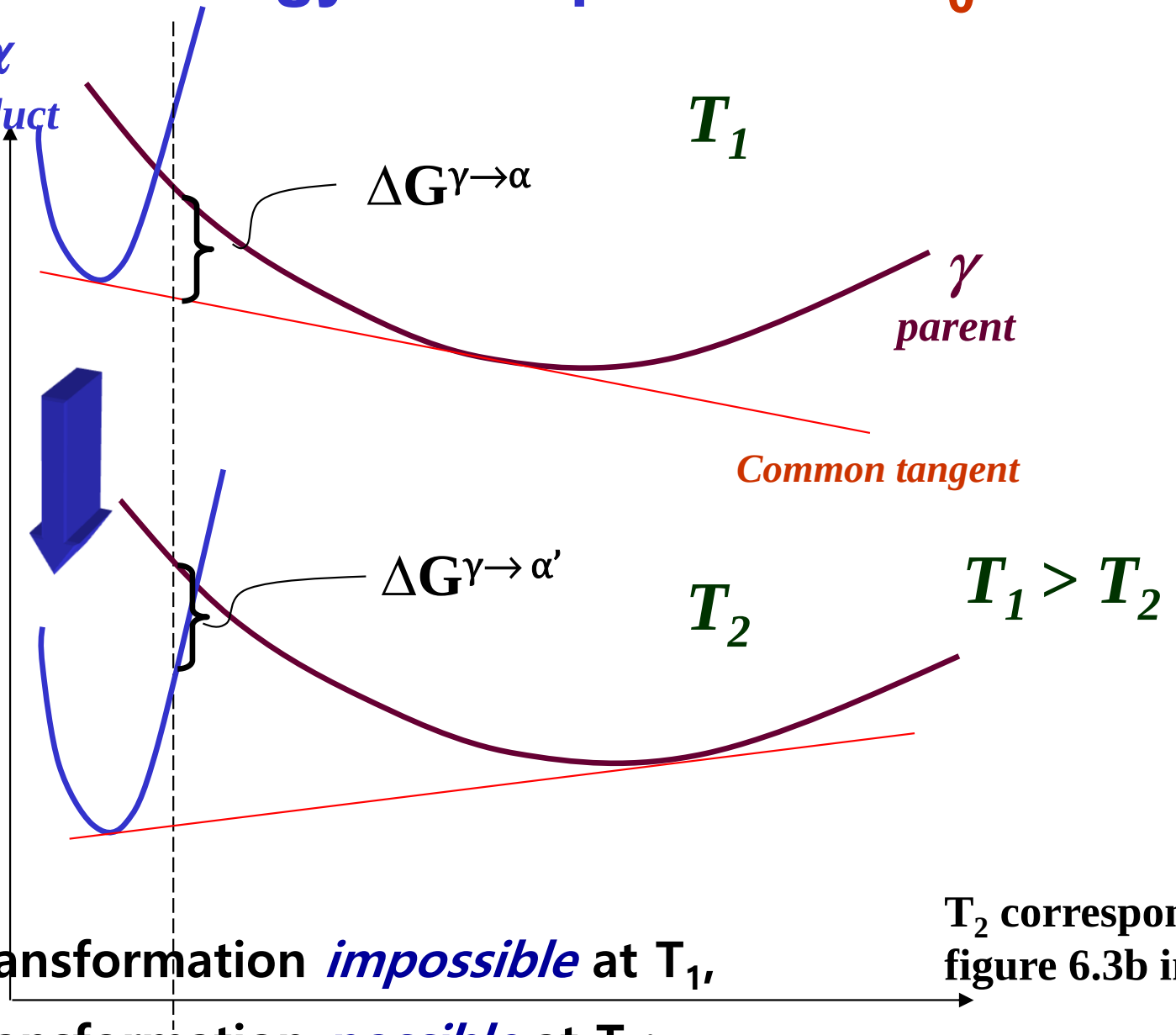

Diffusionless transformation *impossible* at T_1,

Diffusionless transformation *possible* at T_2;

T_2 corresponds to figure 6.3b in P&E.

"T_0" is defined by no difference in free energy between the phases, $\Delta G=0$.

Driving Force Estimation

- The driving force for a martensitic transformation can be estimated in exactly the same way as for other transformations such as solidification.

- Provided that an enthalpy (latent heat of transformation) is known for the transformation, the driving force can be estimated as proportional to **the latent heat** and **the undercooling below T_0**.

$$\Delta G = \frac{L\Delta T}{T_m} \Rightarrow \Delta G^{\gamma\rightarrow\alpha'} = \Delta H^{\gamma\rightarrow\alpha'}\Delta T/T_0 = \Delta H^{\gamma\rightarrow\alpha'}\frac{(T_0 - M_S)}{T_0}$$

Alloy	$\Delta H^{\gamma\rightarrow\alpha'}$ (J mol^{-1})	$T_0 - M_s$(K)	$-\Delta G^{\gamma\rightarrow\alpha'}$ (J mol^{-1})
Ti–Ni	1550	20	92
Cu–Al	170–270	20–60	19.3 ± 7.6
Au–Cd	290	10	11.8
Fe–Ni 28%	1930	140	840
Fe–C			1260
Fe–Pt 24% Ordered	340	10	17
Fe–Pt Disordered	2390	~150	~1260

(a relatively small ΔT)

*** Large differences in $\Delta G^{\gamma\rightarrow\alpha'}$ btw disordered and ordered alloys**

Source: From Guénin, G., PhD thesis, Polytechnical Institute of Lyon, 1979.

Table 6.1. Comparisons of Calorimetric Measurements of Enthalpy and Undercooling in some M alloys

Various ways of
showing the martensite transformation

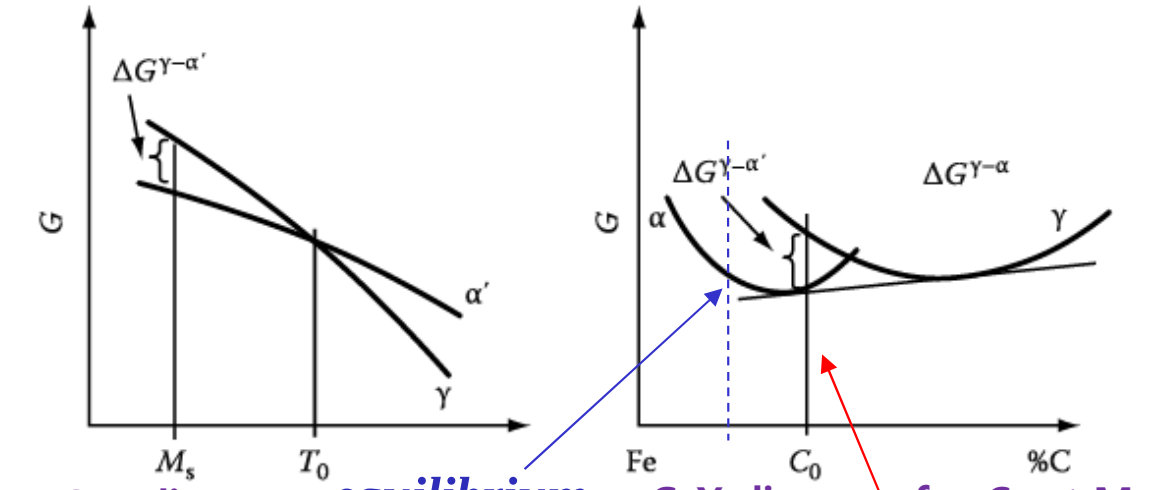

(a) G-T diagram *equilibrium* (b) G-X diagram for C_0 at M_s

diffusionless

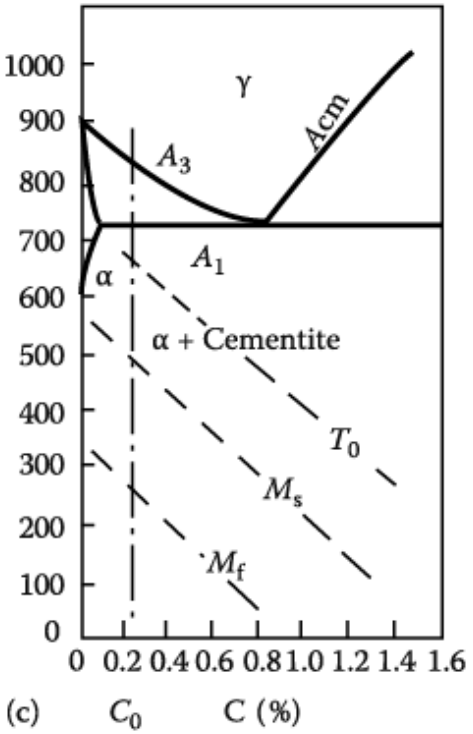

Fe-C phase diagram
Variation of $T_0/M_s/M_f$

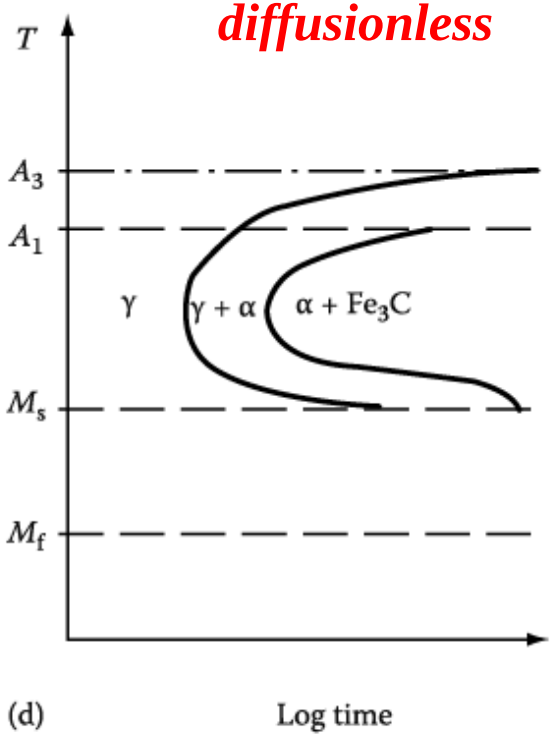

TTT diagram
for alloy C_0 in (c)

Note that the M_s line is horizontal in the TTT diagram; also, the M_f line.

Some retained austenite can be left even below M_f. In particular, as much as 10%-15% retained austenite is a common feature of especially the higher C content alloys such as those used for ball bearing steels.

(f) M 변태시 핵생성은 불균일 핵생성에 의해 일어나며,
열활성화 **(thermal activation)** 없이 핵생성과 성장이 일어나는 경우**: athermal M**
열활성화에 의해 핵생성이 일어나는 경우**: isothermal M = thermally activated M**

(g) M 변태에 대한 구동력이 주어지면, **M** 변태가 일어나는 부피분율이 결정되며,
M 변태가 일어나는 부피분율을 더 증가시키기 위해서는 변태구동력을 키워야 함**.**

(h) M 변태시 정합 또는 부분정합을 이루는 활주계면 **(glissile interface)**을 가로질러
원자들이 협동적으로 이동하기 때문에 모상의 이웃원자들이 **M**에서도 이웃원자로 유지
(Military transformation, the distance any one atom moves is less than an interatomic spacing.)

(i) M 변태시 정합계면을 유지한 채 전단변형이 일어나는 것은 모상 **(γ)**과 생성상**(α')**에
내부 응력과 그로 인한 변형을 유발**.** 따라서, 변형에너지 효과 **(strain E effect)**가 중요하며,
외부 응력이나 자기력 등이 **M** 변태에 영향을 미친다**. (e.g. Stress-induced M** 변태**)**

(j) 일부 **M** 변태는 변태 구동력을 반대로 하면 **(T or stress)** 원래의 모상으로 되돌아 옴
(가역 상변태, **reversible transformation): Thermoelastic M ↔ Non-thermoelastic M**

6.1 Introduction to M in Ferrous system

M transformation : γ (fcc) → α' martensite (bct, body centered tetragonal) (e.g. Fe-C-X)

γ (fcc) with low stacking fault E at room temp.
(cooling or stress) → ε M (hcp) (e.g. Fe-Cr-Ni, Fe-Mn (high Mn steel))

동소변태 : **Ti, Mn, Fe, Co, Zr…**

일반적으로 **fcc** 혹은 **hcp** (조밀격자)
→낮은 내부 **E &** 엔탈피→낮은 온도
영역 안정, **bcc** (낮은 충진율) → 높은 **vibrational entropy** → 높은
온도영역 안정 : **Ti, Mn, Co, Zr**

But

Fe의 경우, **bcc α** 저온 안정/ **Fcc γ**
고온안정 → γ상과 α상의 자기적
성질에 기인 → "복잡한 상변화 거동"

bcc α 와 bcc δ 사이에서 Fcc γ 안정

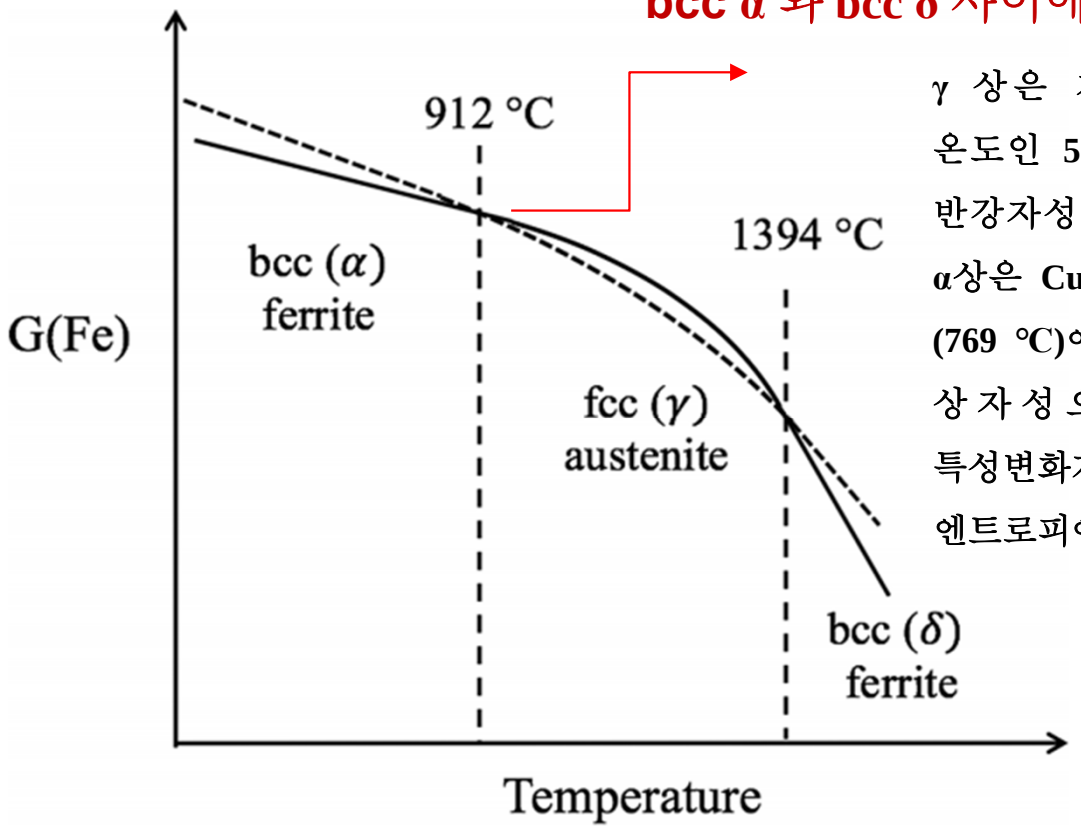

γ 상은 자기특성이 **Neel** 온도인 **50 K (-223°C)**에서 반강자성에서 상자성으로, **α**상은 **Curie** 온도인 **1042K (769 °C)**에서 반강자성에서 상자성으로 → 자기적 특성변화가 두 상의 내부**E**와 엔트로피에 영향

FIGURE 6.1 Schematic representation of the Gibbs free energy of iron as a function of temperature. Full line bcc and dashed line fcc.

Ref. CALPHAD: Comput. Coupling Phase Diagrams Thermochem., 33: 3 (2009)

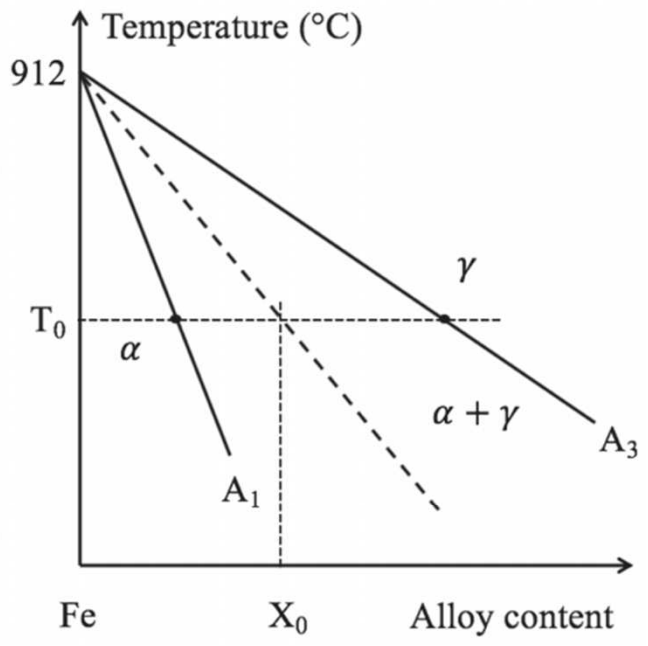

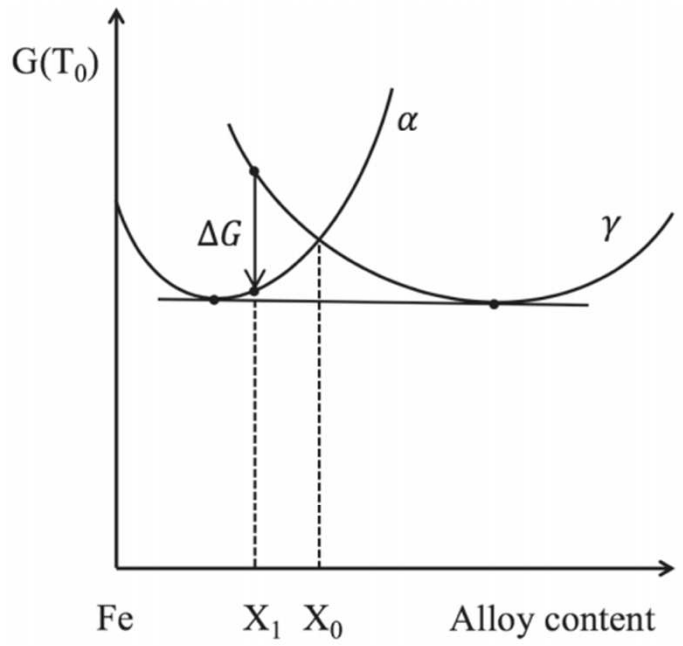

(C, Mn, Cr, Ni, Cu 등)

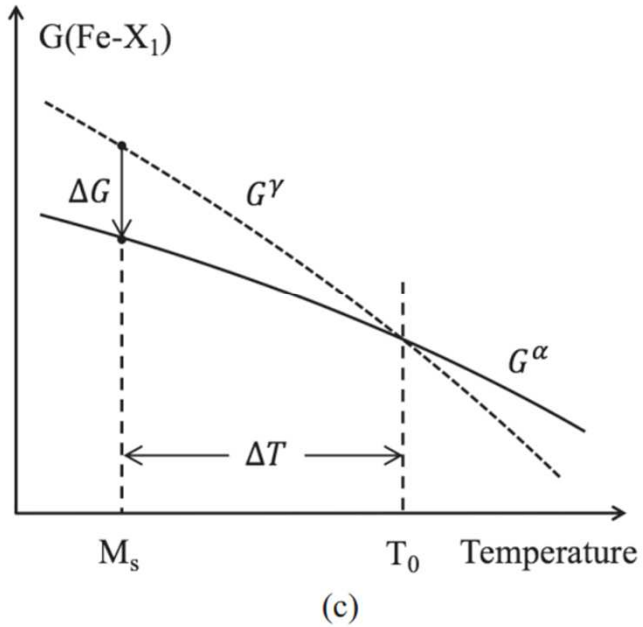

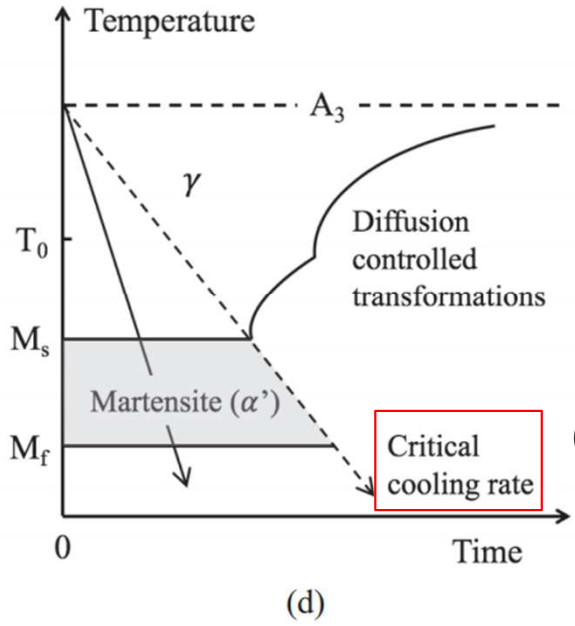

M_s 온도 : 조성에 민감하게 변화
e.g. Pure Fe의 M_s 540°C(813K),
Fe-31Ni-10Co-3Ti 합금 -190°C (83K)

M_f 온도: 100% M 변태 조건 찾기 어려움/ M_s 보다 불분명

(순금속 ~10^5 K/s, 고합금강인 18Ni 마레이징 강 < 10^{-2} K/s)

FIGURE 6.2 Conditions for the $\gamma \rightarrow \alpha'$ transformation in ferrous systems on cooling. (a) Schematic binary phase diagram showing the compositions of γ and α in equilibrium and the equilibrium temperatures A_1 and A_3. (b) Schematic Gibbs free energy vs. composition diagram for the temperature T_0 in (a). (c) Free energy vs. temperature for composition X_1 in (b). (d) CCT diagram for composition X_1.

6.2 ferrous Martensite Morphologies and Crystallography

저탄소 혹은 중탄소 범위 저 합금강 **M transformation : γ (fcc) → bcc 혹은 bct M**

bcc 혹은 bct M 3가지 대표 형상: lath / lenticular plate (렌즈형 판상) / thin plate

6.2.1 Lath Martensite: 저탄소강, 저합금 구조용강, **Ni** 함량이 **28%** 이하인 **Fe-Ni** 합금
고강도 고인성 **e.g.** 고인성 **cryogenic** 합금 **9%Ni**강의 주요 구성상
다른 형상 **M** 보다 상대적으로 높은 상변화 온도 **e.g.** 저합금 탄소강 M_s~400 ℃, M_f~200℃

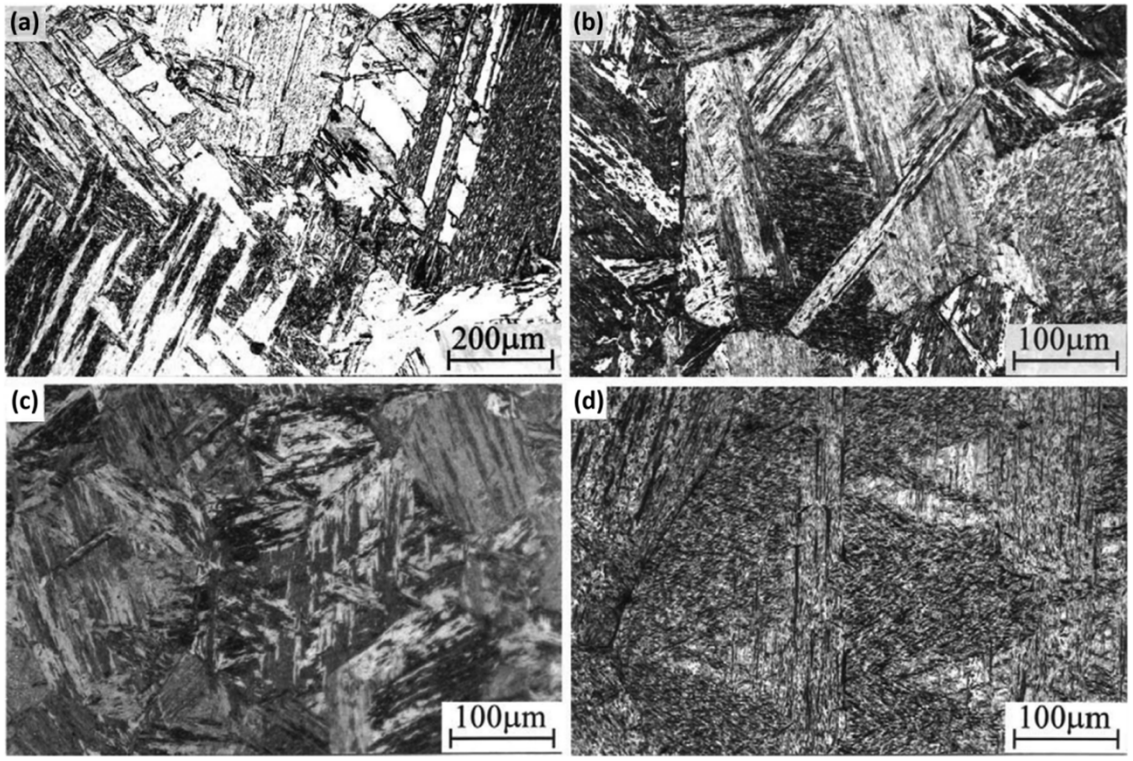

FIGURE 6.3 Light optical micrographs of lath martensite in Fe–C alloys with carbon contents in wt.% (a) 0.0026, (b) 0.18, (c) 0.38 and (d) 0.61. Etched in 3% nital solution. (Reprinted from *Acta Materialia* Vol. 51, S. Morito, H. Tanaka, R. Konishi, T. Furuhara, T. Maki, The morphology and crystallography of lath martensite in Fe–C alloys, 1789–1799 (2003), with permission from Elsevier.)

*** 결정립 – Packet – Sub-block – Lath 구조**

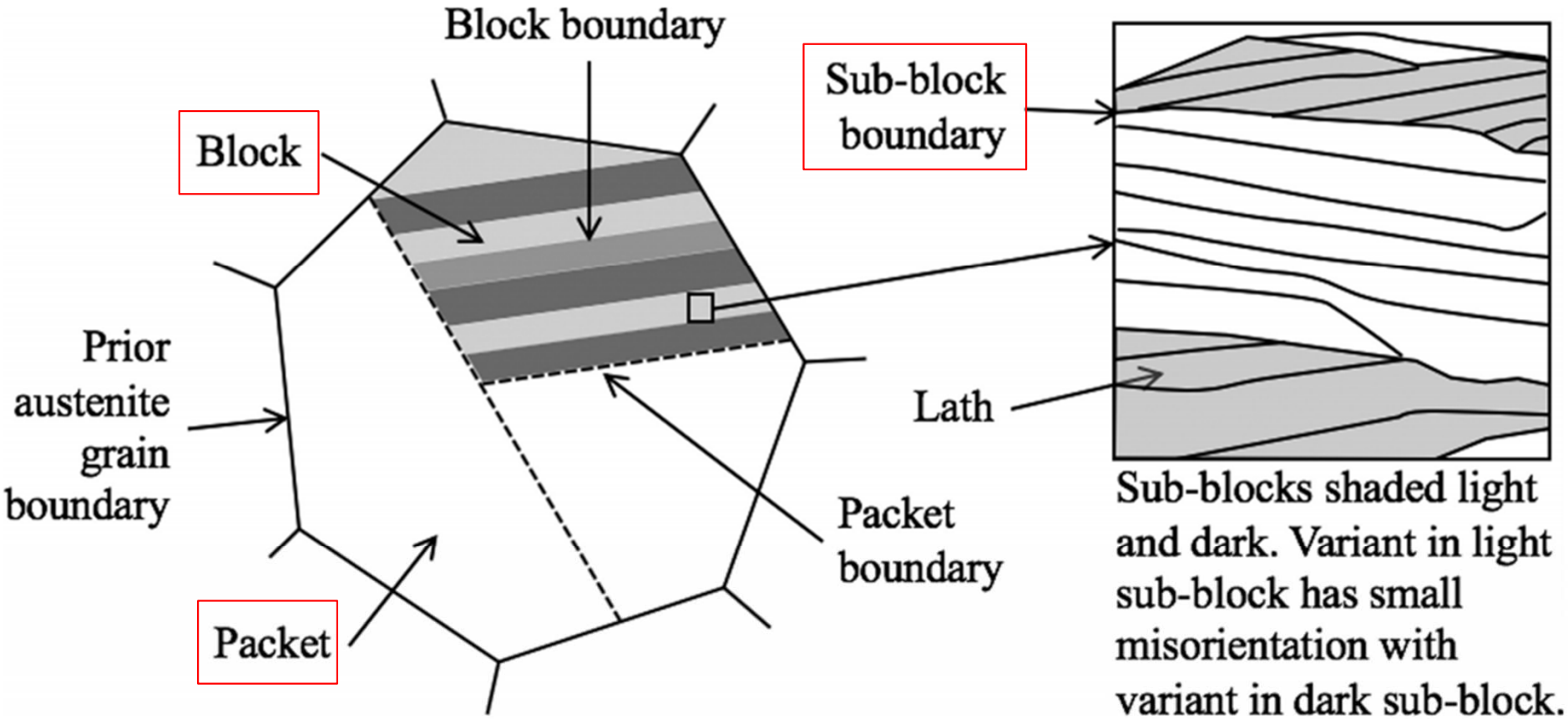

FIGURE 6.4 Schematic representation of lath martensite morphology in low-carbon alloys and steels.

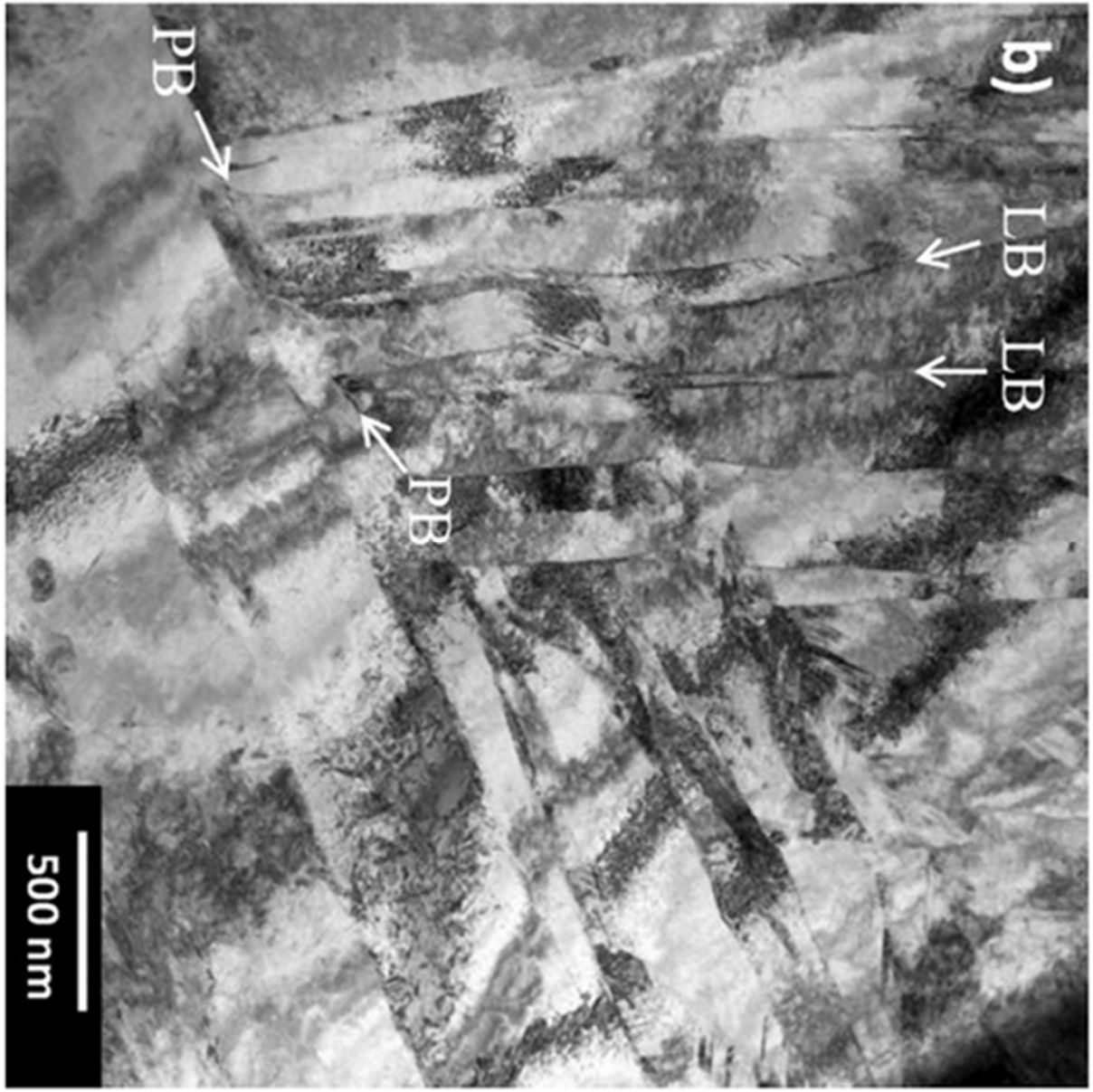

Lath에서 마주보는 면이
완전히 평행하지 않기 때문에
3차원 이미징 기술을 이용해야
lath 폭과 길이 결정 가능

대략적으로 약 **0.1~ 1 μm**

10^{15} m^{-2}의 매우 높은 전위 밀도

Lath 결정구조 **: bcc**

$$\{110\}_{\alpha'} \| \{111\}_{\gamma}$$

KS 방위관계/ **Greninger-Troiano** 방위관계/ **NW** 방위관계 **(KS** 대비 **5.26°)**

FIGURE 6.5 Bright-field transmission electron microscope image of lath martensite in a thin foil of a low-carbon steel. Two lath boundaries and one packet boundary are marked (LB, PB). The distances between the lath boundaries vary from 50 to 500 nm. The dark–light banding is due to bending of the thin foil causing changes in the diffraction conditions. (Courtesy of Shashank Ramesh Babu.)

*** 결정립 – Packet – Sub-block – Lath 구조**

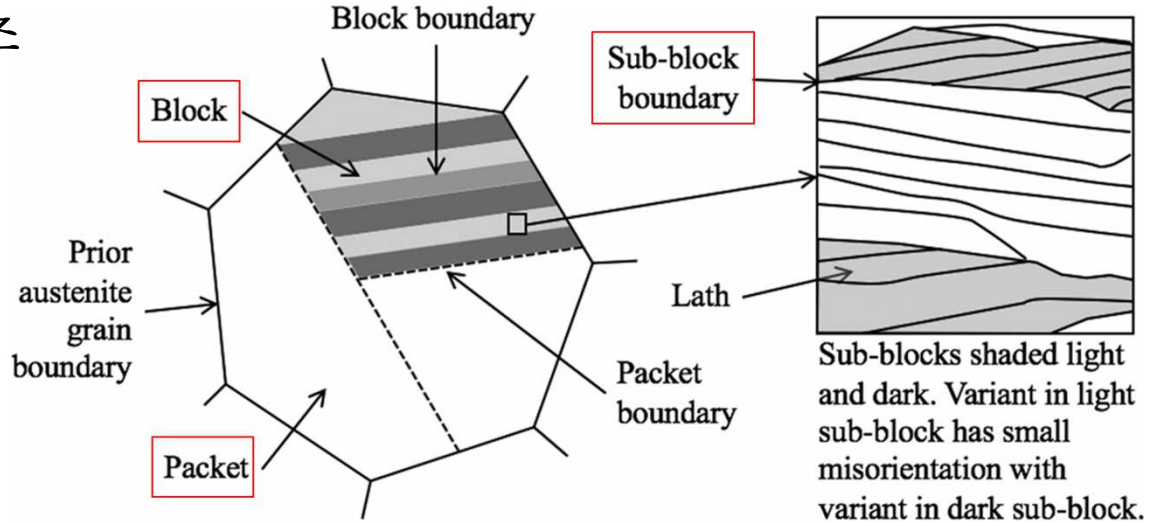

FIGURE 6.4 Schematic representation of lath martensite morphology in low-carbon alloys and steels.

- 변태전 γ 결정립은 Packet으로 분리 - 이 안에 모든 Lath는 {111} 면 변형에 의한 K-S 방위관계 따라서, 한 Packet에는 V1-V6 의 6rodml 이형이 존재

- 저탄소 합금이나 저탄소강의 경우 패킷은 블록으로 나눠지며, 각 블록에 있는 모든 Lath는 V1과 V4 같이 서로 근접한 방위를 갖는 이형들로 구성되어 있으며, 블록 내의 같은 이형 모임을 Sub-block이라고 함. Lath의 habit plane은 서브블록마다 어느정도는 변할 수 있음.

- Sub-block 내 Lath의 방위는 4° 이하에서 변할 수 있으며, 이들 Lath 사이의 경계는 소경각 입계가 됨. 블록간의 경계면은 조밀면에 평행하게 유지하려하며, 따라서 49.5-70.5° 범위의 고경각입계를 이룸

- 고탄소 합금의 경우 패킷과 블록의 크기가 감소 저탄소 합금에 비해 작으며, 각각의 블록은 단 한가지의 방위 이형을 가짐.

- 모상 γ의 결정립 크기가 감소하면 패킷과 블록의 크기가 감소.

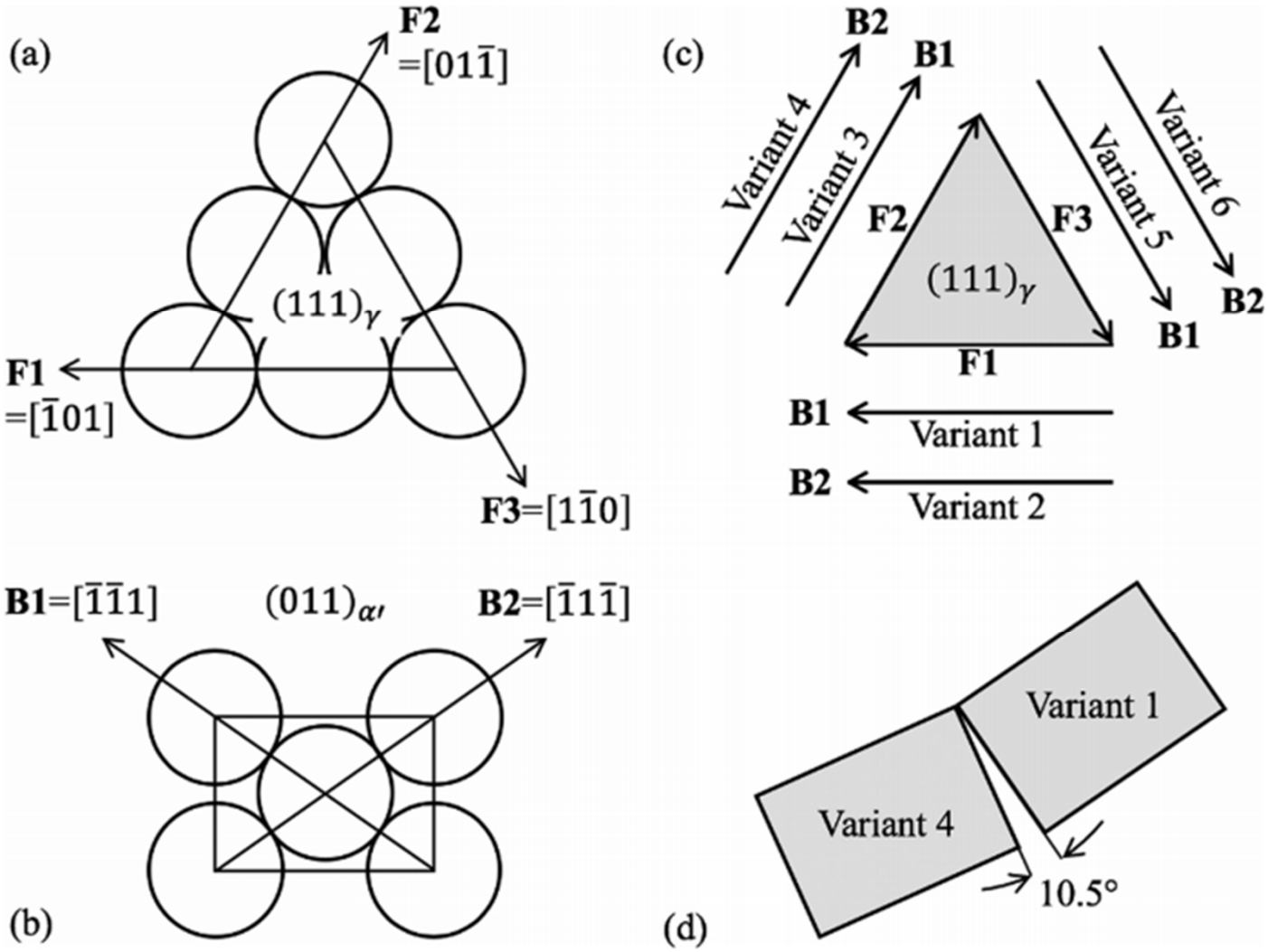

FIGURE 6.6 Variants of the Kurdjumov–Sachs orientation relationship for one close-packed austenite plane $(111)_\gamma$. (a) Atomic arrangement and the three close-packed directions on $(111)_\gamma$. For brevity, the symbols F1, F2 and F3 are used in place of the Miller indices (F meaning fcc). (b) The two close-packed directions in a $(011)_{\alpha'}$ plane abbreviated to B1 and B2 (B meaning bcc). (c) The six ways of aligning the close-packed directions in the two lattices giving six orientation variants. (d) $(011)_{\alpha'}$ sections through the bcc unit cells for variants 1 and 4 showing that there is only a 10.5° rotation about $[011]_{\alpha'}$. The same misorientation exists for the corresponding variant pairs V2-V5 and V3-V6.

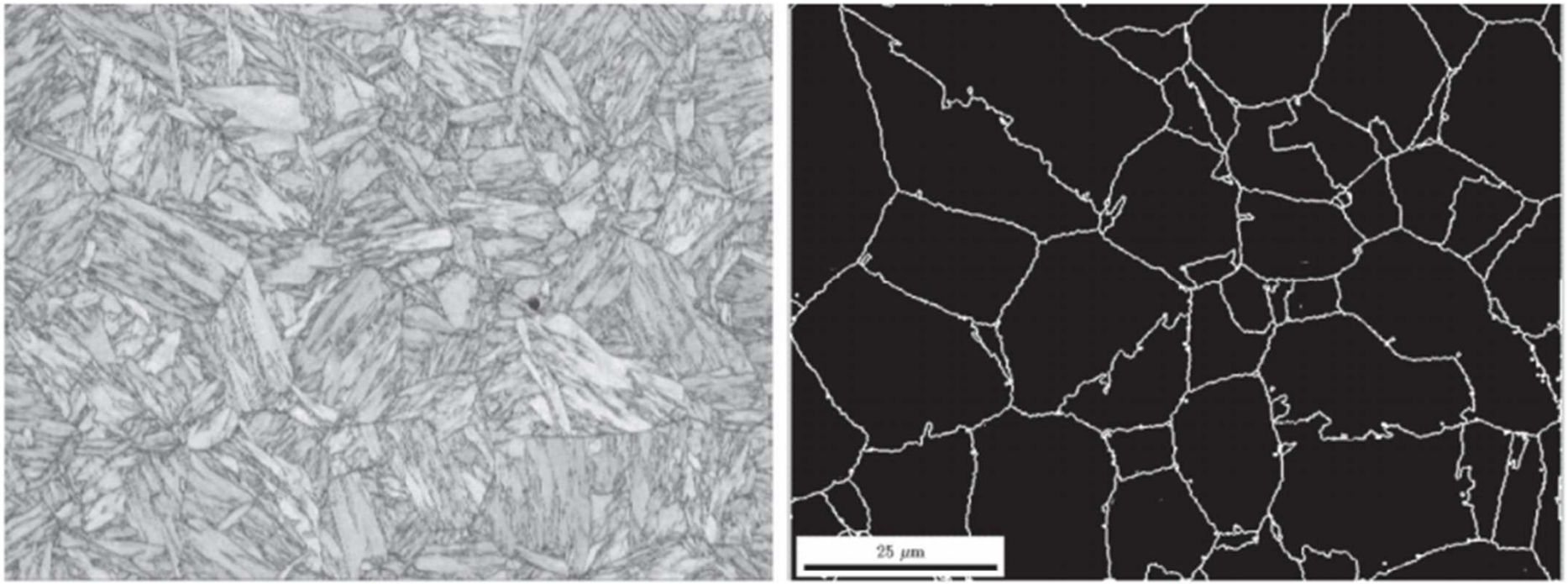

FIGURE 6.7 Lath martensite in a steel containing 0.13C–0.7Si–1.7Mn–0.3Cr. (a) Scanning electron backscattered diffraction band contrast image showing block structure. (b) Prior austenite grain boundaries reconstructed from the pixel orientation data assuming a K–S orientation relationship. Note that the jaggedness of some boundaries is due to misindexing of the diffraction patterns near the boundaries. Courtesy of Shashank Ramesh Babu and Matias Jaskari.